

國立臺灣大學生命科學院基因體與系統生物學學位學程

碩士論文

Genome and Systems Biology Degree Program

College of Life Science

National Taiwan University

Master Thesis



透過適應性演化研究牛痘病毒 A56/K2 蛋白複合體如何抑制病毒進入細胞

Adaptive evolution of vaccinia virus to bypass viral entry
inhibition of A56/K2 protein complex

洪冠琦

Guan-Ci Hong

指導教授：張雯 博士

Advisor: Wen Chang, Ph.D.

中華民國 109 年 7 月

July 2020



國立臺灣大學碩士學位論文

口試委員會審定書

透過適應性演化研究牛痘病毒 A56/K2 蛋白複合體如何抑制病毒進
入細胞

Adaptive evolution of vaccinia virus to bypass viral entry
inhibition of A56/K2 protein complex

本論文係洪冠琦君 (R07B48002) 在國立臺灣大學基因
體與系統生物學學位學程完成之碩士學位論文，於民國 109
年 7 月 16 日承下列考試委員審查通過及口試及格，特此證
明

口試委員：

張雯

(簽名)

(指導教授)

鄭昭生

薛麗冰

~~~~~

鄭石通

( 簽名 )

基因體與系統生物學學位學程主任

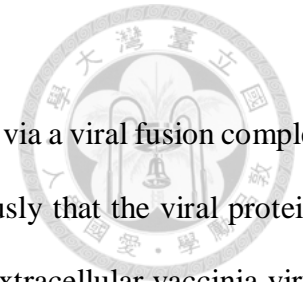
## 摘要



在牛痘病毒進入宿主過程中，牛痘病毒需要通過 11 種蛋白質的病毒融合複合物與宿主膜融合，但詳細機制仍不清楚。先前研究顯示，病毒蛋白 A56 和 K2 會在感染的細胞上表達，並透過與病毒融合複合物的兩個分子（G9 和 A16）結合以防止細胞外痘苗病毒的過度感染，從而抑制膜融合。為了研究 A56 / K2 複合物如何抑制膜融合，我們透過在 HeLa 細胞表面表達 A56 和 K2 蛋白並用三種痘苗病毒 WR，WR $\Delta$ A26 和 WR $\Delta$ B5 進行病毒體外演化實驗，以分離出適應性突變病毒。適應性突變病毒的全基因組定序結果顯示，三種病毒基因對於痘苗病毒克服 A56 / K2 表達的融合抑制作用很重要。我們確定的有一個三種病毒都共同擁有的突變發生在 G9R ORF 中，它在經過多代的篩選後出現了一個單一鹼基突變 C130T，會導致胺基酸 His44 變成 Tyr。G9<sup>H44Y</sup> 突變並不影響病毒融合蛋白複合物的形成，也不影響其與 A56 / K2 蛋白複合物的相互作用。這些結果說明 G9<sup>H44Y</sup> 突變蛋白模擬了酸誘導的中間構象，使膜融合更容易發生。由於此突變共同出現在三個傳代病毒庫中，可能表明該突變是發生病毒適應的主要驅動力。除了 G9<sup>H44Y</sup> 突變之外，有兩個突變只專一性的存在於 WR 傳代病毒中，A28 ORF 中的 P79Q 和 A26 ORF 中發生的多個插入或缺失的適應性突變。A28<sup>P79Q</sup> 突變僅短暫累積，隨後在之後的傳代過程中被 A26 ORF 中發生的多個插入或缺失突變所取代，這也說明了這些基因之間存在著遺傳上相互作用的關係。實際上，我們發現 A26 和 A28 蛋白在免疫共沈澱實驗結果中顯現有相互結合的關係，然而 A28<sup>P79Q</sup> 突變並不影響其與 A26 蛋白的結合。最後，我們發現雙重突變病毒 WR-G9<sup>H44Y</sup> + A28<sup>P79Q</sup> 具有比 WR-G9<sup>H44Y</sup> 好的病毒傳播能力，這結果可能暗示著 A28<sup>P79Q</sup> 控制著 mature virus (MV) 到 extracellular virus (EV) 的運輸或 EV 釋放的步驟。

**Keywords:** 牛痘病毒膜融合機制，膜融合蛋白複合物(EFC)，膜融合抑制子，病毒體外演化實驗

## ***Abstract***



For cell entry, vaccinia virus requires fusion with the host membrane via a viral fusion complex of 11 proteins, but the mechanism remains unclear. It was shown previously that the viral proteins A56 and K2 are expressed on infected cells to prevent superinfection by extracellular vaccinia virus through binding to two components of the viral fusion complex (G9 and A16), thereby inhibiting membrane fusion. To investigate how the A56/K2 complex inhibits membrane fusion, I performed experimental evolutionary analyses by repeatedly passaging three vaccinia viruses—WR, WR $\Delta$ A26 and WR $\Delta$ B5—in HeLa cells overexpressing the A56 and K2 proteins to isolate adaptive mutant viruses. Genome sequencing of adaptive mutants revealed that three viral genes are important for vaccinia virus to overcome fusion inhibition by A56/K2 expression. The first viral open reading frame (ORF) I identified is G9R, which harbors a specific mutation (C130T) from adaptive selection, resulting in a His44Tyr amino acid change. G9H44Y did not affect viral fusion protein complex formation nor its interaction with A56/K2 protein complex. These results suggest that G9H44Y mutant protein mimics an acid-induced intermediate conformation more prone to membrane fusion. Since this mutation is shared by all three passaged virus pools, this mutation appears to be the major driving force for virus adaptation. In addition to G9H44Y, I also identified two viral mutations specific to adaptive mutants derived from WR passaging, i.e., P79Q of A28 ORF and multiple insertions/deletions of A26 ORF. A28P79Q only accumulated transiently and was subsequently replaced by insertions/deletions of A26 ORF in subsequent passaging events, indicating genetic interplay between these two genes. Indeed, a co-immunoprecipitation experiment revealed that A26 and A28 protein bind to each other and that the P79Q mutation of A28 does not affect its binding to A26 protein. Finally, I observed that the double mutant virus WR-G9H44Y+A28P79Q exhibits enhanced virus spreading relative to WR-G9H44Y, indicating that A28P79Q controls the transition of mature virus (MV) to extracellular virus (EV) or the EV release step.

**Keywords:** Vaccinia virus entry, Entry fusion complex (EFC), Fusion suppressor, Experimental evolution



# Table of Contents

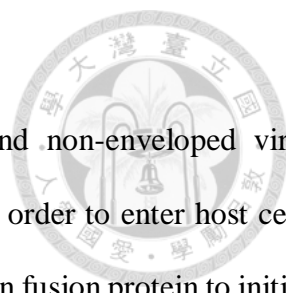


|                                                                                                                                                              |     |
|--------------------------------------------------------------------------------------------------------------------------------------------------------------|-----|
| 口試委員會審定書                                                                                                                                                     | I   |
| 摘要                                                                                                                                                           | II  |
| Abstract                                                                                                                                                     | III |
| Table of Contents                                                                                                                                            | V   |
| The List of Figures and Supplementary Figures                                                                                                                | VI  |
| Introduction                                                                                                                                                 | 1   |
| Materials and Methods                                                                                                                                        | 4   |
| Cell culture, reagents and viruses. ....                                                                                                                     | 4   |
| Construction of a fluorescent recombinant vaccinia virus expressing early Venus and late A4-mCherry protein (WRΔA26-Venus-A4mCherry). ....                   | 5   |
| Construction of a stable cell line expressing A56 and K2 protein complex. ....                                                                               | 5   |
| Construction of a fluorescent recombinant vaccinia virus expressing late A4-mCherry protein, WRΔB5-A4-mCherry. ....                                          | 6   |
| Experimental passaging of WRΔA26, WR and WRΔB5 viruses on HeLa and HeLa-A56/K2 cells for adaptive mutant virus selection. ....                               | 6   |
| Viral genome sequencing and data analyses. ....                                                                                                              | 6   |
| Generation of G9 <sup>H44Y</sup> recombinant virus of WRΔA26, WR and WRΔB5 vaccinia viruses. ....                                                            | 8   |
| Growth analyses of the viruses in HeLa and HeLa-A56/K2 cells. ....                                                                                           | 8   |
| Vaccinia MV-triggered cell fusion from-without at neutral and acidic pH. ....                                                                                | 9   |
| Vaccinia EV-triggered cell fusion from-within. ....                                                                                                          | 9   |
| Coimmunoprecipitation and immunoblot analyses. ....                                                                                                          | 10  |
| Results                                                                                                                                                      | 12  |
| Chapter 1: To investigate EV-mediated entry fusion inhibition process in WRΔA26 through in vitro experimental evolution. ....                                | 12  |
| Chapter 2: WR-G9 <sup>H44Y</sup> mutants require additional mutations in A28 and A26 genes in order to overcome growth inhibition on HeLa-A56/K2 cells. .... | 19  |
| Discussion                                                                                                                                                   | 27  |
| References                                                                                                                                                   | 30  |

## *The List of Figures and Supplementary Figures*

|                                                                                                                                                                              |    |
|------------------------------------------------------------------------------------------------------------------------------------------------------------------------------|----|
| <b>Figure 1.</b> Generation of HeLa-A56/K2 cells co-expressing vaccinia A56 and K2 proteins to inhibit WRΔA26 infection.....                                                 | 34 |
| <b>Figure 2.</b> Experimental passaging of WRΔA26 in HeLa and HeLa-A56/K2 cells.....                                                                                         | 36 |
| <b>Figure 3.</b> Whole genome sequencing identified genome variations present in WRΔA26 <sup>HeLa</sup> and WRΔA26 <sup>HeLa-A56/K2</sup> virus pools.....                   | 37 |
| <b>Figure 4.</b> Generation of recombinant WRΔA26-G9 <sup>H44Y</sup> virus.....                                                                                              | 39 |
| <b>Figure 5.</b> WRΔA26-G9 <sup>H44Y</sup> mutant virus forms plaques with a cell fusion phenotype on HeLa and HeLa-A56/K2 cells.....                                        | 41 |
| <b>Figure 6.</b> Coimmunoprecipitation of G9 <sup>H44Y</sup> protein with A16, A56/K2 protein complex and multiple components of the viral EFC in virus-infected cells.....  | 42 |
| <b>Figure 7.</b> Acid titration of WRΔA26-G9 <sup>H44Y</sup> virus-mediated fusion activation in HeLa-A56/K2 cells.....                                                      | 44 |
| <b>Figure 8.</b> The entry of mature virion and extracellular virion.....                                                                                                    | 46 |
| <b>Figure 9.</b> Experimental passaging of WR and WRΔB5 in HeLa and HeLa-A56/K2 cells.....                                                                                   | 48 |
| <b>Figure 10.</b> Whole genome sequencing identified genome variations present in different pools of WR and WRΔB5 passaged virus.....                                        | 50 |
| <b>Figure 11.</b> An identical G9 <sup>H44Y</sup> mutation occurred in WRΔA26 <sup>HeLa-A56/K2</sup> , WR <sup>HeLa-A56/K2</sup> and WRΔB5 <sup>HeLa-A56/K2</sup> virus..... | 51 |
| <b>Figure 12.</b> Generation of recombinant WR-G9 <sup>H44Y</sup> and WRΔB5-G9 <sup>H44Y</sup> virus.....                                                                    | 52 |
| <b>Figure 13.</b> The additional mutation revealed on WR <sup>HeLa-A56/K2</sup> virus.....                                                                                   | 54 |
| <b>Figure 14.</b> Coimmunoprecipitation of wild type A28 protein, A28 <sup>P79Q</sup> protein, A26, wild type G9 and G9 <sup>H44Y</sup> .....                                | 56 |
| <b>Figure 15.</b> The EV of WR-G9 <sup>H44Y</sup> and WR-G9 <sup>H44Y</sup> +A28 <sup>P79Q</sup> virus triggered a cell fusion phenotype on HeLa and HeLa-A56/K2 cells.....  | 57 |
| <b>Figure 16.</b> Acid titration of WR-G9 <sup>H44Y</sup> and WR-G9 <sup>H44Y</sup> +A28 <sup>P79Q</sup> virus-mediated fusion activation in HeLa-A56/K2 cells.....          | 58 |
| <b>Figure 17.</b> EV spreading ability assessment by liquid plaque assay.....                                                                                                | 60 |
| <b>Figure 18.</b> Hypothesis of the regulatory role of A28 <sup>P79Q</sup> in EV spreading.....                                                                              | 61 |
| <b>Supplementary 1.</b> Whole genome sequencing data for passaged WR virus pools.....                                                                                        | 62 |
| <b>Supplementary 2.</b> Acid titration of WR-G9 <sup>H44Y</sup> and WR-G9 <sup>H44Y</sup> +A28 <sup>P79Q</sup> virus-mediated fusion activation in HeLa cells.....           | 69 |

## ***Introduction***



Viruses are divided into two main categories, enveloped virus and non-enveloped virus. Enveloped virus presents attachment and fusion proteins on its surface in order to enter host cells. Not only do such viruses need to bind to host cells, they also utilize their own fusion protein to initiate fusion between viral and cell membranes, enabling release of viral cores into cells (1, 2). Despite different viruses binding to different receptors, they all use viral fusion proteins to mediate this critical fusion step. There are three classes of viral fusion proteins, categorized according to structure: Class I viral fusion proteins, such as influenza HA2 and HIVgp41 proteins, contain an N-terminal fusion peptide and exhibit a triple helix structure (3); Class II fusion proteins, such as flavivirus virus E protein, contain an internal fusion loop (4); and Class III fusion proteins, such as vesicular stomatitis virus G protein, are often regarded as a hybrid type since they combine structural features of both Class I and II fusion proteins (5). Membrane fusion necessitates attainment of a thermodynamically stable state, achieved by overcoming a high-energy barrier (40–50 kcal/mol) to initiate a hemi-fusion event (2, 6). How viral fusion proteins overcome this energy barrier and trigger the conformational changes necessary to complete host entry is a critical topic for virologists.

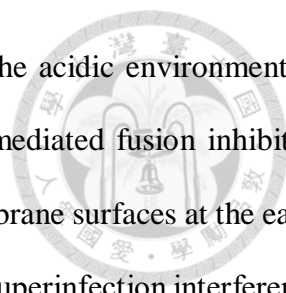
Vaccinia virus (VACV) is a member of the Poxviridae family. It is a complex and enveloped virus with a large double-stranded DNA (dsDNA) genome of approximately 200 kilobases (kb) encoding about 200 proteins. The virions are brick-shaped and ~360x270x250 nm in size. VACV produces two infectious forms of infective particles, i.e., mature virus (MV) and extracellular virus (EV) (7). MVs are released after cell lysis and are important for transmission between hosts. EVs are released from infected cell surfaces and contribute to efficient cell-to-cell transmission. MV has a single membrane that is derived from endoplasmic reticulum (ER) and incorporates viral membrane proteins (8). Each MV particle consists of at least 80 viral proteins, of which 20 or more are involved in virus entry. These latter include four attachment proteins [H3 (9), D8 (10), A27 (11) and A26 (12)] and an entry fusion protein complex (EFC) of eleven components [G9 (13), A16 (14), A28 (15), F9



(16), L1 (17), L5 (18), H2 (19), G3 (20), J5 (21), O3 (22) and A21 (23)] that mediates fusion between host and viral membranes during virus entry (24-26). EV has one additional Golgi-derived membrane that contains at least six viral proteins—A34, A33, B5, F13, A56, A36—distinct from those of MV (27). When EV binds to cells, its outer membrane ruptures on the host plasma membrane, exposing the internal viral fusion complex that completes membrane fusion with host cells (28, 29). Therefore, the vaccinia viral EFC is required for both MV and EV to fuse to host cells (25, 30).

The 11 components of vaccinia virus EFC are known to be essential for virus-mediated membrane fusion, but few detailed studies have been conducted on their biochemical structures and functional relationships. Five components of the EFC (A21, A28, G3, H2 and O3) are type II transmembrane (TM) proteins, whereas another six (A16, G9, F9, L1, J5 and L5) are type I TM proteins. It is also known that in the absence of A28 protein, subcomplexes of G9&A16 and G3&L5 are detected (30). Super-resolution microscopy has revealed that EFC components are localized to the tips of MV particles, suggesting that their spatial orientation on the virion may affect viral fusion activity (31). It is conceivable that viral EFC activity must be tightly regulated such that viral particles do not lose infectivity due to spontaneous fusion activation.

Although the viral EFC is required for membrane fusion of MV and EV with host cells, previous studies have identified two sets of viral fusion regulatory proteins that can curtail membrane fusion i.e., A26 and the A56/K2 protein complex. These regulatory proteins use an acid-sensitivity mechanism to inhibit the EFC-mediated fusion activity of MV and EV (32-34). A26 is an MV-specific protein that binds individually to the G9 and A16 proteins of the EFC at neutral PH to inhibit EFC fusion activity (32, 35). Only when MV is endocytosed in the cytoplasm, can the acidic environment of endosomes trigger a conformational change in A26 protein to induce EFC fusion activation and then, following viral membrane fusion with the endosome, viral cores are released into the cytoplasm. A previous study showed that WRΔA26-MV particles mimic EV particles to directly



trigger plasma membrane and viral membrane fusion without requiring the acidic environment of endosomes (36). This finding also suggests that A26 protein is an MV-mediated fusion inhibitor. Unlike A26 protein, the A56/K2 protein complex is expressed on cell membrane surfaces at the early stage of viral infection to inhibit EV-mediated fusion, in a process termed “superinfection interference” (33, 37-42). Overexpression of A56/K2 on cell surfaces can inhibit entry of both MV and EV into cells (43). Deletion of the A56R or K2L open reading frames (ORF) from the viral genome caused cell-cell fusion of infected cells (39, 42, 44). Coimmunoprecipitation (co-IP) experiments have also revealed that the A56/K2 protein complex on cell surfaces is associated with the G9/A16 components of the EFC (45, 46). Thus, both A26 protein and the A56/K2 protein complex inhibit EFC-mediated membrane fusion by binding to the G9/A16 subunits.

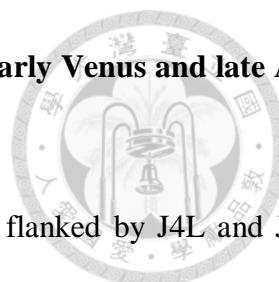
In order to understand how the A56/K2 protein complex inhibits the viral EFC, I employed an experimental evolution strategy to continuously passage vaccinia virus in the presence of A56/K2 to identify adaptive mutant viruses that overcome A56/K2-mediated fusion inhibition. Subsequent viral genome sequencing of these adaptive mutant viruses revealed the mutations and underlying mechanism allowing these mutant viruses to evade A56/K2-mediated fusion inhibition.

## Materials and Methods



### Cell culture, reagents and viruses.

BSC40 cells were cultured in Dulbecco's modified Eagle's medium (DMEM) plus 10% calf serum (CS). CV-1, HeLa and other HeLa-derived cell clones, as well as 293T cells, were cultured in DMEM plus 10% fetal bovine serum (FBS, Invitrogen). The pLKO AS3w.neo, pLKO AS3w.puro, pLKO AS3.1 EGFP3', pLKO AS3.1w tRFP-C, pCMV-ΔR8.91 and pMD.G lentiviral vectors were obtained from the National RNAi Core (Academia Sinica, Taiwan). The pMyc-G9R, pHA-A16L, pA56R-GFP and pK2L-Flag plasmids were described previously (35). A28L was constructed in pLKO AS3w.puro vector, and the A28L P79Q mutant plasmid was generated using *in vitro* mutagenesis. The pMyc-G9R His44Tyr mutant plasmid was also generated using *in vitro* mutagenesis (QuickChange Lightning site-directed mutagenesis kit; Agilent Technologies Inc.). The wild-type Western Reserve (WR) strain of vaccinia virus, the A26L deletion virus (WR-ΔA26), as well as WRΔA26-A4mCherry, WRΔB5 and VTF7-3 (ATCC® VR-2153™), were all propagated in BSC40 cells, and virus titers were determined by plaque assays as described previously (32, 35, 47). Generation of HeLa cells expressing GFP or RFP was as described previously (32, 36). Anti-H3 (9), anti-D8 (10), anti-G3 (20), anti-A4 (48), anti-L1 (35), anti-G9 (35), anti-L5 (35) and anti-A16 antibodies (35) were all described previously. Anti-A56 monoclonal antibody (mAb) was provided by Yasuo Ichihashi (44, 49). Anti-K2 mAb was provided by Richard W. Moyer (50). Anti-Flag mAb was purchased from Sigma Inc. Anti-GFP antibody was purchased from Bioscience Inc. Anti-A28, anti-H2, anti-F9 and anti-O3 are rabbit antibodies raised, respectively, against the following four synthetic peptides: A28(92-112): N'-QAEVGPNNTRSIRKFNTMQQC-C'; H2(81-102): N'-KLESDRGRLLAAGKDDIFEFKC-C'; F9(80-107): KDRRAIAEEIGIDLDDVPSAVSKLEKNC-C'; and O3(14-35): N'-CSWLSYSYLRPYISTKELNKSRC'.



### **Construction of a fluorescent recombinant vaccinia virus expressing early Venus and late A4-mCherry protein (WRΔA26-Venus-A4mCherry).**

Viral genomic DNA containing an early Venus expression cassette flanked by J4L and J5R sequences was obtained from Dr. John H. Connor (51, 52) and used as the template to obtain a PCR fragment that was subsequently cloned into a Topo plasmid, resulting in pTopo-J4R-Venus-J5L, in which Venus is expressed from a viral early promoter of the C11R gene (51). The plasmid was sequenced to ensure accuracy and subsequently transfected into CV1 cells that had been infected with WRΔA26-A4mCherry (47). The lysates were harvested at 24 hours post-infection (hpi) and virus titration was performed on BSC40 cells to isolate WRΔA26-Venus-A4mCherry virus through multiple rounds of plaque purification under fluorescence microscopy until 100% purity.

### **Construction of a stable cell line expressing A56 and K2 protein complex.**

Vaccinia A56R and K2L genes were synthesized using codons optimized for mammalian expression (GenScript Inc.). Vaccinia A56R and K2L ORFs were inserted into the vectors pLKO AS3w.neo and pLKO AS3w.puro and subsequently packaged into lentiviral vectors (provided by the RNAi Core, Academia Sinica, Taiwan). HeLa cells were infected with lentiviral vectors expressing A56 and cultured in medium containing G418 (1 mg/ml) for 2 weeks. These A56-expressing HeLa cells were subsequently infected with lentivirus expressing K2 and selected in medium containing puromycin (1 µg/ml) for 1 week. The resulting cell clones were assessed for A56 and K2 protein expression using anti-A56 and anti-K2 mAbs, respectively, by fluorescence-activated cell sorting (FACS) and immunofluorescence under confocal microscopy, as described previously (47). HeLa-A56/K2 cells expressing GFP or RFP were subsequently generated using FACS as described previously (32, 36). In brief, HeLa-A56/K2 cells were infected with lentiviral vectors expressing GFP or RFP (RNAi Core, Academia Sinica, Taiwan) and selected for GFP-positive or RFP-positive cells by FACS analyses.

## **Construction of a fluorescent recombinant vaccinia virus expressing late A4-mCherry protein, WRΔB5-A4-mCherry.**

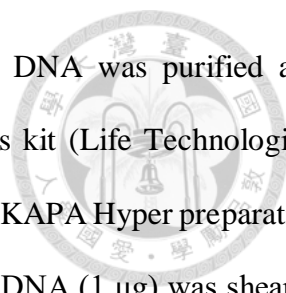
The CV-1 cells were transfected with linear A4-mCherry plasmid and infected with WRΔB5 virus. Cell lysate was harvested at 24 hpi and m-Cherry-positive virus was sorted by FACS. Virus titration was then performed on BSC40 cells to isolate WRΔB5-A4-mCherry virus through multiple rounds of plaque purification under fluorescence microscopy until 100% purity.

## **Experimental passaging of WRΔA26, WR and WRΔB5 viruses on HeLa and HeLa-A56/K2 cells for adaptive mutant virus selection.**

HeLa-A56/K2 cells ( $10^6$  cells /100 mm) were infected with WRΔA26, WR or WRΔB5 virus at a multiplicity of infection (MOI) of 0.02, 0.1 or 0.1 plaque-forming units (PFU) per cell and cultured for 2-3 days until infection had completed. The cells were harvested, denoted as the P1 pools of WRΔA26<sup>HeLa-A56/K2</sup>, WR<sup>HeLa-A56/K2</sup> or WRΔB5<sup>HeLa-A56/K2</sup>, respectively, and then used to infect fresh HeLa-A56-K2 cells to obtain the P2 pool. This process was repeated 10 times to obtain a total of 10 virus pools, denoted P1 to P10 of WRΔA26<sup>HeLa-A56/K2</sup>, WR<sup>HeLa-A56/K2</sup> or WRΔB5<sup>HeLa-A56/K2</sup>, respectively. We then continued with 10 more passages at an MOI of 0.002 or 0.01 PFU per cell of WRΔA26 to obtain the P11 to P20 pools. As a control, HeLa cells were infected and passaged with WRΔA26 as described above to obtain 20 virus pools, denoted P1-P20 of WRΔA26<sup>HeLa</sup>. To observe the plaque phenotypes of these passaged viruses, the P1 to P20 virus pools of WRΔA26<sup>HeLa-A56/K2</sup> and WRΔA26<sup>HeLa</sup> or WR<sup>HeLa-A56/K2</sup> and WR<sup>HeLa</sup> were simultaneously titrated on HeLa and HeLa-A56/K2 cells to determine plaque numbers and size at 3 days post-infection (dpi) after 1% crystal violet staining. The P1 to P20 virus pools of WRΔB5<sup>HeLa</sup> and WRΔB5<sup>HeLa-A56/K2</sup> were infected with HeLa and HeLa-A56/K2 cells with an MOI=0.1 per cell to detect viral late m-Cherry expression at 8 hpi.

## **Viral genome sequencing and data analyses.**

Vaccinia viral genomic DNA isolation, sequencing and data analyses were performed as



previously described with minor modifications (36). All viral genomic DNA was purified and quantified using a Qubit 3.0 fluorometer and a Qubit ds DNA BR assays kit (Life Technologies, Carlsbad, USA). Whole genome sequencing libraries were prepared using a KAPA Hyper preparation kit (Roche, KAPA Biosystems) protocol for Illumina Platforms. Genomic DNA (1 µg) was sheared to an average length of 350 base pairs (bp) using an M220 focused ultrasonicator (Covaris). For each library, 100 ng fragmented DNA was end-repaired and 3'-adenylated using a proprietary master mix before being ligated to the barcoded adapter from an Illumina index kit (Illumina Inc., San Diego, CA, USA). The adaptor-ligated DNA was enriched using a KAPA Hyper Library Preparation kit with nine cycles of PCR, and then purified using KAPA Pure Beads (Roche, KAPA Biosystems). The quality and size distribution of the libraries was verified on an Agilent 2100 Bioanalyzer using an Agilent DNA High Sensitivity kit. Concentrations of the libraries were determined using a Kapa Library Quantification Kit (Roche, KAPA Biosystems). Libraries were sequenced using NextSeq Paired-end (PE) 150-cycles version 2.5 reagents on an Illumina NextSeq 500 system (Illumina, Inc., USA) at the Genomics Core facility of the Institute of Molecular Biology, Academia Sinica (Taiwan). To obtain 150 bp paired-end reads, base-calling was conducted using bcl2fastq (version 2.17.1.14) conversion software and BCL files were converted to FASTQ format.

The resulting sequence data were uploaded to CLC Genomics Workbench 11.0.1 (Qiagen, Aarhus, Denmark) for raw sequence trimming, sequence mapping, and variant detection. Raw sequencing reads were trimmed by removing adapter sequences, low-quality sequences (Phred quality score <Q30) and sequencing fragments of shorter than 30 nucleotides. Sequencing reads were mapped to the human genome (GRCh38, from [ftp.ensembl.org/pub/release-82/fasta/homo\\_sapiens/dna/](ftp.ensembl.org/pub/release-82/fasta/homo_sapiens/dna/)) with stringent parameters (mismatches cost = 2, insertion cost = 3, deletion cost = 3, minimum fraction length = 0.9, minimum fraction similarity = 0.9). All host genome sequences that met the above parameters were removed, before mapping the remaining paired-end reads to the vaccinia virus WR genome (GenBank NC\_006998) (53). We removed duplicate reads

and performed a local realignment, and then used the Basic Variant Detection tool in CLC Genomics Workbench 11.0.1 to call single nucleotide polymorphisms (SNPs) and insertions/deletions (InDels) with the following customized parameters to identify mutation positions: (1) minimum frequency = 1% and minimum coverage = 10 reads; and (2) minimum quality of SNPs/InDels >Q25 and the neighborhood quality (upstream/downstream five bases) >Q20.

We also used the paired-end reads, after removing host genome sequences, to generate mutant and revertant viral genomes by *de novo* genome assembly but excluding the terminal repeat sequences of vaccinia virus. Using the alignment program MAFFT version 7 (54, 55), we aligned our parental WRΔA26 strain, P5 pool, P7 pool, P10 pool and P20 pool viral genome sequences with the reference WR strain (GenBank NC\_006998) to identify differences among viruses.

#### **Generation of G9<sup>H44Y</sup> recombinant virus of WRΔA26, WR and WRΔB5 vaccinia viruses.**

A *G8R-GFP-G9R* cassette containing the p11k-driven G9R ORF, the p7.5K-driven GFP gene and 500 bp of the G8R sequence at the 3' end was cloned into pBluescript plasmid using the NEBuilder® HiFi DNA Assembly Cloning Kit to obtain pBluescript-*G8R-GFP-G9R* plasmid. We then generated G9R His44Tyr mutant plasmid using *in vitro* mutagenesis (QuickChange Lightning site-directed mutagenesis kit; Agilent Technologies Inc.). To generate recombinant WRΔA26-G9<sup>H44Y</sup>, WRΔA26-G9-Rev, WR-G9<sup>H44Y</sup> and WR-G9-Rev viruses, we infected CV-1 cells with WRΔA26, WR or WRΔB5 at an MOI of 5 PFU per cell. The CV-1 cells were subsequently transfected with pBluescript-*G8R-GFP-G9R* plasmid and pBluescript-*G8R-GFP-G9RH44Y* plasmid and cultured for 3 days before cell harvesting for the next round of infection to enrich for GFP-positive cells using FACS. These GFP-positive cells were used to further purify GFP-positive recombinant virus plaques after five rounds of plaque purification.

#### **Growth analyses of the viruses in HeLa and HeLa-A56/K2 cells.**

HeLa cells (2x10<sup>5</sup>/well) and HeLa-A56/K2 cells (2x10<sup>5</sup>/well) in 6-well plates were infected with

each virus at an MOI of 0.02 PFU per cell, washed and incubated with growth medium at 37 °C, and the cells were then harvested at 0 and 24 hpi for virus titer determination. We determined virus growth by dividing virus titers at 24 hpi with the respective values at 0 hpi as previously described (36).

### **Vaccinia MV-triggered cell fusion from-without at neutral and acidic pH.**

Cell-cell fusion induced by vaccinia MV infections was performed as described previously (32, 36). In brief, HeLa-A56/K2 cells expressing GFP or RFP were mixed at a 1:1 ratio and seeded in 96-well plates. The next day, these cells were pretreated with 40 µg/ml cordycepin or 3'-deoxyadenosine (Sigma) for 60 min and subsequently infected with MV of WRΔA26, WRΔA26-G9<sup>H44Y</sup>, WRΔA26-G9-Rev, WR, WR-G9<sup>H44Y</sup>, WR-G9-Rev, or WR-G9<sup>H44Y</sup>+A28<sup>P79Q</sup> virus at an MOI of 100 PFU per cell. Cordycepin was present in culture media throughout the experiments to inhibit viral early gene expression. After infection at 37 °C for 60 min, cells were treated with PBS of various pH (pH 7.4, 6.5, 6, 5.5 or 4.7) at 37 °C for 3 min, washed with growth medium, further incubated at 37 °C for 1 h, and then photographed using a Zeiss Axiovert fluorescence microscope. Percentage cell fusion was quantified using MetaXpress software as the image area of GFP<sup>+</sup>RFP<sup>+</sup> double-fluorescent cells divided by that of single-fluorescent cells, as described previously (36). Experiments were repeated three times and statistical analyses were performed using Student's *t* tests in Prism (version 5) software (GraphPad). Statistical significance is represented as \*, *P* value <0.05, \*\* <0.01, and \*\*\* <0.001.

### **Vaccinia EV-triggered cell fusion from-within.**

HeLa or HeLa-A56/K2 cells expressing GFP or RFP were mixed at a 1:1 ratio and seeded in 60 mm plates. The next day, cells were infected with only 20-50 plaques of either WRΔA26, WRΔA26-G9<sup>H44Y</sup> or WRΔA26-G9-Rev. Resulting plaque formation was monitored from 1-2 dpi and individual plaques were photographed at 2 dpi using a Zeiss LSM710 fluorescence microscope. Although WRΔA26-G9<sup>H44Y</sup> and WRΔA26-G9-Rev harbor a GFP marker, its expression level was relatively



weak relative to the fluorescence intensities of HeLa-GFP and HeLa-A56/K2-GFP, so viral GFP was calibrated as the background value. Percentage cell fusion was quantified using MetaXpress software as the image area of GFP<sup>+</sup>RFP<sup>+</sup> double-fluorescent cells divided by that of single-fluorescent cells, as described previously (36). Experiments were repeated twice and statistical analysis was performed with a total of 14 plaques using Student's *t* tests in Prism (version 5) software (GraphPad). Statistical significance is represented as \*, *P* value <0.05, \*\* <0.01, and \*\*\* <0.001. Alternatively, we performed EV-mediated fusion assays using Giemsa solution (Merck Inc.) and monitored syncytia formation directly under light microscopy and found that the resulting data were consistent with the outcomes of fluorescence microscopy.

### **Coimmunoprecipitation and immunoblot analyses.**

Cell lysates used for coimmunoprecipitation (co-IP) were prepared from cells as previously described (35) under five different conditions: (1) 293T cells (8x10<sup>6</sup>/100 mm) were transfected with 3 µg pMyc-G9R and pHA-A16L using a calcium phosphate transfection protocol and harvested 24 h later; (2) 293T cells (8x10<sup>6</sup>/100 mm) were infected with VTF7-3 at an MOI of 5 PFU per cell before being transfected with 3 µg of pMyc-G9R, pHA-A16L, pA56R-GFP and pK2L-Flag using a calcium phosphate transfection protocol, and then harvested 24 h later; (3) 293T cells (8x10<sup>6</sup>/100 mm) were infected with WRΔA26, WRΔA26-G9<sup>H44Y</sup>, WRΔA26-G9-Rev viruses at an MOI of 5 PFU per cell and harvested 24 hpi; (4) 293T cells (8x10<sup>6</sup>/100 mm) were transfected with 3 µg pA26L-V5 and pA28L using a calcium phosphate transfection protocol and harvested 24 h later; and (5) 293T cells (8x10<sup>6</sup>/100 mm) were transfected with 3 µg pMyc-G9R and pA28L using a calcium phosphate transfection protocol and harvested 24 h later. Cells were then lysed in a lysis buffer consisting of 20 mM Tris-HCl (pH 8.0), 200 mM NaCl, 0.5% NP40, 1 mM EDTA, and protease inhibitor cocktail containing 2 µg/ml Aprotinin, 1 µg/ml Leupeptin, 0.7 µg/ml Pepstatin, and 1 mM PMSF. Lysates were cleared by low-speed centrifugation, incubated at 4 °C overnight with anti-Myc, anti-GFP

(1:100), anti-G9 (1:50) or anti-V5 antibody conjugated to agarose beads (Sigma) or protein A beads (GE Healthcare), washed four times with lysis buffer, and centrifuged. The immunoprecipitates were then resuspended in SDS-containing sample buffer, separated by SDS-PAGE, and analyzed by immunoblot analyses as described previously (35).

## *Results*



### **Chapter 1: To investigate EV-mediated entry fusion inhibition process in WRΔA26 through in vitro experimental evolution.**

#### **Expression of A56/K2 on HeLa cell surfaces inhibits WRΔA26 entry.**

I performed experimental evolution to select for and identify adaptive vaccinia mutant viruses that could overcome the fusion inhibition mediated by the A56/K2 complex. Previously, several labs have shown that stable expression of A56 and K2 in uninfected cells is sufficient to prevent virus entry and cell fusion (40, 43). Therefore, I used lentiviral vectors to introduce the mammalian codon-optimized A56 and K2 ORFs into HeLa cells. I established a stable cell line, named HeLa-A56/K2, expressing high levels of A56 and K2 proteins on cell surfaces, as detected by FACS (Figure 1A) and by immunofluorescence staining using anti-A56 and anti-K2 antibodies (Figure 1B). Next, I chose to infect cells with WRΔA26 virus, and not wild type WR virus, for two reasons. First, both A26 and A56/K2 bind to the G9/A16 subunits of the EFC, raising the possibility that A26 on wild type WR MV particles may interfere with binding of MV to A56/K2 protein complex on cell surfaces during experimental passaging. Second, purified EV particles specifically lack A26 protein (56), so by passaging WRΔA26 MV particles on HeLa-A56/K2 cells I could closely approximate “superinfection interference” of EV entry. I infected HeLa and HeLa-A56/K2 with MV of WRΔA26-Venus-A4-mCherry at an MOI of 0.1 PFU per cell and monitored expression of viral early Venus marker and late A4-mCherry genes by FACS at 2 hpi and 8 hpi, respectively (Figure 1C&D). Mean fluorescence intensity in HeLa cells was set as 100% to normalize the relative fluorescence intensity in HeLa-A56/K2 cells. The data revealed that viral early gene expression in HeLa-A56/K2 cells was reduced to 22% that of HeLa cells (Figure 1C), and viral late gene expression in HeLa-A56/K2 cells was 11% of that in HeLa cells (Figure 1D). Furthermore, plaques of WRΔA26 were smaller (<0.35 mm

diameter) and fewer (by 8-10-fold) on HeLa-A56/K2 cells than on HeLa cells (Figure 1E). Thus, expression of A56 and K2 proteins on HeLa-A56/K2 cells significantly inhibited WRΔA26 MV infection, as reported previously for A56/K2 inhibition of wild type WR MV (43).

**Adaptive mutants that have overcome A56/K2 inhibition gradually accumulate upon experimental passaging of WRΔA26 on HeLa-A56/K2 cells for 20 generations.**

I began passaging experiments by infecting HeLa-A56/K2 cells with WRΔA26 at an MOI of 0.02 PFU per cell, and then harvested cells at 3 dpi (Figure 2A). Lysates of the harvested cells were used as the P1 virus pool to initiate the next round of infection on HeLa-A56/K2 cells, with the resulting lysates being harvested as the P2 virus pool. This process was repeated 10 times to obtain a total of 10 virus pools, denoted P1 to P10 of WRΔA26<sup>HeLa-A56/K2</sup>. I continued with another 10 passages at an MOI of 0.002 PFU per cell to obtain viral pools P11 to P20. In general, the proportion of a given viral pool used as inoculum to generate the next pool was relatively small at ~0.1-0.01 %. As a control experiment, WRΔA26 was similarly passaged in parallel on HeLa cells to obtain 20 passaged virus pools, denoted P1 to P20 of WRΔA26<sup>HeLa</sup>. I anticipated that beneficial viral mutations to overcome A56/K2-mediated fusion suppression would be specifically selected for and accumulate in the virus pools of WRΔA26<sup>HeLa-A56/K2</sup>, and spontaneous non-adaptive mutations would be present in virus pools of WRΔA26<sup>HeLa</sup> following long-term virus passaging in control HeLa cells.

Next, I compared plaque size (Figure 2B&D) and titers (Figure 2C&E) of the P1, P5, P10 and P20 pools of WRΔA26<sup>HeLa-A56/K2</sup> and WRΔA26<sup>HeLa</sup> by plating on HeLa and HeLa-A56/K2 cells. I found that the P1 pool of WRΔA26<sup>HeLa-A56/K2</sup> grew well on HeLa but not on HeLa-A56/K2 cells, exhibiting small plaque sizes and low virus titers in these latter (Figure 2B&C). However, I observed gradual virus adaptation through subsequent passaging rounds on HeLa-A56/K2 cells so that by the 20<sup>th</sup> passaging event, the P20 pool of WRΔA26<sup>HeLa-A56/K2</sup> already exhibited large plaque size (Figure 2B) and a high virus titer (Figure 2C) on both HeLa-A56/K2 and HeLa cells. Accordingly, I

concluded that repeated passaging of WRΔA26 on HeLa-A56/K2 cells had specifically selected for variants in the P20 pool of WRΔA26<sup>HeLa-A56/K2</sup> that had overcome the fusion inhibition imposed by the cell surface A56/K2 protein complex. In control passaging experiment, the P1, P5, P10 and P20 pools of WRΔA26<sup>HeLa</sup> all formed large plaques (> 0.35 mm diameter) on HeLa cells and small plaques (< 0.35 mm diameter) on HeLa-A56/K2 cells (Figure 2D). Moreover, the titers of each of those pools of WRΔA26<sup>HeLa</sup> on HeLa cells were always ~8-fold greater than on HeLa-A56/K2 cells (Figure 2E), demonstrating that even after 20 passages on control HeLa cells, WRΔA26<sup>HeLa</sup> remained sensitive to A56/K2-mediated fusion inhibition.

### **Whole genome sequencing of virus pools reveals a specific G9<sup>H44Y</sup> mutation in WRΔA26**

I purified viral genomes from P5, P7, P10 and P20 of WRΔA26<sup>HeLa-A56/K2</sup>, as well as from the P10 and P20 pools of WRΔA26<sup>HeLa</sup>. Whole genome sequencing analyses were performed with a sequencing depth close to an average of 600 reads per base. Genome sequences were aligned with parental WRΔA26 sequences to identify genetic variations that arose during passaging on HeLa-A56/K2 and control HeLa cells. To avoid background fluctuation interfering with data interpretation, I filtered the dataset with a cut-off of 10% variation and identified one mutation of the D8L ORF (C525G) that presented a 13.5% mutation frequency in the P10 and a 93.9% mutation frequency in the P20 pools of WRΔA26<sup>HeLa</sup> (Figure 3A). That same mutation was observed in the P20 pool of WRΔA26<sup>HeLa-A56/K2</sup>, with a mutation frequency of 61.9%. Another unique mutation (C130T) was identified in the G9R ORF solely of WRΔA26<sup>HeLa-A56/K2</sup> virus pools (P7, P10 and P20), which resulted in the H44Y amino acid change of G9 protein (Figure 3A). Although H44 is conserved among G9 proteins of the Orthopoxvirus genus, the respective residue is Q in the parapoxvirus genus, F in Yokavirus, and R in Pteropoxvirus (Figure 3B). The G9<sup>H44Y</sup> mutation frequency increased from 49.2% in the P7 pool to 87% in the P10 pool, and then up to 99.8% in the P20 pool of WRΔA26<sup>HeLa-A56/K2</sup> (Figure 3C). Together, these data demonstrate that the G9<sup>H44Y</sup> genetic mutation is specifically

associated with phenotypic adaptation of WRΔA26<sup>HeLa-A56/K2</sup> virus pools, allowing them to overcome inhibition by the viral A56 and K2 suppressors. Since the C525G mutation of the D8L ORF occurred in pools of both WRΔA26<sup>HeLa</sup> and WRΔA26<sup>HeLa-A56/K2</sup>, I assume that it has little relevance for the adaptation allowing WRΔA26<sup>HeLa-A56/K2</sup> to overcome A56/K2 inhibition.

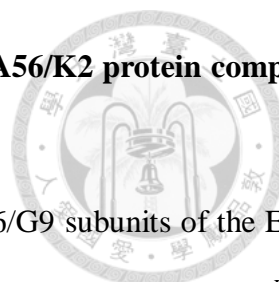
### **Recombinant WRΔA26-G9<sup>H44Y</sup> virus overcomes MV and EV entry inhibition on HeLa-A56/K2 cells**

To verify that the H44Y mutation of G9 protein could overcome A56/K2-mediated fusion inhibition, I generated a recombinant WRΔA26-G9<sup>H44Y</sup> virus that expresses the G9<sup>H44Y</sup> mutant protein as well as a GFP protein to facilitate isolation of virus clones (Figure 4A). I also generated a revertant vaccinia virus, WRΔA26-G9-Rev, expressing a wild type G9R protein and a GFP marker as a control (Figure 4A). Immunoblot analyses of infected cells demonstrated that both WRΔA26-G9<sup>H44Y</sup> and WRΔA26-G9-Rev expressed G9 protein of the same size to that in parental WRΔA26-WT virus (Figure 4B). To ensure that WRΔA26-G9<sup>H44Y</sup> had not reverted back to wild type G9R during the isolation process, I purified the viral genomes from virus stocks, amplified the G9R ORF by PCR, and sequenced the resulting DNA fragments to reconfirm clonal accuracy (data not shown). Next, I infected HeLa and HeLa-A56/K2 cells with MV of WRΔA26-WT, WRΔA26-G9<sup>H44Y</sup> and WRΔA26-G9-Rev at a low MOI of 0.02 and harvested cells at 24 hpi to determine MV titers (Figure 4C). All three viruses grew equally well on HeLa cells, but titers of WRΔA26-G9<sup>H44Y</sup> on HeLa-A56/K2 cells at 24 hpi were significantly higher than for WRΔA26-WT and WRΔA26-G9-Rev, suggesting that the G9<sup>H44Y</sup> mutation had overcome fusion inhibition by A56/K2 proteins (Figure 4C). To confirm that the increased viral yield was due to enhanced MV entry, I infected HeLa and HeLa-A56/K2 cells with ~200 PFU of each virus at 37 °C for 60 min, washed off any unbound virus, added an agar overlay, and then counted plaque number on both cell types at 3 dpi. I divided the number of plaques on HeLa-A56-K2 cells by the respective number on HeLa cells to normalize virus entry

efficiency into HeLa-A56/K2 cells. As shown in Figure 4D, WRΔA26-WT and WRΔA26-G9-Rev formed fewer plaques on HeLa-A56/K2 cells than on HeLa cells, whereas I observed equivalent numbers of WRΔA26-G9<sup>H44Y</sup> plaques on both cell types, supporting that the G9<sup>H44Y</sup> mutation had enhanced virus entry into HeLa-A56/K2 cells.

The viral EFC is also important for facilitating EV-cell fusion during cell-to-cell spreading (57), so I anticipated that WRΔA26-G9<sup>H44Y</sup> should also enhance EV spreading on HeLa-A56/K2 cells. Therefore, I measured plaque sizes formed by WRΔA26-WT, WRΔA26-G9<sup>H44Y</sup> and WRΔA26-G9-Rev on HeLa and HeLa-A56/K2 cells at 3 dpi. As shown in Figure 4E, although all three viruses formed large plaques on HeLa cells, only WRΔA26-G9<sup>H44Y</sup> formed mid-to-large-sized plaques on HeLa-A56/K2 cells, whereas WRΔA26-WT and WRΔA26-G9-Rev formed tiny plaques on HeLa-A56/K2 cells (Figure 4E, quantification in Figure 4F). Taken together, these results show that H44Y mutation of G9 protein is sufficient to improve vaccinia MV entry as well as EV spreading in otherwise resistant HeLa-A56/K2 cells.

Vaccinia A56 and K2 protein on infected cell surfaces function to prevent EV progeny back-fusion (41, 43, 58), but A56R or K2L knockout results in a cell fusion phenotype upon EV spreading in viral plaques (39). I wanted to investigate if the G9<sup>H44Y</sup> mutation overcomes A56/K2-mediated inhibition of fusion by EV. GFP- and RFP-expressing HeLa and HeLa-A56/K2 cells were mixed at a 1:1 ratio and subsequently infected with WRΔA26-WT, WRΔA26-G9<sup>H44Y</sup> or WRΔA26-G9-Rev and we monitored development of plaque morphology with a cell fusion phenotype at 1-2 dpi. As shown in Figure 5A, WRΔA26-WT and WRΔA26-G9-Rev produced plaques lacking a cell fusion phenotype on both HeLa and HeLa-A56/K2 cells. In contrast, WRΔA26-G9<sup>H44Y</sup> developed plaques with a robust cell fusion phenotype on HeLa cells. It also produced plaques with a cell fusion phenotype on HeLa-A56/K2 cells, though the extent of cell fusion was less obvious. Imaging quantification of cell fusion within 14 plaques of each virus confirmed that viral EFC harboring the G9<sup>H44Y</sup> mutation was less inhibited by the A56/K2 protein complex (Figure 5B).



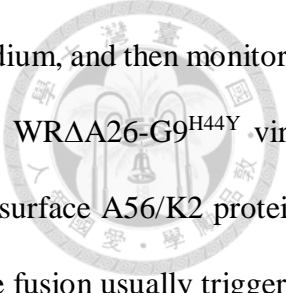
## **H44Y mutation of G9 protein does not alter its ability to bind to the A56/K2 protein complex or other EFC components**

Since it had previously been proposed that A56/K2 directly bind A16/G9 subunits of the EFC to regulate the fusion activity of the EFC (43, 46, 58), I used co-IP to investigate if the G9<sup>H44Y</sup> mutation alters the ability of G9 to bind to A16 or the A56/K2 protein complex. First, I co-transfected plasmids expressing A16 with wild type G9 or the G9<sup>H44Y</sup> mutant into 293T cells and our co-IP showed that both wild type and mutant G9<sup>H44Y</sup> pulled down A16 protein equally well (Figure 6A). Next, I assessed if the G9<sup>H44Y</sup> mutation affects interactions between G9/A16 and the A56/K2 protein complex. Wild type G9 or G9<sup>H44Y</sup> mutant plasmids were co-transfected with three plasmid types expressing A16, A56 and K2 proteins into cells that had been infected with VTF7-3 to induce high-level gene expression (Figure 6B). Co-IP of A56 brought down K2, A16 and wild type G9 protein. Substitution of wild type G9 plasmid with G9<sup>H44Y</sup> mutant plasmid did not alter these co-IP results (Figure 6B). I then performed reciprocal co-IP using myc antibody to pull down wild type G9 or G9<sup>H44Y</sup> mutant protein. Both wild type and mutant G9 proteins brought down A16, A56 and K2 equally well (Figure 6C). Finally, I investigated if the G9<sup>H44Y</sup> mutation affects EFC formation, but my co-IP results revealed little difference between wild type G9 and G9<sup>H44Y</sup> mutant protein in terms of binding to EFC subunits (Figure 6D).

## **WRΔA26-G9<sup>H44Y</sup> mutant virus has altered pH sensitivity to acid-induced membrane fusion in HeLa-A56/K2 cells**

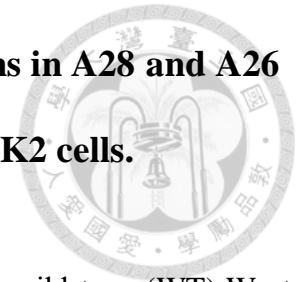
Although co-IP assays revealed that both wild type G9 and mutant G9<sup>H44Y</sup> protein bound to A56/K2 equally well at neutral pH, I could not exclude the possibility that they exhibit differential responses during the acid-dependent fusion activation process. To explore if the WRΔA26-G9<sup>H44Y</sup> mutant virus exhibits any change in acid sensitivity, I infected HeLa-A56/K2 cells with MV of WRΔA26-WT, WRΔA26-G9<sup>H44Y</sup> and WRΔA26-G9-Rev for 1 h so that the incoming viruses could bind to A56/K2 on cell surfaces. I then treated these MV-bound cells briefly with a range of pH





buffers (pH 7.4, 6.5, 6.0, 5.5 or 4.7), washed the cells again with growth medium, and then monitored cell-cell fusion 1-2 h later (Figure 7A). Using this strategy, I found that WRΔA26-G9<sup>H44Y</sup> virus triggered a low level of cell-cell fusion at neutral pH, suggesting that cell surface A56/K2 proteins efficiently bound WRΔA26-G9<sup>H44Y</sup> and inhibited the subsequent membrane fusion usually triggered by vaccinia viruses. When infected HeLa-A56/K2 cells were treated with low pH buffers, both WRΔA26-WT and WRΔA26-Rev only triggered cell-cell fusion at the lowest pH of 4.7. In contrast, cells infected with WRΔA26-G9<sup>H44Y</sup> mutant virus triggered robust cell fusion at pH 6.0, 5.5 and 4.7, as quantified in Figure 7B. This higher pH threshold of membrane fusion activation by the WRΔA26-G9<sup>H44Y</sup> mutant suggests a reduced inhibitory effect of A56/K2 in terms of suppressing EFC-G9<sup>H44Y</sup> fusion activity. The data suggested a model in which H44Y mutation of G9 protein allows viral EFC to overcome a lower energy barrier prior to activation of membrane fusion (Figure 7C). We speculate that G9<sup>H44Y</sup> mutant protein may mimic an “intermediate structure” of wild type G9 protein upon acid treatment that facilitates viral EFC dissociation from the A56/K2 protein complex.

## **Chapter 2: WR-G9<sup>H44Y</sup> mutants require additional mutations in A28 and A26 genes in order to overcome growth inhibition on HeLa-A56/K2 cells.**



In chapter 1, I chose to infect cells with WR $\Delta$ A26 virus, and not the wild-type (WT) Western Reserve (WR) virus, for two reasons. First, both A26 and A56/K2 bind to the G9/A16 subunits of the EFC, raising the possibility that A26 on wild-type WR MV particles may interfere with the binding of MV to the A56/K2 protein complex on cell surfaces during experimental passaging. Second, purified EV particles specifically lack A26 protein (56), so by passaging WR $\Delta$ A26 MV particles on HeLa-A56/K2 cells, I could closely approximate superinfection interference (33, 37-42) of EV entry. My results showed that the G9<sup>H44Y</sup> single mutation is sufficient to overcome the entry fusion inhibition of EV mediated by surface expression of A56/K2. However, these results only provide a partial picture of the natural vaccinia virus life-cycle, which involves both MV- and EV-mediated membrane fusion for virus dissemination (Figure 8A). To differentiate MV- and EV-mediated entry in a natural VACV infection, here in Chapter 2, I repeated the experimental evolution analyses using two viruses, wild type WR and WR $\Delta$ B5 mutant virus, for continuous passaging on HeLa-A56/K2 cells. WR virus passaging involved both MV- and EV-mediated virus dissemination, whereas WR $\Delta$ B5 virus generated only MV during serial passaging events (Figure 8B).

### **All of the WR $\Delta$ A26, WR, and WR $\Delta$ B5 viruses overcame A56/K2 inhibition after 20 generations.**

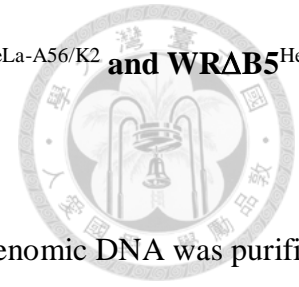
HeLa-A56/K2 cells were infected with either WR or WR $\Delta$ B5 at an MOI of 0.1 PFU per cell, harvested at 3 dpi, and saved as respective P1 virus pools, which were then used to initiate the next round of infection on HeLa-A56/K2 cells. The process was repeated for a total of 10 generations, and these virus stocks were denoted as the P1 to P10 stocks of WR<sup>HeLa-A56/K2</sup> and WR $\Delta$ B5<sup>HeLa-A56/K2</sup>, respectively. Next, I continued with another 10 passages at an MOI of 0.01 PFU per cell to obtain viral pools from P11 to P20. In general, the proportion of a given viral pool used as inoculum to generate the next pool was relatively small at ~0.1-0.01 %. As control experiments, WR and WR $\Delta$ B5

virus were similarly passaged in parallel on HeLa cells to obtain 20 passaged virus pools, denoted P1 to P20 of WR<sup>HeLa</sup> and WRΔB5<sup>HeLa</sup>.

First, I analyzed WR passaging experiment results by comparing plaque size and titers of the P1, P5, P10 and P20 pools of WR<sup>HeLa-A56/K2</sup> and WR<sup>HeLa</sup> on HeLa and HeLa-A56/K2 cells (Figure 9). I found that the P1 pool of WR<sup>HeLa-A56/K2</sup> grew well on HeLa but not on HeLa-A56/K2 cells (Figure 9A), exhibiting small plaque sizes and low virus titers in these latter cells (Figure 9B). However, I observed gradual virus adaptation through subsequent passaging rounds on HeLa-A56/K2 cells so that by the 20<sup>th</sup> passaging event, the P20 pool of WR<sup>HeLa-A56/K2</sup> already exhibited large plaque size (Figure 9A) and a high virus titer (Figure 9B) on HeLa-A56/K2 cells, i.e., similar to HeLa cells. Accordingly, I concluded that repeated passaging of WR on HeLa-A56/K2 cells had specifically selected for variants in the P20 pool of WR<sup>HeLa-A56/K2</sup> that had overcome the fusion inhibition imposed by the cell surface A56/K2 protein complex. In control passaging experiment, even after 20 passages on control HeLa cells, WR<sup>HeLa</sup> remained sensitive to A56/K2-mediated fusion inhibition (Figure 9C and D).

Since WRΔB5 formed tiny plaques that were difficult to detect, I inserted a fluorescent marker (mCherry) fused with a viral late gene (A4) into its genome and isolated the WRΔB5-A4-mCherry virus before performing similar passaging experiments as described above. As expected, initial infection of WRΔB5-A4mCherry virus on HeLa-A56/K2 cells resulted in 10-fold less mCherry expression than observed for control HeLa cells, evidencing robust A56/K2 inhibition of WRΔB5-A4mCherry infection (Figure 9E and F). Next, I passaged WRΔB5-A4mCherry virus 20 times and observed that mCherry expression levels gradually increased throughout the passaging process, suggesting that the WRΔB5-A4mCherry virus had adapted to grow in HeLa-A56/K2 cells (Figure 9E and F). On control HeLa cells, even after 20 passages, the mean fluorescence intensity of mCherry did not vary significantly (Figure 9G and H).

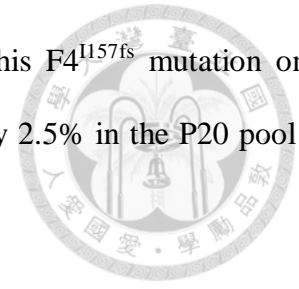
**An identical mutation of G9<sup>H44Y</sup> arises in the WR $\Delta$ A26<sup>HeLa-A56/K2</sup>, WR<sup>HeLa-A56/K2</sup> and WR $\Delta$ B5<sup>HeLa-A56/K2</sup> viruses.**



To identify genetic mutations that facilitate virus adaptation, viral genomic DNA was purified from the P0, P10, and P20 pools of WR<sup>HeLa-A56/K2</sup>, WR<sup>HeLa</sup>, WR $\Delta$ B5<sup>HeLa-A56/K2</sup> and WR $\Delta$ B5<sup>HeLa</sup>, respectively. Whole genome sequencing analyses were performed with a sequencing depth close to an average of 600 reads per base. Genome sequences were aligned with parental WR or WR $\Delta$ B5 sequences to identify genetic variations that arose during passaging on HeLa-A56/K2 and control HeLa cells. To avoid background fluctuation interfering with data interpretation, I also filtered the dataset with a cut-off of 10% variation, as described in Figure 3A. The raw data for whole genome sequencing without the 10% cut-off are included in Supplementary Table 1. In WR passaging experiments, I identified a common C293A mutation of the B4R ORF, which exhibited 37.9% and 11.9% mutation frequencies in the P20 pool of WR<sup>HeLa</sup> and WR<sup>HeLa-A56/K2</sup>, respectively (Figure 10A). In addition, I identified specific mutations in the G9R, A28 and A26 ORFs that were only present in the P10 and P20 pools of WR<sup>HeLa-A56/K2</sup>, but not in WR<sup>HeLa</sup> virus pools. The G9R<sup>C130T</sup> mutation resulted in a H44Y amino acid change to G9 protein, with a frequency of 95.4% in the P10 pool and of 99.9% in the P20 pool of WR<sup>HeLa-A56/K2</sup> (Figure 10A). The A28L<sup>C236A</sup> mutation resulted in a P79Q amino acid change to A28 protein, with a frequency of 63.8% in the P10 pool and of 30.9% in the P20 pool of WR<sup>HeLa-A56/K2</sup> (Figure 10A). Finally, multiple InDel mutations of the A26L ORF were identified, all of which resulted in various truncations of A26 protein. The combined frequency of these various InDels was 55.8% in the P20 pool of WR<sup>HeLa-A56/K2</sup> (Figure 10A).

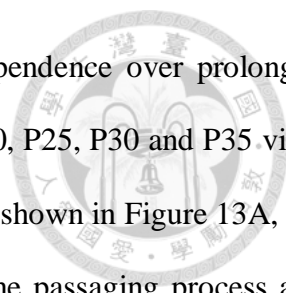
In WR $\Delta$ B5 passaging experiments, I identified two ORFs, G9R and F4L, each containing a single mutation in the WR $\Delta$ B5<sup>HeLa-A56/K2</sup> virus pools but not in control WR $\Delta$ B5<sup>HeLa</sup> virus pools. The G9R<sup>C130T</sup> mutation, which resulted in the H44Y amino acid change of G9 protein, had a frequency of 95.6% in the P10 pool and of 99.9% in the P20 pool of WR $\Delta$ B5<sup>HeLa-A56/K2</sup> (Figure 10B). A F4L<sup>468 $\Delta$ T</sup>

mutation resulted in a frame-shift of F4 protein at residue I157, but this F4<sup>I157fs</sup> mutation only appeared transiently, with a frequency of 35.3% in the P10 pool and only 2.5% in the P20 pool of WRΔB5<sup>HeLa-A56/K2</sup> (Figure 10B and Supplemental Table 1).



When I compared the mutations in the P20 pools of WR<sup>HeLa-A56/K2</sup> and WRΔB5<sup>HeLa-A56/K2</sup> with those of WRΔA26<sup>HeLa-A56/K2</sup>, only the G9<sup>H44Y</sup> mutation existed in all three passaging experiments (Figure 11A), reaching close to 100% with similar kinetics (Figure 11B). In Chapter 1, I have already demonstrated that the G9<sup>H44Y</sup> mutation enhanced virus infectivity on HeLa-A56/K2 cells because it promotes membrane fusion with a lower energy barrier in WRΔA26<sup>HeLa-A56/K2</sup>, so it is conceivable that the G9<sup>H44Y</sup> mutation exerts the same function during passaging of WR and WRΔB5 on HeLa-A56/K2 cells. To provide direct evidence of this possibility, I generated WR-G9<sup>H44Y</sup> and WRΔB5-G9<sup>H44Y</sup> recombinant viruses and tested their enhanced ability to grow in HeLa-A56/K2 cells, i.e., similar to WRΔA26-G9<sup>H44Y</sup> (Figure 12). As a control, I also generated two revertant viruses, WR-G9-Rev and WRΔB5-G9-Rev, that expressed wild type G9 protein (Figure 12A and D). As anticipated, both the WR-G9<sup>H44Y</sup> and WRΔB5-G9<sup>H44Y</sup> recombinant viruses formed more plaques (Figure 12B and E) and grew to higher titers (Figure 12C and F) than wild type and revertant viruses on HeLa-A56/K2 cells, respectively. These data show that G9<sup>H44Y</sup> indeed is an important adaptive mutation that plays a critical role for all three viruses to bypass A56/K2 protein entry inhibition.

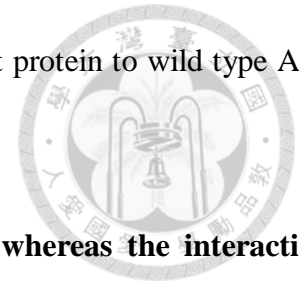
Unlike the G9<sup>H44Y</sup> mutation, which was common to the P20 pools of all three viruses, the A28<sup>P79Q</sup> mutation and the multiple A26 InDel mutations were only detected in the P20 pool of WR<sup>HeLa-A56/K2</sup> virus, but not in WRΔA26<sup>HeLa-A56/K2</sup> or WR-ΔB5<sup>HeLa-A56/K2</sup>. Interestingly, the frequency of A28<sup>P79Q</sup> in the P10 pool (63.8%) was reduced to 30.9% in the P20 pool in which the sum of A26<sup>InDel</sup> increased to 55.8%, implying that A26 mutations impose a negative effect on the A28<sup>P79Q</sup> mutation. This is a puzzling observation since, to my knowledge, no studies have reported functional interplay between A26 and A28 proteins. Therefore, I decided to continue passaging the P20 pool of WR<sup>HeLa-</sup>



A56/K2 to P35 in order to observe if these two mutations exhibit interdependence over prolonged passaging. I then sequenced the virus genomes purified from the P1 to P10, P25, P30 and P35 virus pools and analyzed mutation frequencies using 1% as the cut-off value. As shown in Figure 13A, the G9<sup>H44Y</sup> mutation increased steadily from the P5 virus pool throughout the passaging process and reached a frequency of 100% in the P20 pool. However, the A28<sup>P79Q</sup> mutation increased transiently from the P5 pool, peaked in the P10 pool at 63.8%, and then subsequently declined to 9.8% in the P35 pool. A combined A26<sup>InDel</sup> mutation frequency of 4.6% was detected in the P5 pool, which gradually increased to 77.6% in the P35 pool. This outcome indeed confirms that an inverse relationship exists between the A28<sup>P79Q</sup> and A26<sup>InDel</sup> mutations during WR<sup>HeLa-A56/K2</sup> passaging. To investigate if these mutations impact A28 and A26 proteins, I performed immunoblot analyses with cells infected with the P1, P5, P10, P20, and P35 pools of WR<sup>HeLa-A56/K2</sup>. Consistent with the multiple A26<sup>InDel</sup> mutations identified above, amounts of full-length A26 protein became significantly reduced (Figure 13B). In contrast, amounts of A28 protein were relatively consistent across the P1 to P35 pools, suggesting that the P79Q mutation did not alter A28 protein stability.

To further understand the mutational composition of WR<sup>HeLa-A56/K2</sup> virus pools, I randomly picked 10 virus clones from the P10 pool of WR<sup>HeLa-A56/K2</sup> virus and found that two of the virus clones contained a single G9<sup>H44Y</sup> mutation and eight of them harbored G9<sup>H44Y</sup> and A28<sup>P79Q</sup> double mutations. Next, to verify if A28<sup>P79Q</sup> and A26<sup>InDel</sup> mutations co-evolved at the clonal level, I chose one of the virus clones harboring the G9<sup>H44Y</sup> and A28<sup>P79Q</sup> double mutation (denoted WR-G9<sup>H44Y</sup>+A28<sup>P79Q</sup>) and performed 30 bouts of clonal passaging on both HeLa and HeLa-A56/K2 cells. Immunoblot analyses of lysates collected from the P1, P5, P10, P15, P20, P25 and P30 pools of this virus clone revealed a significant decrease in full-length A26 protein (Figure 13C). Most importantly, genome sequencing analyses of these clonal passages confirmed that frequency of the A28<sup>P79Q</sup> mutation gradually diminished from P1 to P30 (data analyses in progress). Taken together, these data reveal that, for virus adaptation to occur, the G9<sup>H44Y</sup> and A28<sup>P79Q</sup> mutations precede A26 truncations, with these

latter in turn providing a selective advantage to revert the A28<sup>P79Q</sup> mutant protein to wild type A28 protein.



**A28 protein directly interacts with individual G9 or A26 protein, whereas the interaction between A28<sup>P79Q</sup> and G9<sup>H44Y</sup> mutant proteins is unstable.**

The above-described data reveals a co-evolutionary relationship between A26 and A28, so I tested if these two proteins interact with each other. Since it was established previously that A26 binds to G9 and A16 proteins (35), I wanted to define the relationships among A28, A26 and G9. First, I co-transfected plasmids expressing A26 with wild type A28 and a co-IP experiment showed that A26 protein indeed interacted with A28 protein in the transfected cells (Figure 14A). I then co-transfected the A28-expressing plasmid with other constructs expressing various truncation forms of A26 protein to determine which region of A26 protein is important for the interaction with A28. The results show that the C-terminal region (aa 321-500) of A26 protein is sufficient for binding to A28 protein (Figure 14B). In fact, the C-terminal region of A26 protein appeared to interact with A28 better than did full-length A26 protein and, interestingly, this C-terminal region is absent from all of the A26<sup>InDel</sup> mutations described above (Figure 10A), implying existence of selection pressure to dissociate the A26 and A28 protein interaction during WR-virus passaging on A56/K2 cells.

Next, I tested if the A28<sup>P79Q</sup> mutation affects the interaction of A28 with A26 protein. CoIP experiments showed that both wild type and A28<sup>P79Q</sup> mutant protein bound equally well to full-length as well as various truncated forms of A26 protein (Figure 14B), demonstrating that the P79Q mutation does not affect the interaction of A28 with A26 protein. I further tested if the A28<sup>P79Q</sup> mutation affects its interaction with G9 protein. Respective co-IP data showed that wild type A28 and A28<sup>P79Q</sup> mutant protein bound equivalently to wild type G9. Similarly, wild type G9 and G9<sup>H44Y</sup> mutant bound equally well to wild type A28. However, binding between A28<sup>P79Q</sup> and G9<sup>H44Y</sup> mutant proteins seemed to be slightly reduced (Figure 14C).

Taken together, the passaging experiments revealed genetic interplay between G9, A28 and A26 proteins during WR virus selection against A56/K2-mediated fusion inhibition. Co-IP experiments also demonstrated that biochemical interactions exist among these three proteins. I also observed diminished interaction between A28<sup>P79Q</sup> and G9<sup>H44Y</sup> mutant proteins, implying that despite the P79Q mutation transiently appearing to be beneficial, it ultimately disappeared from the population, perhaps because it somehow has a negative effect on EFC function. The relationships between A28/A28<sup>P79Q</sup>, G9/G9<sup>H44Y</sup> and A26 protein warrant further experimental investigation.

**MV and EV membrane fusion ability of WR-G9<sup>H44Y</sup> and WR- G9<sup>H44Y</sup>+A28<sup>P79Q</sup> viruses are similar, suggesting that the G9 H44Y mutation alone is sufficient for both MV and EV host entry.**

Based on the outcomes of the experiments described in the previous section, I hypothesized that viral EFC containing both the G9<sup>H44Y</sup> and A28<sup>P79Q</sup> mutations should be more fusionogenic than that containing G9<sup>H44Y</sup> alone, and that A26<sup>InDel</sup> mutation could substitute for the effect of the A28<sup>P79Q</sup> mutation. Therefore, I compared the fusion ability of EV particles produced by the WR-G9<sup>H44Y</sup> and WR-G9<sup>H44Y</sup>+A28<sup>P79Q</sup> viruses in virus-infected cells (Figure 15A). GFP- and RFP-expressing HeLa and HeLa-A56/K2 cells were mixed at a 1:1 ratio and infected with WR-WT, WR-G9<sup>H44Y</sup>, WR-G9-Rev or WR-G9<sup>H44Y</sup>+A28<sup>P79Q</sup> virus at a M.O.I of 5 PFU per cell and cell-cell fusion was photographed at 20 hpi. As shown in Figure 15A, the control, WR-WT and WR-G9-Rev viruses did not trigger cell-cell fusion on HeLa or HeLa-A56/K2 cells. However, the WR-G9<sup>H44Y</sup> and WR-G9<sup>H44Y</sup>+A28<sup>P79Q</sup> viruses triggered a similar cell fusion phenotype on both HeLa and HeLa-A56/K2 cells, with little difference apparent between the two mutant viruses. I repeated these experiments three times and average outputs are shown in Figure 15B. Consequently, I concluded that the A28<sup>P79Q</sup> mutation does not render EV more fusionogenic.

Next, I compared the ability of MV particles produced by the WR-G9<sup>H44Y</sup> and WR-



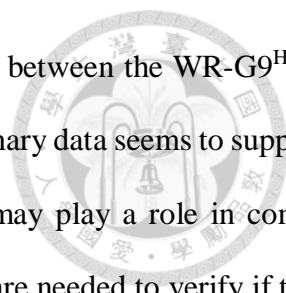
G9<sup>H44Y</sup>+A28<sup>P79Q</sup> viruses to trigger acid-dependent cell fusion. MV-bound HeLa-A56/K2 cells were briefly treated with a range of low pH buffers (pH 7.4, 6.5, 6.0, 5.5 or 4.7), washed, and then cell-cell fusion was monitored 1-2 h later (Figure 16A). A similar infection protocol was performed on HeLa cells (data shown in Supplementary Figure 2). The results clearly showed that both the WR-G9<sup>H44Y</sup> and WR-G9<sup>H44Y</sup>+A28<sup>P79Q</sup> viruses triggered acid-dependent fusion at pH4.7, whereas WR-WT and WR-G9-Rev did not (Figure 16A & B). These results indicate that the G9<sup>H44Y</sup> mutation can enhance EFC fusion activation at low pH, but the A28<sup>P79Q</sup> mutation does not.

When I further examined plaque phenotypes of the P1 to P35 pools of WR<sup>HeLa-A56/K2</sup> on both HeLa and HeLa-A56/K2 cells I noticed an increased number of comet-shaped formations surrounding the viral plaques, suggesting enhanced EV spread (Figure 17A). I then checked if the same comet phenotype is present in plaques formed by the WR-G9<sup>H44Y</sup> and WR-G9<sup>H44Y</sup>+A28<sup>P79Q</sup> viruses. Figure 17B indeed reveals that WR-G9<sup>H44Y</sup>+A28<sup>P79Q</sup> virus generates comet-shaped plaques, whereas plaques of WR-G9<sup>H44Y</sup> are more rounded. These results raise the interesting possibility that the A28<sup>P79Q</sup> mutation may enhance EV spread upon passaging in HeLa-A56/K2 cells (Figure 18). I plan to further quantify EV production by WR-G9<sup>H44Y</sup> and WR-G9<sup>H44Y</sup>+A28<sup>P79Q</sup> viruses to establish if the A28<sup>P79Q</sup> mutation facilitates EV spread during WR virus adaptation on HeLa-A56/K2 cells.

## Discussion

Vaccinia virus can infect cells either via endocytosis or plasma membrane fusion in a virus strain-dependent and cell type-dependent manner. I have established the strain-dependence and shown that A26 protein on MV particles dictates the acid-dependent fusion property of vaccinia MV particles. Thus, wild type MV fusion with the endosomal membrane is acid-dependent, whereas removal of A26 enables the MV of WRΔA26 to effect plasma membrane fusion into cells. In contrast, EV particles never incorporate A26 protein, so they can directly fuse with the plasma membrane of cells at neutral pH, exhibiting neither strain-dependence nor acid-dependence. Here, I used three different viruses to perform experimental evolutionary analyses to identify the adaptive mutations derived from either acid-dependent membrane fusion or plasma membrane fusion. I found that MV and EV virions produced from WRΔA26-infected cells use plasma membrane fusion for subsequent virus spread. However, MV progeny from WR virus harbor A26 so they adopt acid-dependent membrane fusion for virus spread. In contrast, EV produced by WR virus lack A26 protein so it can only use the plasma membrane fusion pathway. WRΔB5 virus is defective in EV formation, so it only spreads via MV that employs endocytic fusion for viral spread. It is significant that after 20 passages, all three viruses contained a common G9<sup>H44Y</sup> mutation, which seems to adopt an intermediate fusion conformation to allow viruses overcome the fusion barrier created by A56/K2 proteins. Supporting evidence of this scenario came from the MV-mediated and EV-mediated membrane fusion assays (described in Figure 5, 7, 15 and 16) in which the G9<sup>H44Y</sup> mutant protein always induced greater fusion activity than the wild type G9 protein.

However, it is puzzling why the A28<sup>P79Q</sup> mutation and multiple InDels of A26 protein were identified in the P20 virus pools of WR virus. The fact that the A28<sup>P79Q</sup> mutation preceded A26 OFR InDels implies a cause-and-effect relationship. Two immediate questions that arise are what is the role of the A28<sup>P79Q</sup> mutation in the adaptive mutation process and what is the driving force that reverts A28<sup>P79Q</sup> to wild type while enabling A26 truncation? I endeavored to answer the first of those



questions by comparing growth and fusion properties and EFC interaction between the WR-G9<sup>H44Y</sup> single mutant and WR-G9<sup>H44Y</sup>+A28<sup>P79Q</sup> double mutant viruses. My preliminary data seems to support that A28<sup>P79Q</sup> does not affect EFC fusion activity, unlike G9<sup>H44Y</sup>, but it may play a role in comet formation by EV and subsequent EV spread. Clearly, further experiments are needed to verify if this hypothesis is true. As yet, I have no definitive answer to the second question. However, given the relationship between the A28 and A26 mutations, I was prompted to investigate if their genetic interaction translates into a biochemical interaction. Indeed, my co-IP data shows that A28 binds to the C-terminal region of A26, which is lacking from the multiple A26 InDel mutants. One possibility is that the A28 and A26 proteins on MV play an opposing role in MV transport to Golgi for EV membrane wrapping, i.e., A28 facilitates EV wrapping whereas A26 inhibits MV to EV wrapping. Although a role for A28 in EV wrapping has not been reported previously, several studies have shown that A26 on MV targets the virus particles to inclusion bodies, thereby reducing EV trafficking/formation. Clearly, further experiments are required to clarify these issues.

The multi-subunit nature of the vaccinia virus EFC complicates efforts to understand how the virus executes membrane fusion during viral entry. X-ray crystallization approaches are useful for identifying novel structural features of viral fusion proteins but, thus far, only L1 (59) and F9 (60) proteins of vaccinia EFC have been crystallized and their structures do not share significant homology with the known viral fusion proteins. My results reveal that G9 plays an important role in the EFC for viral entry. Although G9<sup>H44Y</sup> mutant protein facilitates escape from A56/K2-mediated membrane fusion, my co-IP experiments did not reveal any biochemical differences contributed by the H44Y mutation since both wild type and G9<sup>H44Y</sup> mutant protein bound to A16, A56/K2 and other EFC components. Notably, vaccinia virus expresses three major forms of A56, i.e., proteins of 85 kD, 62 kD, and 58 kD (61-63), and a monoclonal antibody recognizing the 85 kD form was previously shown to inhibit vaccinia virus infection and syncytia formation (43, 44). Moreover, a vaccinia G9/A16 protein subcomplex was previously shown to bind to A56/K2 proteins in detergent-treated extracts,

though which form of A56 protein was brought down by G9 protein in those co-IP experiments was not clear (46). My co-IP experiments have revealed that both wild type and mutant G9 protein preferentially and consistently interacted with the two under-glycosylated forms of A56 protein (58 kD and 62 kD) instead of the fully glycosylated (85 kD) form (Figure 6B). How glycosylation of A56 protein influences its interaction with G9/A16 proteins is an interesting topic for future study.

Since WRΔA26-G9<sup>H44Y</sup> could trigger cell fusion at pH 6, I hypothesize that the G9<sup>H44Y</sup> mutant protein adopts an intermediate conformation more prone to acid-induced membrane fusion. Residue H44Y is located within the N-terminal region of G9 protein that was previously reported to play a role in fusion regulation since insertion of a small tag at the N-terminal region of G9 protein increased spontaneous fusion at neutral pH (13). Why the H44Y mutation was selected out of my experimental evolution assay to overcome A56/K2-mediated inhibition is currently unclear. It would be very informative to obtain the crystal structure of G9 protein in order to fully explain how the H44Y mutation modulates EFC fusion activity. Finally, G9 protein is known to interact with A16 protein in the EFC, but I did not select out any mutation of the A16 ORF during the 20 passages of my experimental evolution assay. Why this might be is not clear. The acid sensitivity of A56/K2 inhibition of membrane fusion by the EFC suggests that a biochemical regulatory mechanism operates that may involve acid-dependent conformational changes. That possibility requires further investigation.

The advantage of the experimental evolution approach I deployed here is that I could identify functionally important mutations, but it has the limitations of being time-consuming and necessitating narrow-spectrum selective pressure. In the future, other functionally important motifs or domains in subunits of the vaccinia EFC should be determined in order to further dissect the membrane fusion mechanism mediated by the poxviral EFC.

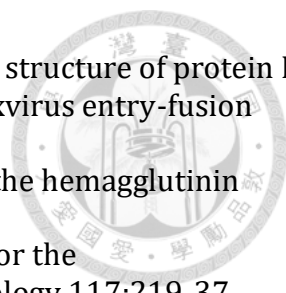
## References



1. Harrison SC. 2005. Mechanism of membrane fusion by viral envelope proteins. *Adv Virus Res* 64:231-61.
2. Harrison SC. 2008. Viral membrane fusion. *Nat Struct Mol Biol* 15:690-8.
3. Kielian M, Rey FA. 2006. Virus membrane-fusion proteins: more than one way to make a hairpin. *Nat Rev Microbiol* 4:67-76.
4. Kielian M. 2006. Class II virus membrane fusion proteins. *Virology* 344:38-47.
5. Backovic M, Jardetzky TS. 2011. Class III viral membrane fusion proteins. *Adv Exp Med Biol* 714:91-101.
6. Harrison JS, Higgins CD, O'Meara MJ, Koellhoffer JF, Kuhlman BA, Lai JR. 2013. Role of electrostatic repulsion in controlling pH-dependent conformational changes of viral fusion proteins. *Structure* 21:1085-96.
7. Condit RC, Moussatche N, Traktman P. 2006. In a nutshell: structure and assembly of the vaccinia virion. *Adv Virus Res* 66:31-124.
8. Weisberg AS, Maruri-Avidal L, Bisht H, Hansen BT, Schwartz CL, Fischer ER, Meng X, Xiang Y, Moss B. 2017. Enigmatic origin of the poxvirus membrane from the endoplasmic reticulum shown by 3D imaging of vaccinia virus assembly mutants. *Proc Natl Acad Sci U S A* 114:E11001-e11009.
9. Lin CL, Chung CS, Heine HG, Chang W. 2000. Vaccinia virus envelope H3L protein binds to cell surface heparan sulfate and is important for intracellular mature virion morphogenesis and virus infection in vitro and in vivo. *J Virol* 74:3353-65.
10. Hsiao JC, Chung CS, Chang W. 1999. Vaccinia virus envelope D8L protein binds to cell surface chondroitin sulfate and mediates the adsorption of intracellular mature virions to cells. *J Virol* 73:8750-61.
11. Chung CS, Hsiao JC, Chang YS, Chang W. 1998. A27L protein mediates vaccinia virus interaction with cell surface heparan sulfate. *J Virol* 72:1577-85.
12. Chiu WL, Lin CL, Yang MH, Tzou DL, Chang W. 2007. Vaccinia virus 4c (A26L) protein on intracellular mature virus binds to the extracellular cellular matrix laminin. *J Virol* 81:2149-57.
13. Ojeda S, Domi A, Moss B. 2006. Vaccinia virus G9 protein is an essential component of the poxvirus entry-fusion complex. *J Virol* 80:9822-30.
14. Ojeda S, Senkevich TG, Moss B. 2006. Entry of vaccinia virus and cell-cell fusion require a highly conserved cysteine-rich membrane protein encoded by the A16L gene. *J Virol* 80:51-61.
15. Senkevich TG, Ward BM, Moss B. 2004. Vaccinia virus A28L gene encodes an essential protein component of the virion membrane with intramolecular disulfide bonds formed by the viral cytoplasmic redox pathway. *J Virol* 78:2348-56.
16. Brown E, Senkevich TG, Moss B. 2006. Vaccinia virus F9 virion membrane protein is required for entry but not virus assembly, in contrast to the related L1 protein. *J Virol* 80:9455-64.
17. Bisht H, Weisberg AS, Moss B. 2008. Vaccinia virus l1 protein is required for cell entry and membrane fusion. *J Virol* 82:8687-94.
18. Townsley AC, Senkevich TG, Moss B. 2005. The product of the vaccinia virus L5R gene is a fourth membrane protein encoded by all poxviruses that is required for cell entry and cell-cell fusion. *J Virol* 79:10988-98.
19. Senkevich TG, Moss B. 2005. Vaccinia virus H2 protein is an essential component of a complex involved in virus entry and cell-cell fusion. *J Virol* 79:4744-54.

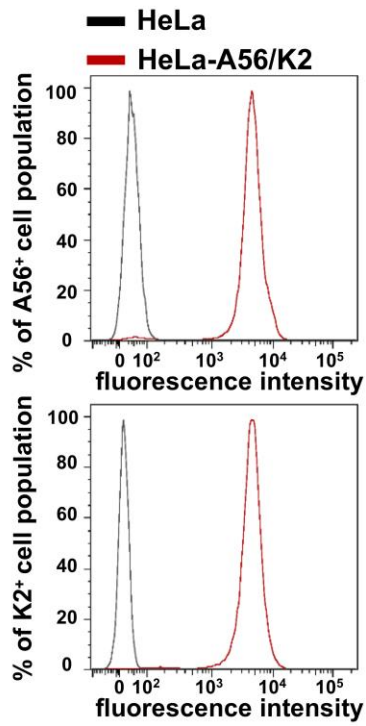
20. Izmailyan RA, Huang CY, Mohammad S, Isaacs SN, Chang W. 2006. The envelope G3L protein is essential for entry of vaccinia virus into host cells. *J Virol* 80:8402-10.
21. Senkevich TG, Ojeda S, Townsley A, Nelson GE, Moss B. 2005. Poxvirus multiprotein entry-fusion complex. *Proc Natl Acad Sci U S A* 102:18572-7.
22. Satheshkumar PS, Moss B. 2009. Characterization of a newly identified 35-amino-acid component of the vaccinia virus entry/fusion complex conserved in all chordopoxviruses. *J Virol* 83:12822-32.
23. Townsley AC, Senkevich TG, Moss B. 2005. Vaccinia virus A21 virion membrane protein is required for cell entry and fusion. *J Virol* 79:9458-69.
24. Laliberte JP, Weisberg AS, Moss B. 2011. The membrane fusion step of vaccinia virus entry is cooperatively mediated by multiple viral proteins and host cell components. *PLoS Pathog* 7:e1002446.
25. Moss B. 2012. Poxvirus cell entry: how many proteins does it take? *Viruses* 4:688-707.
26. Townsley AC, Weisberg AS, Wagenaar TR, Moss B. 2006. Vaccinia virus entry into cells via a low-pH-dependent endosomal pathway. *J Virol* 80:8899-908.
27. Smith GL, Vanderplasschen A, Law M. 2002. The formation and function of extracellular enveloped vaccinia virus. *J Gen Virol* 83:2915-2931.
28. Law M, Carter GC, Roberts KL, Hollinshead M, Smith GL. 2006. Ligand-induced and nonfusogenic dissolution of a viral membrane. *Proc Natl Acad Sci U S A* 103:5989-94.
29. Schmidt FI, Bleck CK, Helenius A, Mercer J. 2011. Vaccinia extracellular virions enter cells by macropinocytosis and acid-activated membrane rupture. *Embo j* 30:3647-61.
30. Moss B. 2016. Membrane fusion during poxvirus entry. *Semin Cell Dev Biol* 60:89-96.
31. Gray RDM, Albrecht D, Beerli C, Huttunen M, Cohen GH, White IJ, Burden JJ, Henriques R, Mercer J. 2019. Nanoscale polarization of the entry fusion complex of vaccinia virus drives efficient fusion. *Nature Microbiology* 4:1636-1644.
32. Chang SJ, Chang YX, Izmailyan R, Tang YL, Chang W. 2010. Vaccinia virus A25 and A26 proteins are fusion suppressors for mature virions and determine strain-specific virus entry pathways into HeLa, CHO-K1, and L cells. *J Virol* 84:8422-32.
33. Ichihashi Y, Dales S. 1971. Biogenesis of poxviruses: interrelationship between hemagglutinin production and polykaryocytosis. *Virology* 46:533-43.
34. Sanderson CM, Frischknecht F, Way M, Hollinshead M, Smith GL. 1998. Roles of vaccinia virus EEV-specific proteins in intracellular actin tail formation and low pH-induced cell-cell fusion. *J Gen Virol* 79 ( Pt 6):1415-25.
35. Chang SJ, Shih AC, Tang YL, Chang W. 2012. Vaccinia mature virus fusion regulator A26 protein binds to A16 and G9 proteins of the viral entry fusion complex and dissociates from mature virions at low pH. *J Virol* 86:3809-18.
36. Chang HW, Yang CH, Luo YC, Su BG, Cheng HY, Tung SY, Carillo KJD, Liao YT, Tzou DM, Wang HC, Chang W. 2019. Vaccinia viral A26 protein is a fusion suppressor of mature virus and triggers membrane fusion through conformational change at low pH. *PLoS Pathog* 15:e1007826.
37. Blackman KE, Bubel HC. 1972. Origin of the vaccinia virus hemagglutinin. *J Virol* 9:290-6.
38. Law KM, Smith GL. 1992. A vaccinia serine protease inhibitor which prevents virus-induced cell fusion. *J Gen Virol* 73 ( Pt 3):549-57.
39. Turner PC, Moyer RW. 1992. An orthopoxvirus serpinlike gene controls the ability of infected cells to fuse. *J Virol* 66:2076-85.
40. Turner PC, Moyer RW. 2006. The cowpox virus fusion regulator proteins SPI-3 and hemagglutinin interact in infected and uninfected cells. *Virology* 347:88-99.

41. Turner PC, Moyer RW. 2008. The vaccinia virus fusion inhibitor proteins SPI-3 (K2) and HA (A56) expressed by infected cells reduce the entry of superinfecting virus. *Virology* 380:226-33.
42. Zhou J, Sun XY, Fernando GJ, Frazer IH. 1992. The vaccinia virus K2L gene encodes a serine protease inhibitor which inhibits cell-cell fusion. *Virology* 189:678-86.
43. Wagenaar TR, Moss B. 2009. Expression of the A56 and K2 proteins is sufficient to inhibit vaccinia virus entry and cell fusion. *J Virol* 83:1546-54.
44. Seki M, Oie M, Ichihashi Y, Shida H. 1990. Hemadsorption and fusion inhibition activities of hemagglutinin analyzed by vaccinia virus mutants. *Virology* 175:372-84.
45. Wagenaar TR, Moss B. 2007. Association of vaccinia virus fusion regulatory proteins with the multicomponent entry/fusion complex. *J Virol* 81:6286-93.
46. Wagenaar TR, Ojeda S, Moss B. 2008. Vaccinia virus A56/K2 fusion regulatory protein interacts with the A16 and G9 subunits of the entry fusion complex. *J Virol* 82:5153-60.
47. Kasani SK, Cheng HY, Yeh KH, Chang SJ, Hsu PW, Tung SY, Liang CT, Chang W. 2017. Differential Innate Immune Signaling in Macrophages by Wild-Type Vaccinia Mature Virus and a Mutant Virus with a Deletion of the A26 Protein. *J Virol* 91.
48. Chung CS, Huang CY, Chang W. 2005. Vaccinia virus penetration requires cholesterol and results in specific viral envelope proteins associated with lipid rafts. *J Virol* 79:1623-34.
49. Oie M, Shida H, Ichihashi Y. 1990. The function of the vaccinia hemagglutinin in the proteolytic activation of infectivity. *Virology* 176:494-504.
50. Brum LM, Turner PC, Devick H, Baquero MT, Moyer RW. 2003. Plasma membrane localization and fusion inhibitory activity of the cowpox virus serpin SPI-3 require a functional signal sequence and the virus encoded hemagglutinin. *Virology* 306:289-302.
51. Dower K, Rubins KH, Hensley LE, Connor JH. 2011. Development of Vaccinia reporter viruses for rapid, high content analysis of viral function at all stages of gene expression. *Antiviral Res* 91:72-80.
52. Rozelle DK, Filone CM, Dower K, Connor JH. 2014. Vaccinia reporter viruses for quantifying viral function at all stages of gene expression. *J Vis Exp* doi:10.3791/51522.
53. Brister JR A-AD, Bao Y, Blinkova O. . 2015. NCBI viral genomes resource. *Nucleic Acids Res* 43.
54. Shigehiro Kuraku CMZ, Osamu Nishimura, Kazutaka Katoh. 2013. aLeaves facilitates on-demand exploration of metazoan gene family trees on MAFFT sequence alignment server with enhanced interactivity *Nucleic Acids Research* 41:W22–W28.
55. Katoh K, Rozewicki J, Yamada KD. 2017. MAFFT online service: multiple sequence alignment, interactive sequence choice and visualization. *Brief Bioinform* doi:10.1093/bib/bbx108.
56. Ulaeto D, Grosenbach D, Hruby DE. 1996. The vaccinia virus 4c and A-type inclusion proteins are specific markers for the intracellular mature virus particle. *J Virol* 70:3372-7.
57. Senkevich TG, Ward BM, Moss B. 2004. Vaccinia Virus Entry into Cells Is Dependent on a Virion Surface Protein Encoded by the A28L Gene. *J Virol* 78:2357-66.
58. Wagenaar TR, Moss B. 2007. Association of Vaccinia Virus Fusion Regulatory Proteins with the Multicomponent Entry/Fusion Complex. *J Virol*.
59. Su HP, Garman SC, Allison TJ, Fogg C, Moss B, Garboczi DN. 2005. The 1.51-Å structure of the poxvirus L1 protein, a target of potent neutralizing antibodies. *Proc Natl Acad Sci U S A* 102:4240-5.

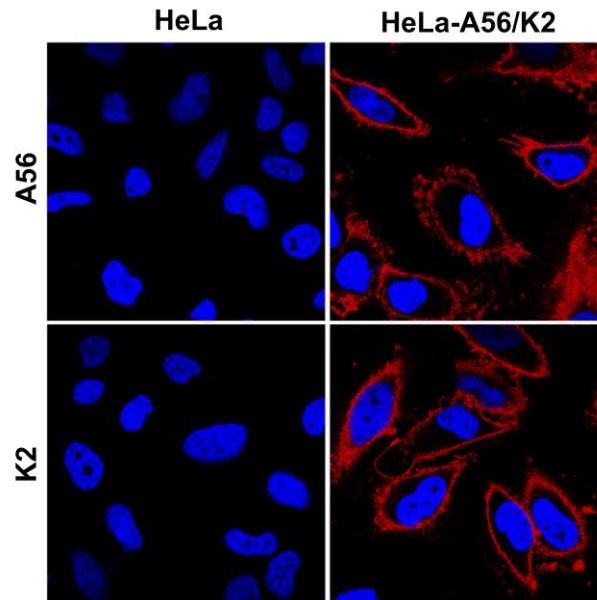
- 
60. Diesterbeck US, Gittis AG, Garboczi DN, Moss B. 2018. The 2.1 Å structure of protein F9 and its comparison to L1, two components of the conserved poxvirus entry-fusion complex. *Sci Rep* 8:16807.
61. Shida H, Dales S. 1981. Biogenesis of vaccinia: carbohydrate of the hemagglutinin molecules. *Virology* 111:56-72.
62. Shida H, Dales S. 1982. Biogenesis of vaccinia: molecular basis for the hemagglutination-negative phenotype of the IHD-W strain. *Virology* 117:219-37.
63. Shida H, Matsumoto S. 1983. Analysis of the hemagglutinin glycoprotein from mutants of vaccinia virus that accumulates on the nuclear envelope. *Cell* 33:423-34.



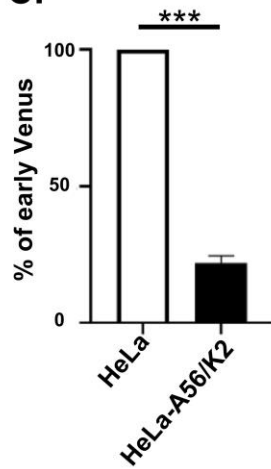
**A.**



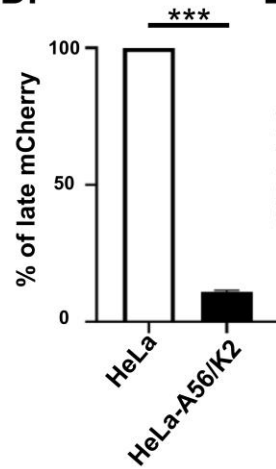
**B.**



**C.**



**D.**



**E.**

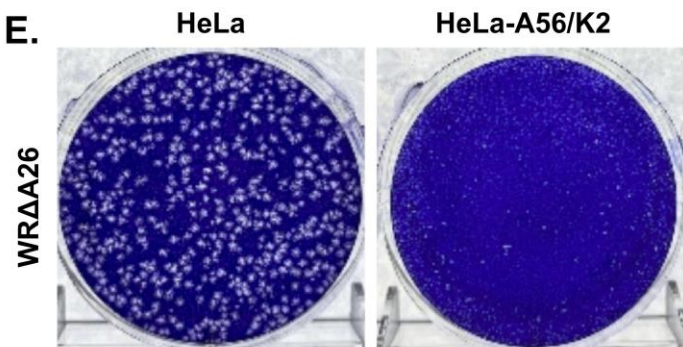


**Figure 1. Generation of HeLa-A56/K2 cells co-expressing vaccinia A56 and K2 proteins to inhibit WRΔA26 infection.** (A). FACS analyses of surface expression of A56 (top panel) and K2 (bottom panel) in HeLa-A56/K2 cells. Control HeLa (black line) and HeLa-A56/K2 cells (red line) were incubated with anti-A56 or anti-K2 mAb, followed by FITC-conjugated goat anti-mouse secondary antibody, washed, and analyzed by FACS. The Y-axis shows the percentage of cell population stained with either anti-A56 (top panel) or anti-K2 (bottom panel) mAb. The X-axis represents fluorescence intensity. (B). Immunofluorescence staining of cell surface A56 and K2 protein using anti-A56 or anti-K2 mAbs in HeLa and HeLa-A56/K2 cells under non-permeable conditions. Blue color represents propidium iodide staining in cell nuclei. (C&D). HeLa and HeLa-A56/K2 cells were infected with MV of WRΔA26-Venus-A4-mCherry at an MOI of 0.1 PFU per cell and expression of viral early Venus marker (in C) and late A4-mCherry genes (in D) was monitored by FACS at 2 hpi and 8 hpi, respectively. Mean fluorescence intensity in HeLa cells was set as 100% to normalize the relative fluorescence intensity in HeLa-A56/K2 cells. Experiments were repeated three times and statistical analyses were performed using a two-tailed unpaired Student's t test. \*,  $P < 0.05$ ; \*\*,  $P < 0.01$ ; \*\*\*,  $P < 0.001$ . (E). Plaque formation of WRΔA26 on HeLa and HeLa-A56/K2 cells. HeLa and HeLa-A56/K2 cells were infected with ~800 PFU of WRΔA26 and incubated for 3 days under agar overlay prior to cell staining with 1% crystal violet.

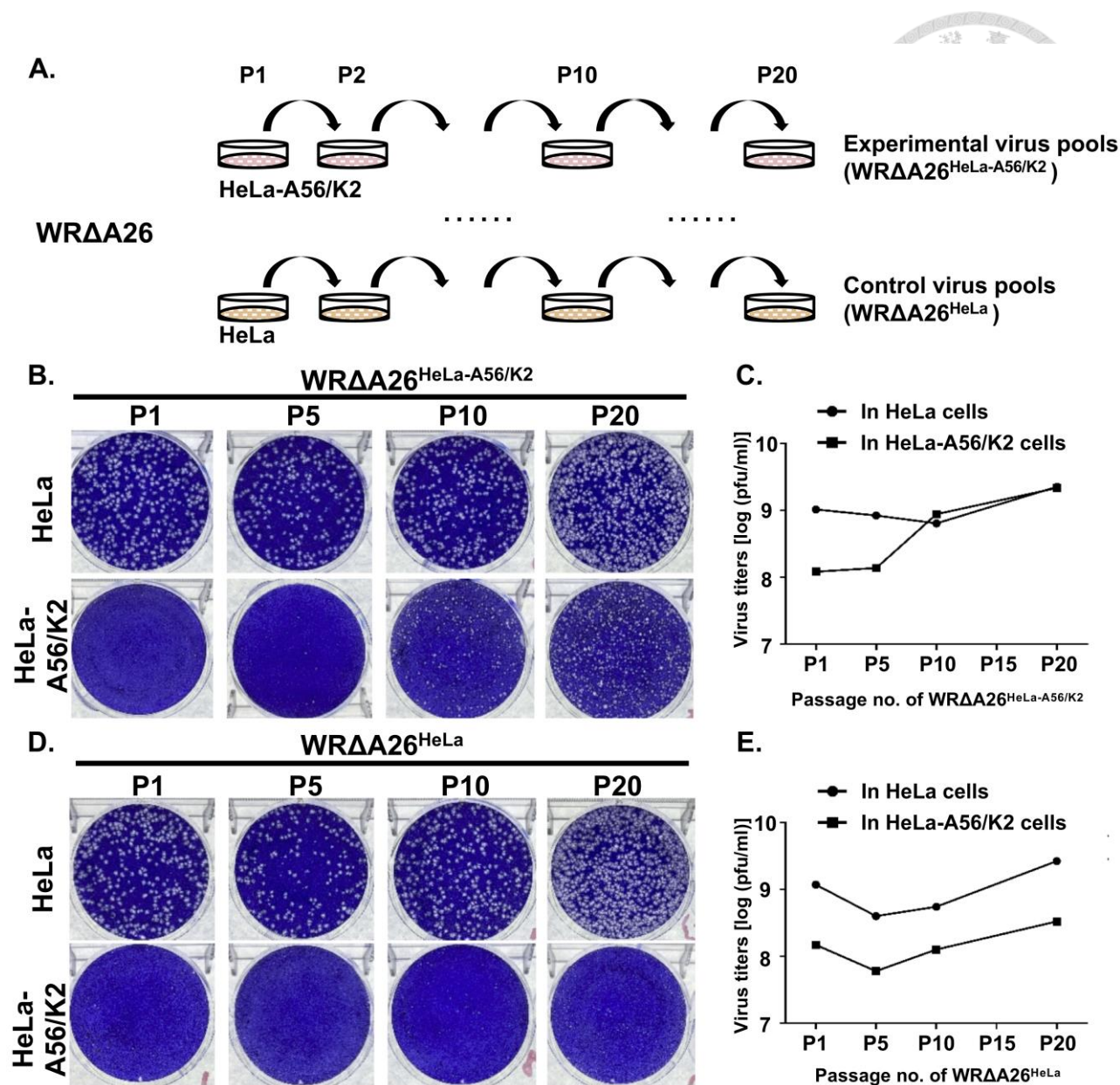
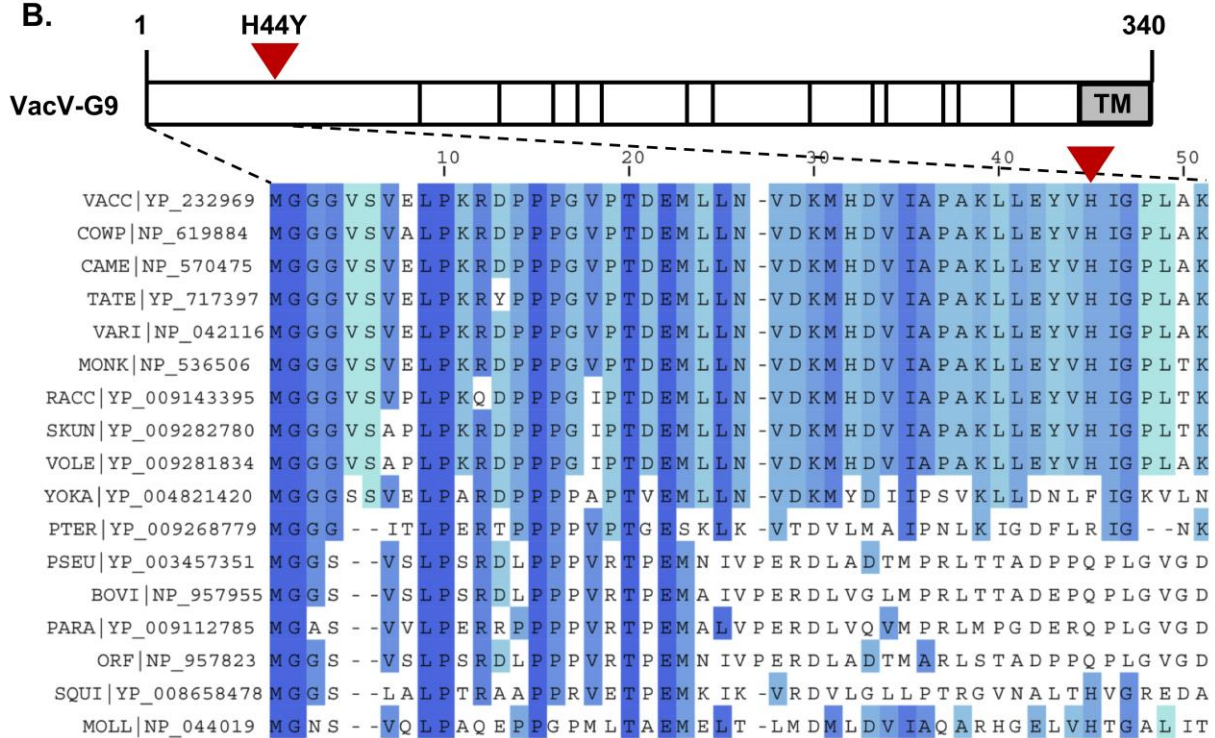


**Figure 2. Experimental passaging of WRΔA26 in HeLa and HeLa-A56/K2 cells.** (A). Schematic representation of our experimental evolution selection process. For P1 to P10 passaging, an MOI of 0.02 PFU per cell was used, whereas for P11 to P20 passaging, an MOI of 0.002 PFU per cell was used. (B). Plaque morphology of WRΔA26<sup>HeLa-A56/K2</sup> from the P1, P5, P10 and P20 virus pools on HeLa and HeLa-A56/K2 cells at 3 dpi after cell staining with 1% crystal violet. (C). Quantification of WRΔA26<sup>HeLa-A56/K2</sup> titers in the P1, P5, P10 and P20 virus pools shown in (B). (D). Plaque morphology of WRΔA26<sup>HeLa</sup> from the P1, P5, P10 and P20 virus pools on HeLa and HeLa-A56/K2 cells at 3 dpi after cell staining with 1% crystal violet. (E). Quantification of WRΔA26<sup>HeLa</sup> titers in the P1, P5, P10 and P20 virus pools shown in (D).

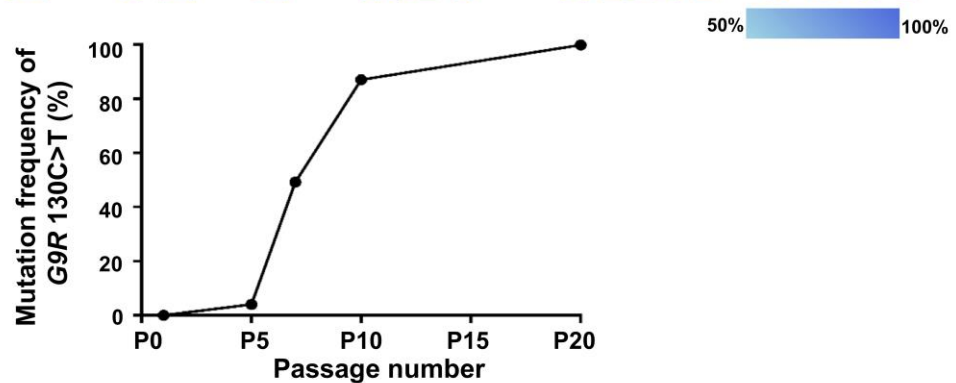
A.

| Passage number (P) | WRΔA26 <sup>Hela</sup> |                   |                        | WRΔA26 <sup>Hela-A56/K2</sup>          |                   |                        |
|--------------------|------------------------|-------------------|------------------------|----------------------------------------|-------------------|------------------------|
|                    | Nucleotide change      | Amino acid change | Mutation frequency (%) | Nucleotide change                      | Amino acid change | Mutation frequency (%) |
| Parental strain    | No mutation            | No mutation       |                        | No mutation                            | No mutation       |                        |
| P5                 | N/D                    | N/D               |                        | No mutation                            | No mutation       |                        |
| P7                 | N/D                    | N/D               |                        | <b>G9R</b> 130C>T                      | H44Y              | 49.2                   |
| P10                | <b>D8L</b> 525C>G      | N175K             | 13.5                   | <b>G9R</b> 130C>T                      | H44Y              | 87.0                   |
| P20                | <b>D8L</b> 525C>G      | N175K             | 93.9                   | <b>G9R</b> 130C>T<br><b>D8L</b> 525C>G | H44Y<br>N175K     | 99.8<br>61.9           |

B.

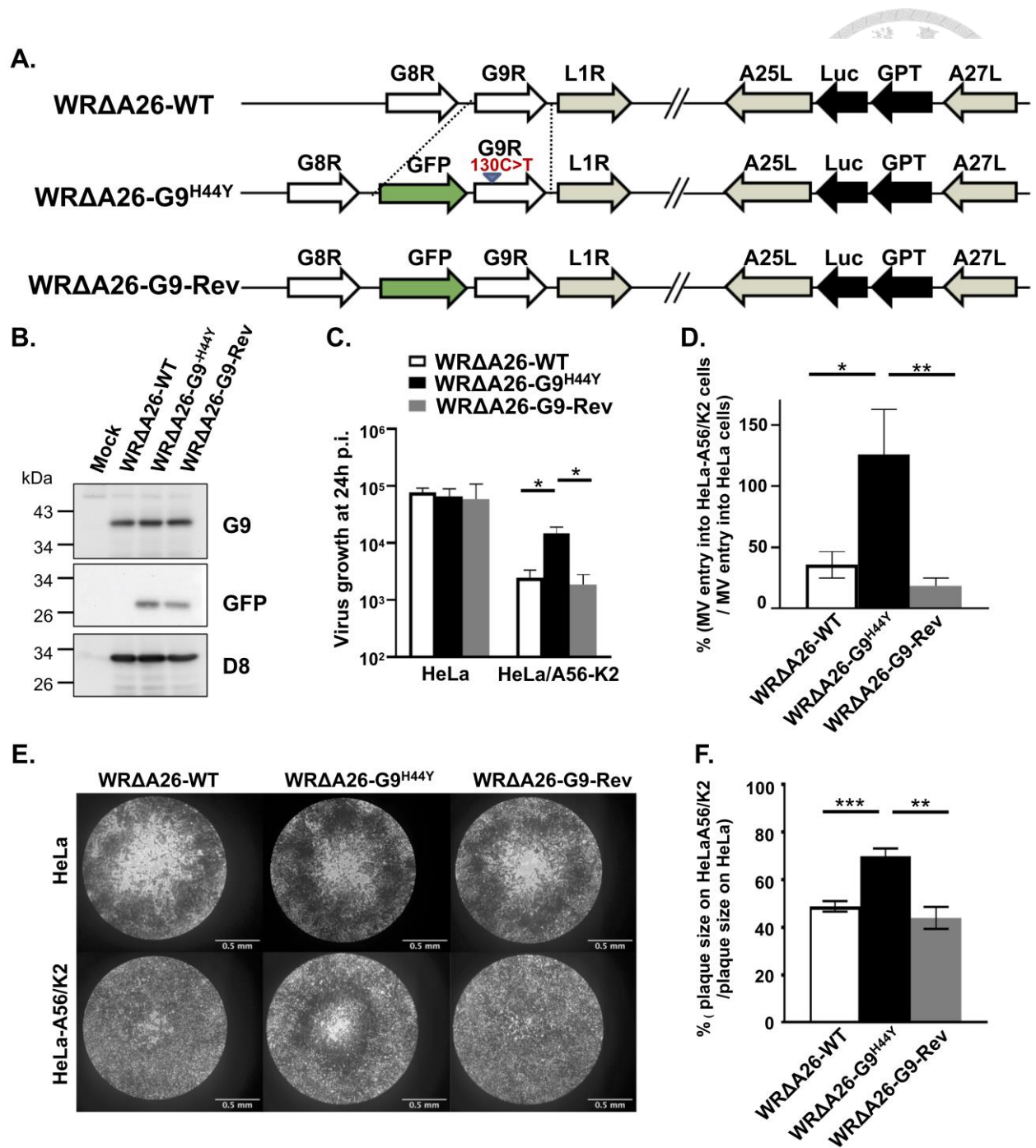


C.

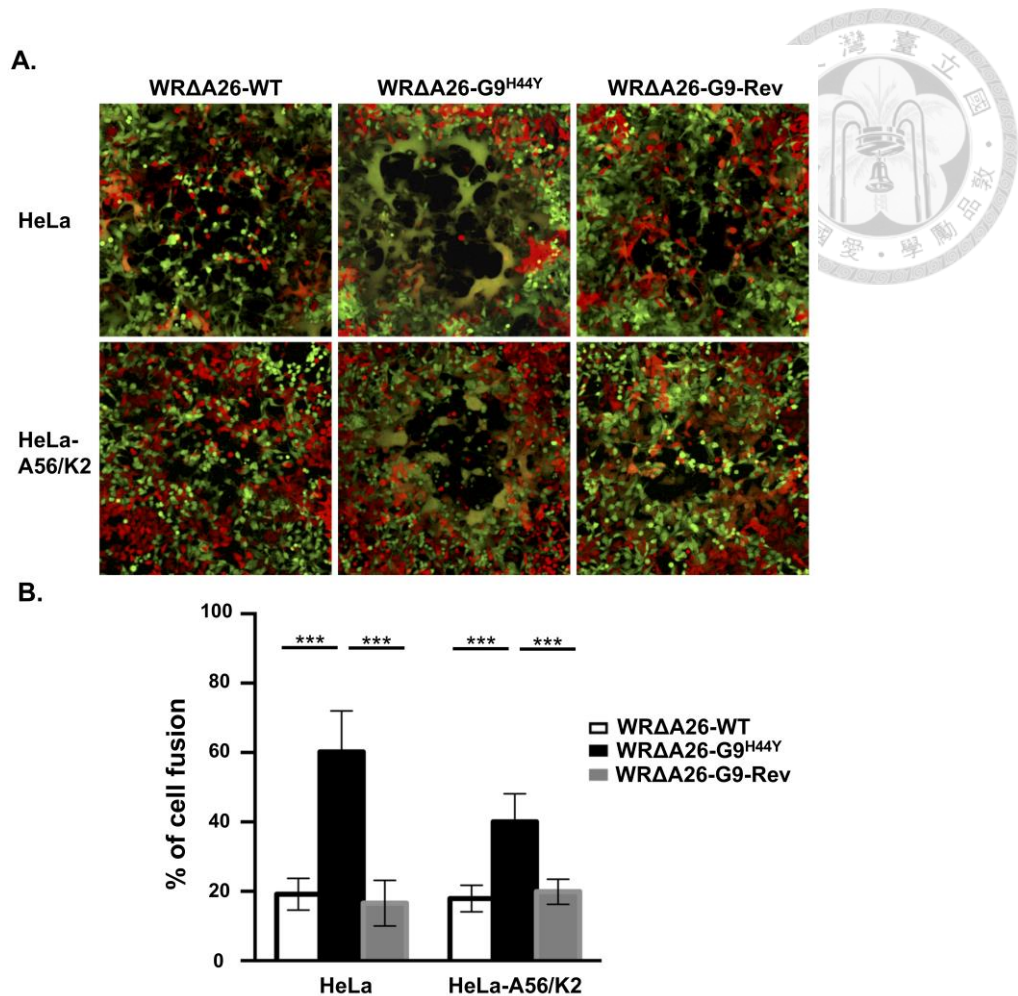


**Figure 3. Whole genome sequencing identified genome variations present in WRΔA26<sup>HeLa</sup> and WRΔA26<sup>HeLa-A56/K2</sup> virus pools.** (A). Mutations of viral genes present in various virus pools derived from populations of WRΔA26<sup>HeLa</sup> and WRΔA26<sup>HeLa-A56/K2</sup>. The dataset was filtered with a cut-off of 10% variation and mutations resulting in amino acid changes are shown. Not done, N/D. (B). Schematic representation of vaccinia G9 protein (amino acids 1-340), showing the single His44Try mutation close to the N-terminal region. TM, transmembrane region. Black bars in the box represent conserved cysteine residues. Multiple sequence alignment of the N-terminal 50 amino acids of vaccinia G9 protein with its orthologues: Vaccinia virus YP\_232969; Cowpox virus NP\_619884; Camelpox virus NP\_570475; Taterapox virus YP\_717397; Variola virus NP\_042116; Monkeypox virus NP\_536506; Raccoonpox virus YP\_009143395; Skunkpox virus YP\_009282780; Volepox virus; YP\_009281834; Yokapox virus YP\_004821420; Pteropox virus YP\_009268779; Pseudocowpox virus YP\_003457351; Bovine papular stomatitis virus NP\_957955; Parapoxvirus YP\_009112785; Orf virus NP\_957823; Squirrelpox virus YP\_008658478; Molluscum contagiosum virus NP\_044019. The color scheme reflects amino acid conservation with a minimum threshold of 50%. (C). The % of 130C>T mutation frequency (representing His44Try) in the G9R ORF that accumulated across the 20 passages of the experimental evolution experiment.



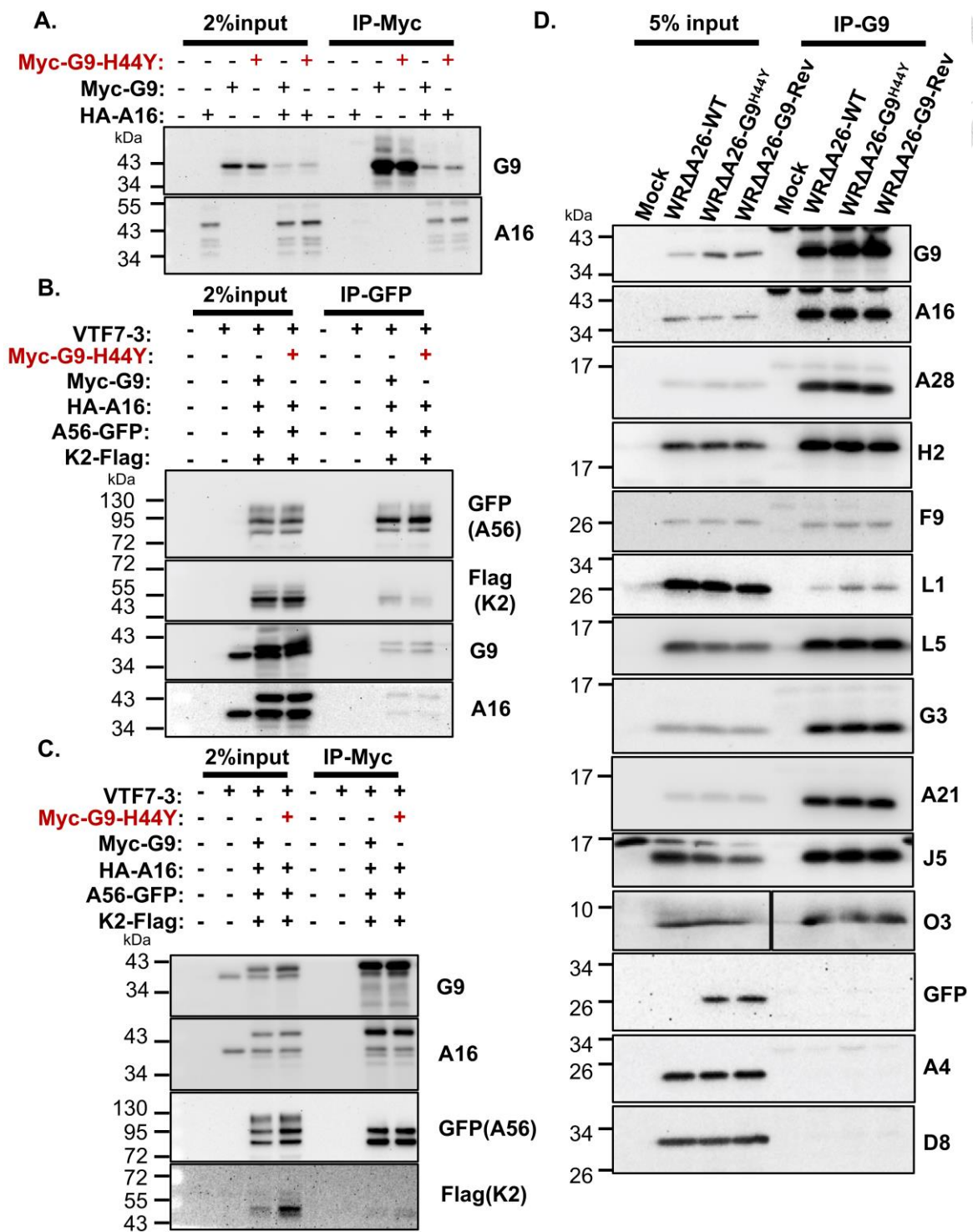


**Figure 4. Generation of recombinant WRΔA26-G9<sup>H44Y</sup> virus.** (A). Schematic representations of WRΔA26-WT, WRΔA26-G9<sup>H44Y</sup> and WRΔA26-G9-Rev recombinant viruses. Luciferase and GPT selection markers replaced the A26L locus in all three viruses. The WRΔA26-G9<sup>H44Y</sup> and WRΔA26-G9-Rev recombinant viruses expressed a p11k-driven G9<sup>H44Y</sup> mutant or wild type G9 protein, respectively, as well as a GFP marker driven by the p7.5K promoter. (B). Immunoblot of G9 proteins in virus-infected cells collected at 24 hpi. GFP is a marker that is present in the WRΔA26-G9<sup>H44Y</sup> and WRΔA26-G9-Rev viruses, and D8 is a viral envelope protein that serves as a positive control. (C). Growth of the WRΔA26-WT, WRΔA26-G9<sup>H44Y</sup>, and WRΔA26-G9-Rev viruses in HeLa and HeLa-A56/K2 cells. HeLa and HeLa-A56/K2 cells were infected with each virus at an MOI of 0.02 PFU per cell and the cells were harvested at 0 and 24 hpi for virus titer determination. The Y-axis represents virus growth, as determined by dividing virus titers at 24 hpi with the respective values at 0 hpi. (D). Relative virus entry efficiency into HeLa and HeLa-A56/K2 cells. HeLa and HeLa-A56/K2 cells were infected with ~200 PFU of each virus for 60 min, washed with PBS to remove unbound viruses, overlaid with agar and PFU number (representing successful entry events) was determined. The Y-axis = (PFU on HeLa-A56/K2 cells / PFU obtained on HeLa cells) x 100%, representing the relative entry efficiency of each virus into HeLa-A56/K2 cells when normalized with that into HeLa cells. (E). Plaque morphology of WRΔA26-WT, WRΔA26-G9<sup>H44Y</sup> and WRΔA26-G9-Rev on HeLa and HeLa-A56/K2 cells after staining with 1% crystal violet. (F). Plaque size quantification for the WRΔA26-WT, WRΔA26-G9<sup>H44Y</sup>, WRΔA26-G9-Rev viruses on HeLa and HeLa-A56/K2 cells. Single plaques on individual cells were randomly selected and the diameters of 30 plaques were determined using Image J. The Y-axis represents normalized plaque size, calculated by dividing plaque diameter on HeLa-A56/K2 cells with the respective value on HeLa cells. Experiments in (C), (D), and (F) were repeated three times and data were analyzed using a two-tailed unpaired Student's t test. \*, P<0.05; \*\*, P<0.01; \*\*\*, P<0.001.

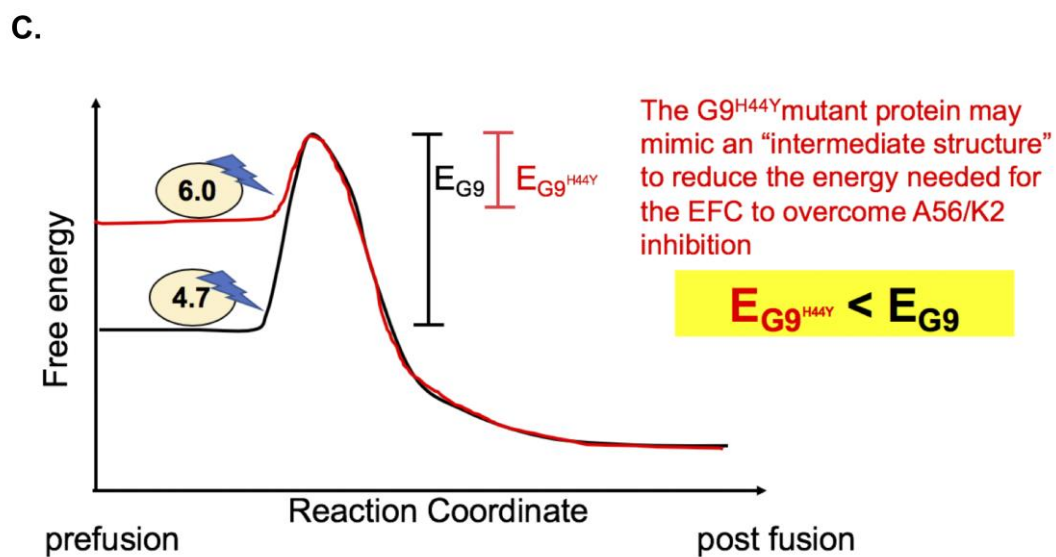
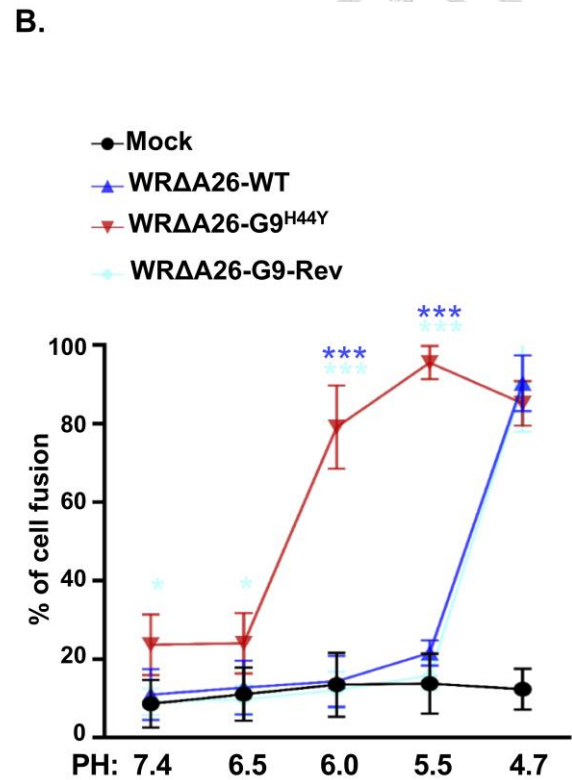
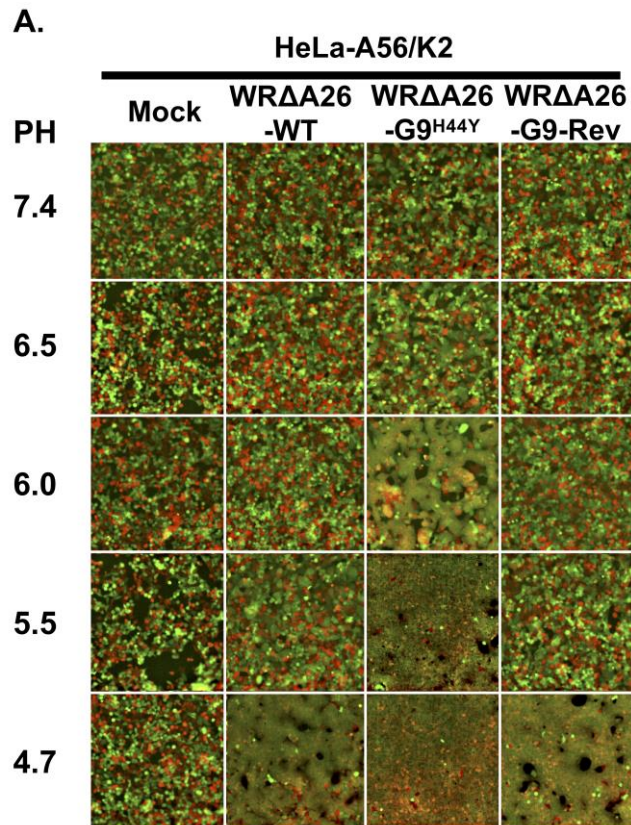


**Figure 5. WRΔA26-G9<sup>H44Y</sup> mutant virus forms plaques with a cell fusion phenotype on HeLa and HeLa-A56/K2 cells.** (A). Images of plaques formed by the WRΔA26-WT, WRΔA26-G9<sup>H44Y</sup>, and WRΔA26-G9-Rev viruses on GFP- and RFP- expressing HeLa and HeLa-A56/K2 cells. HeLa or HeLa-A56/K2 cells expressing GFP or RFP were mixed at a 1:1 ratio and infected with each virus. Plaques were photographed at 2 dpi, as described in the Materials and methods. (B). Quantification of cell fusion in plaques described in (A) from 14 images for each virus. The % cell fusion was quantified using the image area of GFP<sup>+</sup>RFP<sup>+</sup> double-fluorescent cells divided by that of single-fluorescent cells. Although WRΔA26-G9<sup>H44Y</sup> and WRΔA26-G9-Rev harbor a GFP marker, its expression level was relatively weak relative to the fluorescence intensities of HeLa-GFP and HeLa-A56/K2-GFP, so viral GFP was calibrated as the background value. Data from a total of 14 plaques were subjected to statistical analyses using a two-tailed unpaired Student's t test. \*, P<0.05; \*\*, P<0.01; \*\*\*, P<0.001.

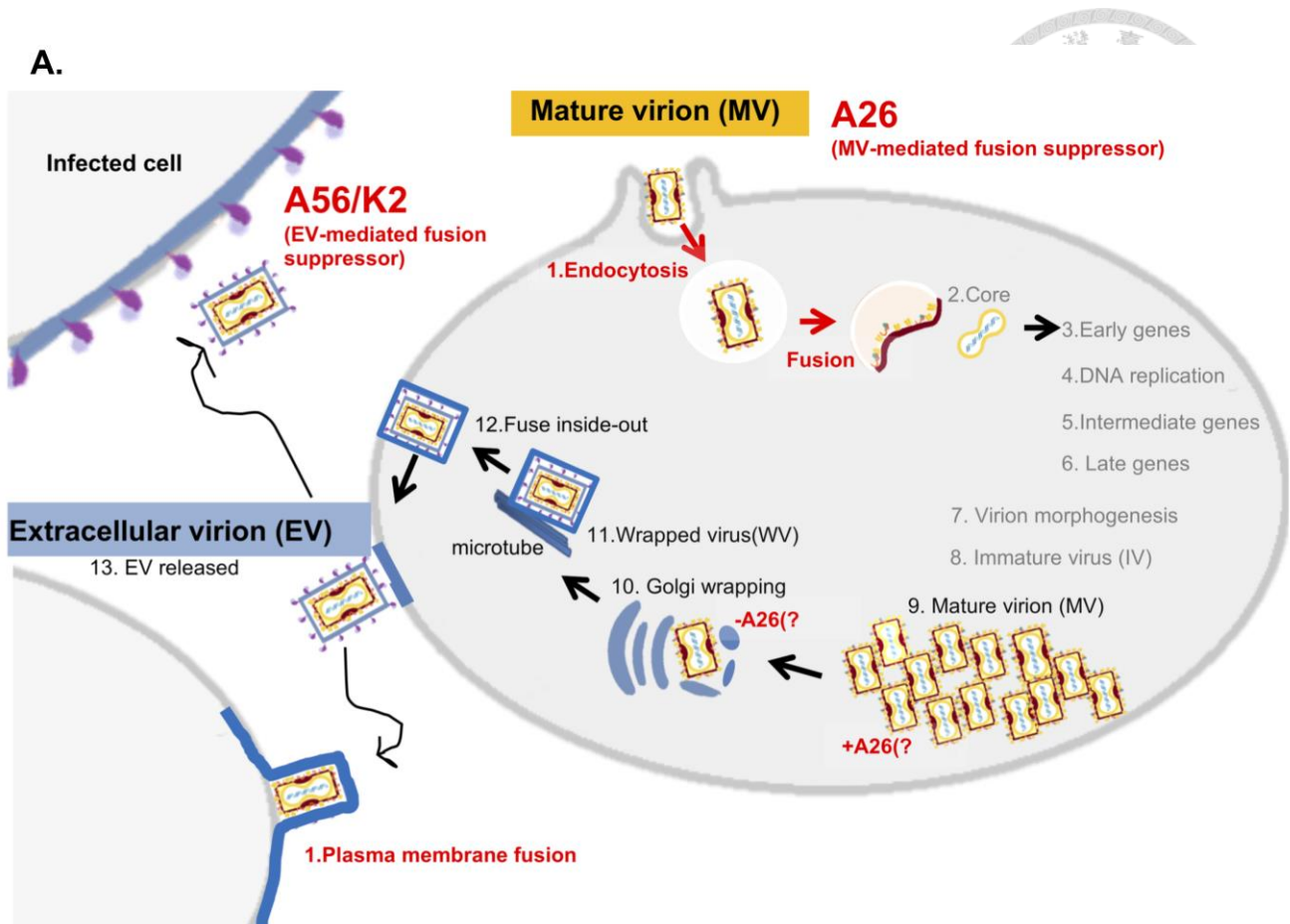




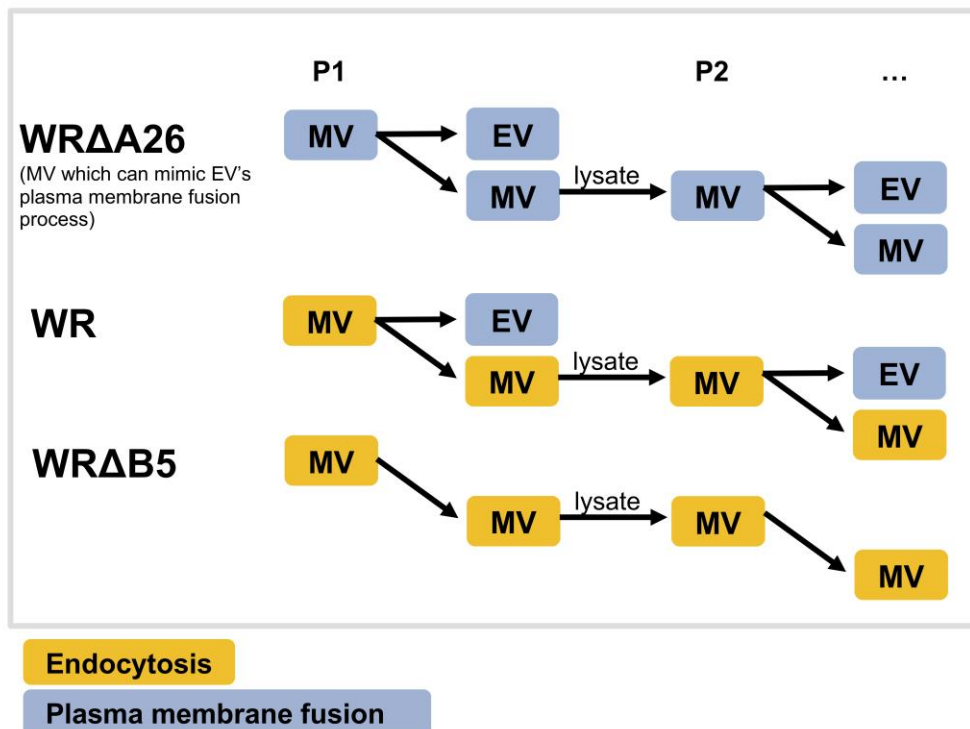
**Figure 6. Coimmunoprecipitation of G9<sup>H44Y</sup> protein with A16, A56/K2 protein complex and multiple components of the viral EFC in virus-infected cells.** (A). Co-IP of G9<sup>H44Y</sup> with A16 in transient transfected cells. 293T cells were transfected with plasmids expressing Myc-G9, Myc-G9<sup>H44Y</sup> and/or HA-A16 and harvested 24 h later for co-IP with anti-Myc agarose beads as described in the Materials and methods. The blot was probed with anti-G9 and anti-A16 antibodies. (B & C). Co-IP of G9<sup>H44Y</sup>/A16 complex with A56/K2 protein complex. 293T cells were infected with VTF7-3 and transfected with plasmids expressing Myc-G9, Myc-G9<sup>H44Y</sup>, HA-A16, A56-GFP and/or K2-Flag, and lysates were harvested 24 h later for co-IP with anti-GFP (in B) or anti-Myc (in C) conjugated agarose beads. Blots were probed with anti-GFP, anti-Flag, anti-G9, or anti-A16 antibodies. (D). Co-IP of G9<sup>H44Y</sup> protein with EFC components in virus-infected cells. 293T cells were either mock infected or infected with individual virus at an MOI of 5 PFU per cell, harvested at 24 hpi for co-IP with anti-G9 conjugated agarose beads, and analyzed by immunoblotting with anti-EFC antibodies as shown at the right side of each panel.



**Figure 7. Acid titration of WRΔA26-G9<sup>H44Y</sup> virus-mediated fusion activation in HeLa-A56/K2 cells.** (A). HeLa-A56/K2 cells expressing GFP or RFP were seeded in a 1:1 ratio. The next day, these cells were pretreated with 40 μg/ml cordycepin for 60 min and subsequently infected with MV of WRΔA26, WRΔA26-G9<sup>H44Y</sup> or WRΔA26-G9-Rev virus at an MOI of 100 PFU per cell. Cordycepin was present in culture media throughout the experiments to inhibit viral early gene expression. After infection at 37 °C for 60 min, cells were treated with a buffer of pH 7.4, 6.5, 6.0, 5.5 or 4.7, respectively, at 37 °C for 3 min, washed with growth medium, further incubated at 37 °C for 1 h, and then photographed using a Zeiss Axiovert fluorescence microscope. (B). Quantification of % cell fusion from the images described in (A). Images from three independent experiments were quantified using the image area of GFP<sup>+</sup>RFP<sup>+</sup> double-fluorescent cells divided by that of single-fluorescent cells. Data from three independent experiments were subjected to statistical analysis using a two-tailed unpaired Student's t test. \*, P<0.05; \*\*, P<0.01; \*\*\*, P<0.001. Cyan asterisks represent the level of significant difference between WRΔA26-G9<sup>H44Y</sup> and WRΔA26-G9-Rev. Blue asterisks represent the level of significant difference between WRΔA26-G9<sup>H44Y</sup> and WRΔA26-WT. (C). A model of G9<sup>H44Y</sup> protein allows viral EFC to overcome a lower energy barrier prior to activation of membrane fusion.



**B.**



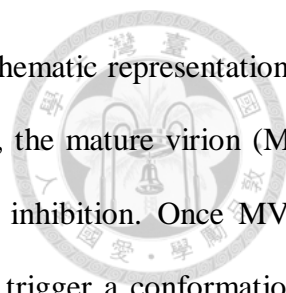


**Figure 8. The entry of mature virion and extracellular virion.** (A). Schematic representation of the vaccinia virion entry pathway. For P1 to P10 passaging Steps 1 to 2, the mature virion (MV) entered cells by endocytosis because A26 binds on G9/A16 for fusion inhibition. Once MV is packaged into an endosome, the acid environment of the endosome can trigger a conformational change in A26 protein to induce EFC fusion activation. Then, the viral membrane fuses with the endosome, releasing viral cores into the cytoplasm. For Steps 2 to 11, upon viral core release, the virus replicates the viral genome and forms MV and is transmitted to the Golgi for packaging (wrapped virus, WV). It remains unclear how the assembly process of MV to EV operates that results in EV without A26 protein. For Steps 11 to 12, WV fuses from within to the outer plasma membrane and the WV outer membrane is removed. The EV can then further spread to another cell, entering it by plasma membrane fusion. The A56/K2 protein complex is expressed on cell membrane surfaces at the early stage of viral infection to inhibit EV-mediated fusion in a process termed “superinfection interference. (B). Schematic representation of the selection process for endocytosis or plasma membrane fusion of MV or EV in  $WR\Delta A26^{\text{HeLa-A56/K2}}$ ,  $WR^{\text{HeLa-A56/K2}}$  and  $WR\Delta B5^{\text{HeLa-A56/K2}}$  viruses.



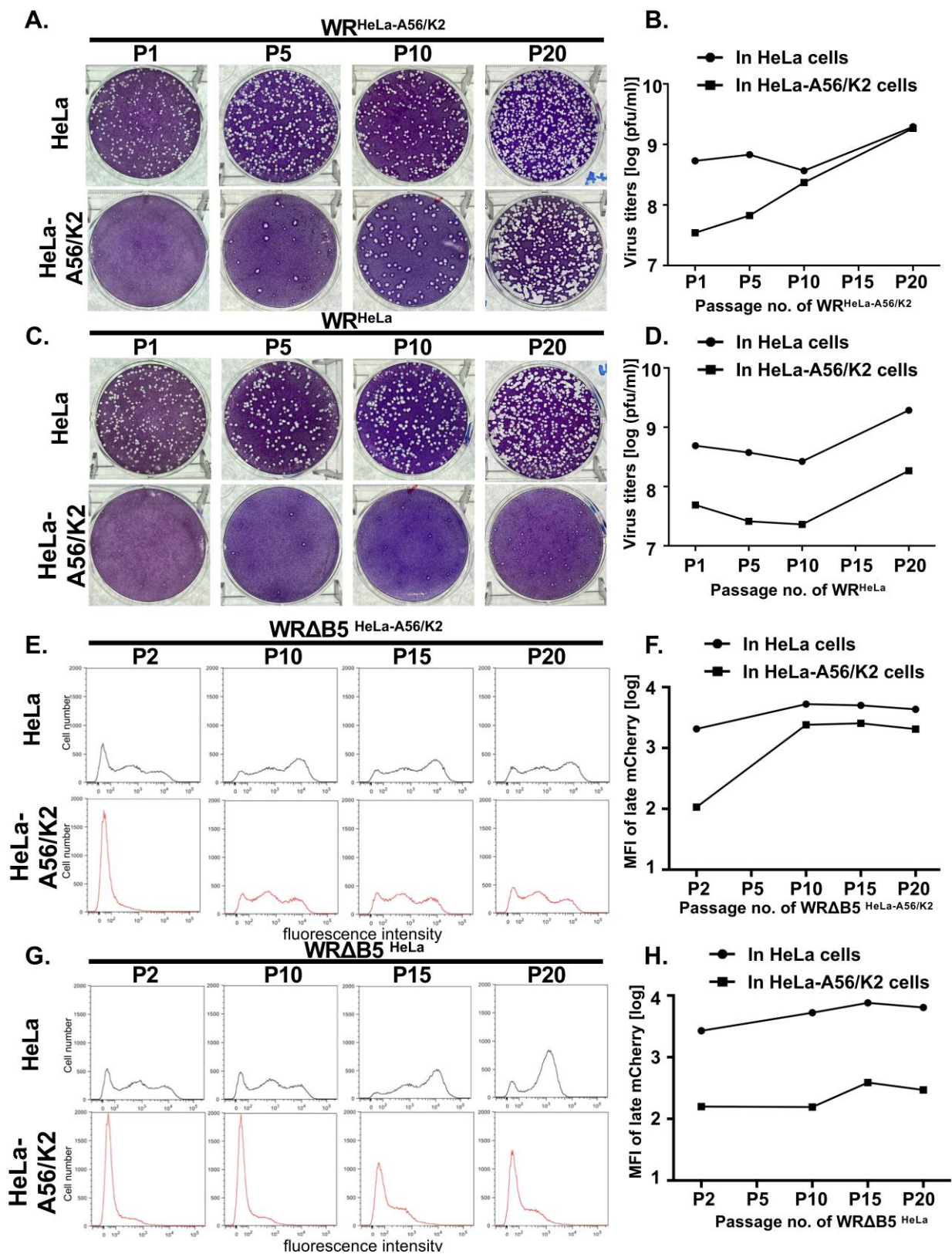


**Figure 9. Experimental passaging of WR and WR $\Delta$ B5 in HeLa and HeLa-A56/K2 cells.** (A). Plaque morphology of WR<sup>HeLa-A56/K2</sup> from the P1, P5, P10 and P20 virus pools on HeLa and HeLa-A56/K2 cells at 3 dpi after cell staining with 1% crystal violet. (B). Quantification of WR<sup>HeLa-A56/K2</sup> titers in the P1, P5, P10 and P20 virus pools shown in (A). (C). Plaque morphology of WR<sup>HeLa</sup> from the P1, P5, P10 and P20 virus pools on HeLa and HeLa-A56/K2 cells at 3 dpi after cell staining with 1% crystal violet. (D). Quantification of WR<sup>HeLa</sup> titers in the P1, P5, P10 and P20 virus pools shown in (C). (E and F). HeLa and HeLa-A56/K2 cells were infected with MV of WR $\Delta$ B5-A4-mCherry<sup>HeLa-A56/K2</sup> from the P2, P10, P15, and P20 pools at an MOI of 0.1 PFU per cell and expression of viral late A4-mCherry genes was monitored by FACS at 8 hpi. (G and H). HeLa and HeLa-A56/K2 cells were infected with MV of WR $\Delta$ B5-A4-mCherry<sup>HeLa</sup> from the P2, P10, P15, and P20 pools at an MOI of 0.1 PFU per cell and expression of viral late A4-mCherry genes was monitored by FACS at 8 hpi.



A.

| Passage number (P) | WR <sup>HeLa</sup> |                   |                        | WR <sup>HeLa-A56/K2</sup>                                                                                                                                                                                                                                                                                                                         |                                                                                                                                                                   |                                                                                                                                                  |
|--------------------|--------------------|-------------------|------------------------|---------------------------------------------------------------------------------------------------------------------------------------------------------------------------------------------------------------------------------------------------------------------------------------------------------------------------------------------------|-------------------------------------------------------------------------------------------------------------------------------------------------------------------|--------------------------------------------------------------------------------------------------------------------------------------------------|
|                    | Nucleotide change  | Amino acid change | Mutation frequency (%) | Nucleotide change                                                                                                                                                                                                                                                                                                                                 | Amino acid change                                                                                                                                                 | Mutation frequency (%)                                                                                                                           |
| Parental strain    | No mutation        | No mutation       |                        | No mutation                                                                                                                                                                                                                                                                                                                                       | No mutation                                                                                                                                                       |                                                                                                                                                  |
| P10                | No mutation        | No mutation       |                        | <b>G9R</b> 130C>T<br><b>A28L</b> 236C>A                                                                                                                                                                                                                                                                                                           | H44Y<br>P79Q                                                                                                                                                      | 95.4<br>63.8                                                                                                                                     |
| P20                | <b>B4R</b> 293C>A  | S98*              | 37.9                   | <b>G9R</b> 130C>T<br><b>A28L</b> 236C>A<br><b>A26L</b> multiple mutations<br>1. 771_772dup<br>2. 230delC<br>3. 188_189dup<br>4. 112delA<br>5. 1471_1472delAT<br>6. 1420_1421delCT<br>7. 1245dup<br>8. 973delG<br>9. 947dup<br>10. 910dup<br>11. 578_579delTA<br>12. 570G>A<br>13. 421dup<br>14. 301_302dup<br>15. 149dup<br><br><b>B4R</b> 293C>A | H44Y<br>P79Q<br><br>L258fs<br>P77fs<br>P64fs<br>I38fs<br>I491fs<br>L474fs<br>D416fs<br>V325fs<br>R317fs<br>E304fs<br>V193fs<br>W190*<br>I141fs<br>S102fs<br>N50fs | 99.9<br>30.9<br><b>55.8</b><br>5.9<br>4.4<br>4.6<br>8.9<br>7.6<br>1.1<br>2.7<br>5.8<br>2.3<br>1.3<br>1.1<br>6.7<br>1.2<br>1.2<br>1.0<br><br>11.9 |

B.

| Passage number (P) | WRΔB5 <sup>HeLa</sup> |                   |                        | WRΔB5 <sup>HeLa-A56/K2</sup>            |                   |                        |
|--------------------|-----------------------|-------------------|------------------------|-----------------------------------------|-------------------|------------------------|
|                    | Nucleotide change     | Amino acid change | Mutation frequency (%) | Nucleotide change                       | Amino acid change | Mutation frequency (%) |
| Parental strain    | No mutation           | No mutation       |                        | No mutation                             | No mutation       |                        |
| P10                | No mutation           | No mutation       |                        | <b>G9R</b> 130C>T<br><b>F4L</b> 468delT | H44Y<br>I157fs    | 95.6<br>35.3           |
| P20                | No mutation           | No mutation       |                        | <b>G9R</b> 130C>T                       | H44Y              | 99.9                   |

**Figure 10. Whole genome sequencing identified genome variations present in different pools of WR and WRΔB5 passaged virus.** (A). Mutations of viral genes present in various virus pools derived from populations of WR<sup>HeLa</sup> and WR<sup>HeLa-A56/K2</sup>. (B). Mutations of viral genes present in various virus pools derived from populations of WRΔB5<sup>HeLa</sup> and WRΔB5<sup>HeLa-A56/K2</sup>. (A and B) The dataset was filtered with a cut-off of 10% variation, and mutations resulting in amino acid changes are shown.

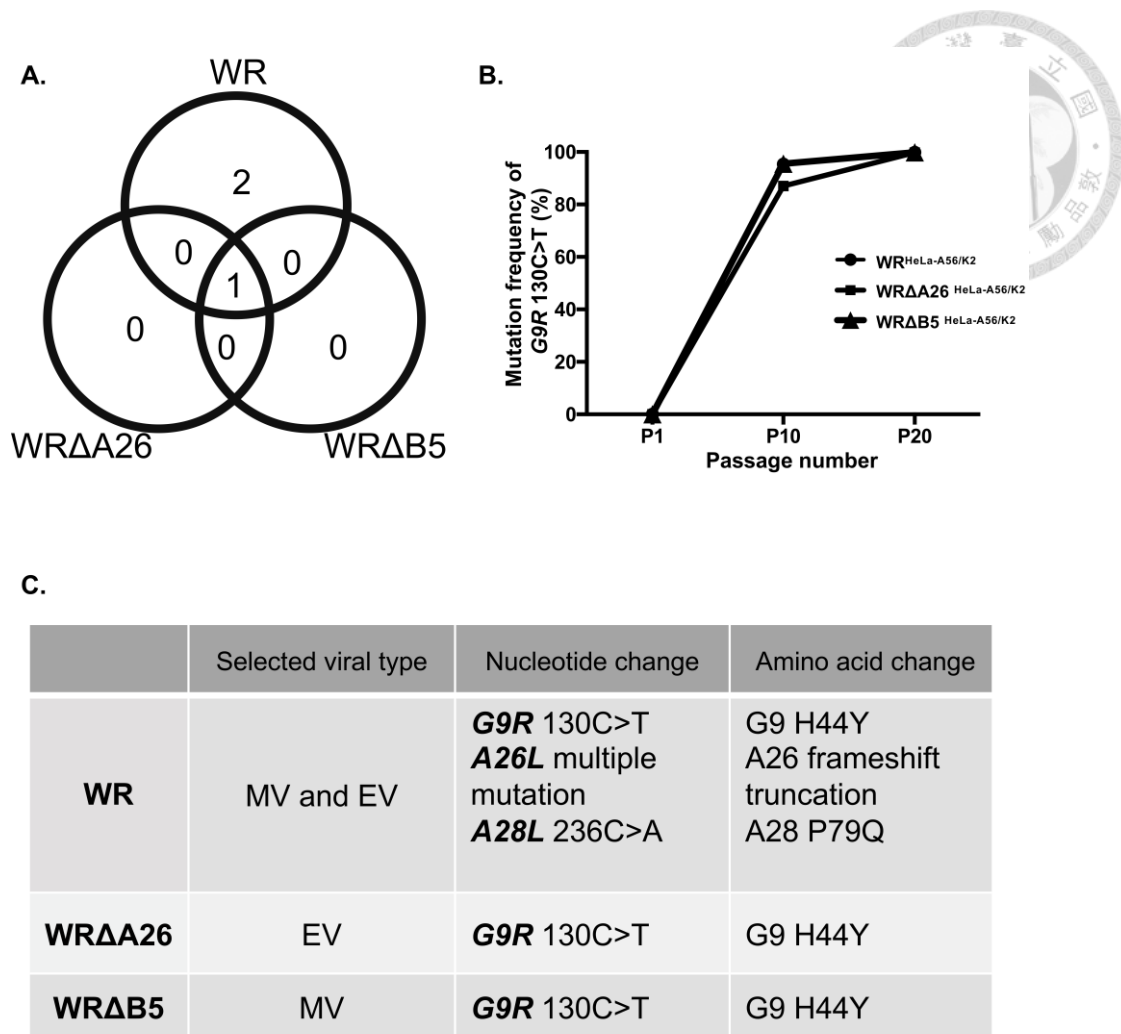


**Figure 11.** An identical G9<sup>H44Y</sup> mutation occurred in WRΔA26<sup>HeLa-A56/K2</sup>, WR<sup>HeLa-A56/K2</sup> and WRΔB5<sup>HeLa-A56/K2</sup> viruses. (A). The Venn diagram illustrates mutation number in the P20 pool of WRΔA26<sup>HeLa-A56/K2</sup>, WR<sup>HeLa-A56/K2</sup> and WRΔB5<sup>HeLa-A56/K2</sup> viruses. (B). The % of 130C>T mutation frequency (representing His44Try) in the G9R ORF that accumulated across the 20 passages of WRΔA26<sup>HeLa-A56/K2</sup>, WR<sup>HeLa-A56/K2</sup> and WRΔB5<sup>HeLa-A56/K2</sup> viruses. (C). The table summarizes the selected viral type, nucleotide change, and amino acid change in the P20 pool of WRΔA26<sup>HeLa-A56/K2</sup>, WR<sup>HeLa-A56/K2</sup> and WRΔB5<sup>HeLa-A56/K2</sup>.

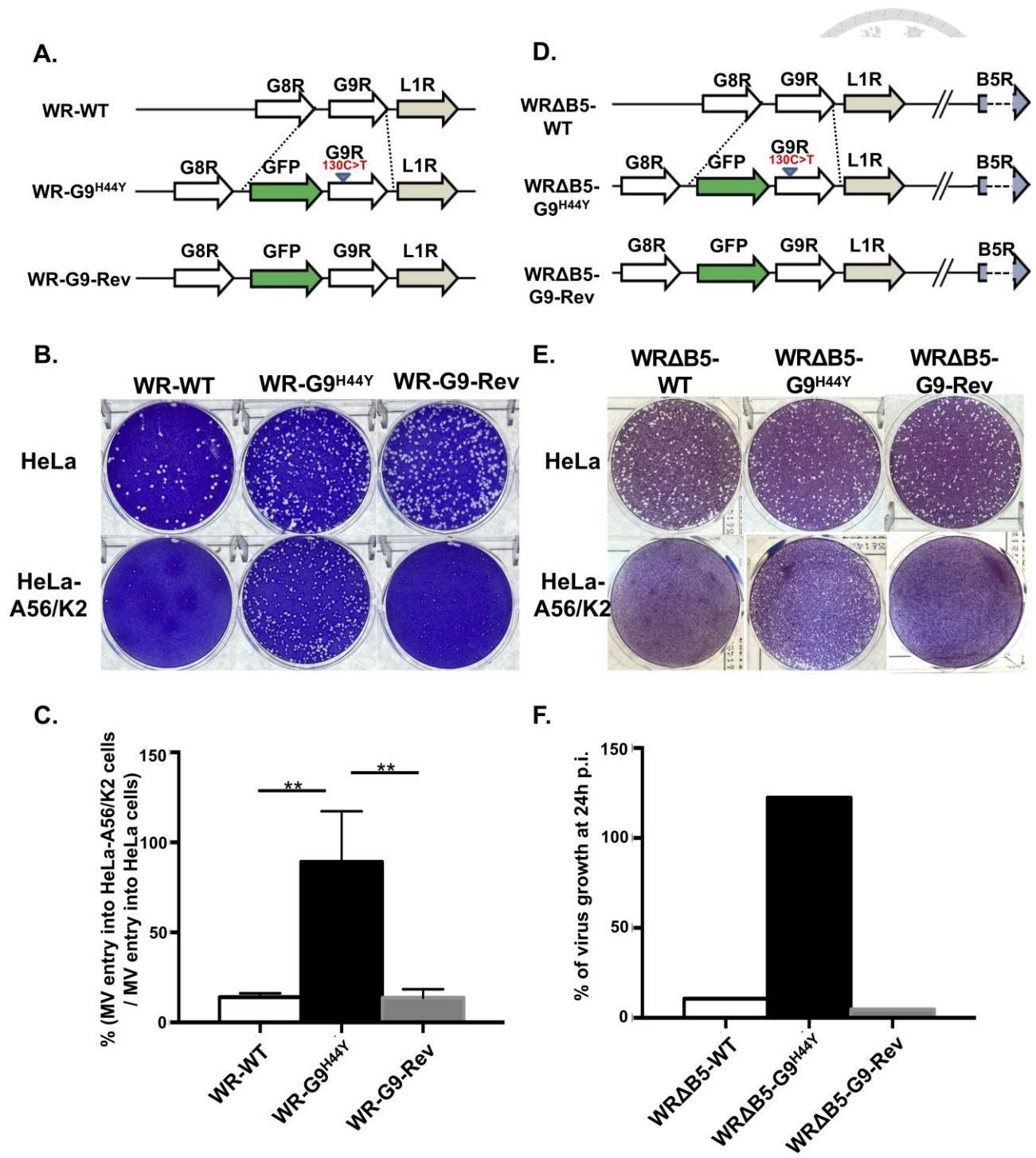


**Figure 12. Generation of recombinant WR-G9<sup>H44Y</sup> and WRΔB5-G9<sup>H44Y</sup> virus.** (A and D). Schematic representations of (A) WR-WT, WR-G9<sup>H44Y</sup> and WR-G9-Rev recombinant viruses and (D) WRΔB5-WT, WRΔB5-G9<sup>H44Y</sup> and WRΔB5-G9-Rev recombinant viruses. The G9<sup>H44Y</sup> and G9-Rev recombinant viruses expressed a p11k-driven G9<sup>H44Y</sup> mutant or wild type G9 protein, respectively, as well as a GFP marker driven by the p7.5K promoter. (B and E). Plaque morphology of (B) WR-WT, WR-G9<sup>H44Y</sup> and WR-G9-Rev and (E) WRΔB5-WT, WRΔB5-G9<sup>H44Y</sup> and WRΔB5-G9-Rev recombinant viruses on HeLa and HeLa-A56/K2 cells after staining with 1% crystal violet. (C). Relative virus entry efficiency into HeLa and HeLa-A56/K2 cells. HeLa and HeLa-A56/K2 cells were infected with ~200 PFU of each virus for 60 min, washed with PBS to remove unbound viruses, overlaid with agar, and PFU number (representing successful entry events) was determined. The Y-axis = (PFU on HeLa-A56/K2 cells / PFU obtained on HeLa cells) x 100%, representing the relative entry efficiency of each virus into HeLa-A56/K2 cells when normalized with that into HeLa cells. Experiments in (C) were repeated three times and data was analyzed using a two-tailed unpaired Student's t test. \*, P<0.05; \*\*, P<0.01; \*\*\*, P<0.001. (F). Growth of the WRΔB5WT, WRΔB5-G9<sup>H44Y</sup>, and WRΔB5-G9-Rev viruses in HeLa and HeLa-A56/K2 cells. HeLa and HeLa-A56/K2 cells were infected with each virus at an MOI of 0.1 PFU per cell and the cells were harvested at 0 and 24 hpi for virus titer determination. The Y-axis represents virus growth, as determined by dividing virus titers at 24 hpi with the respective values at 0 hpi, and reflect relative abundance of HeLa-A56/K2 cells when normalized with that of HeLa cells.

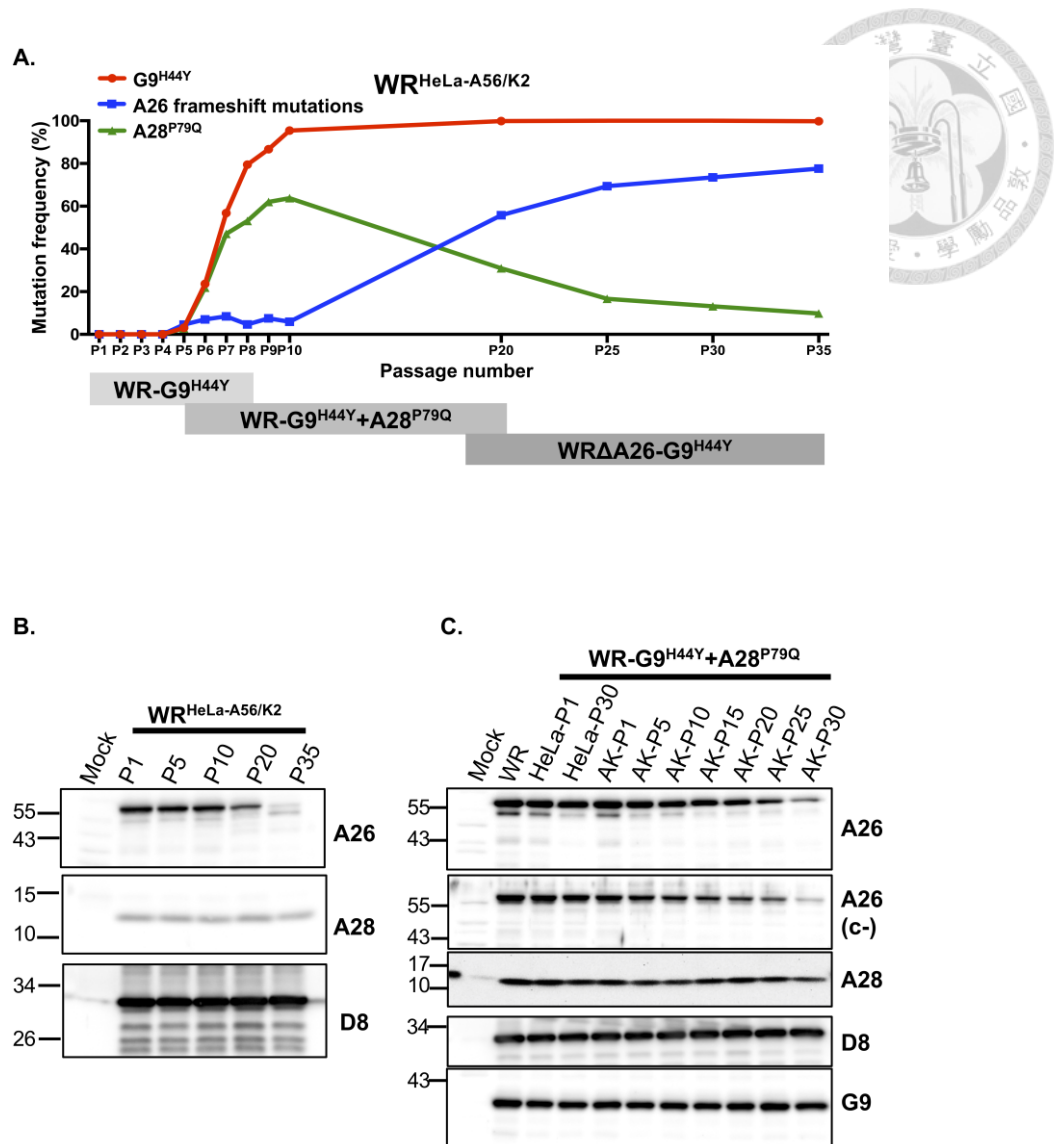
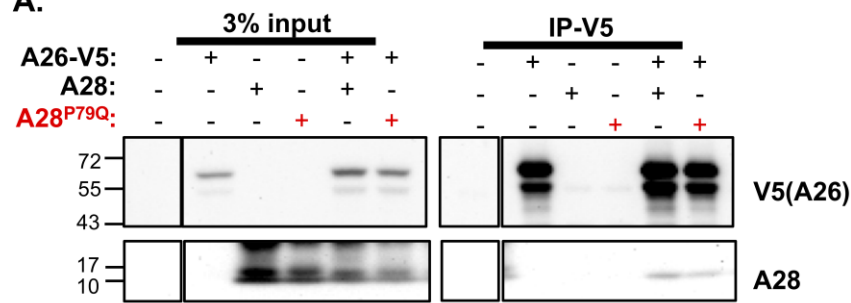
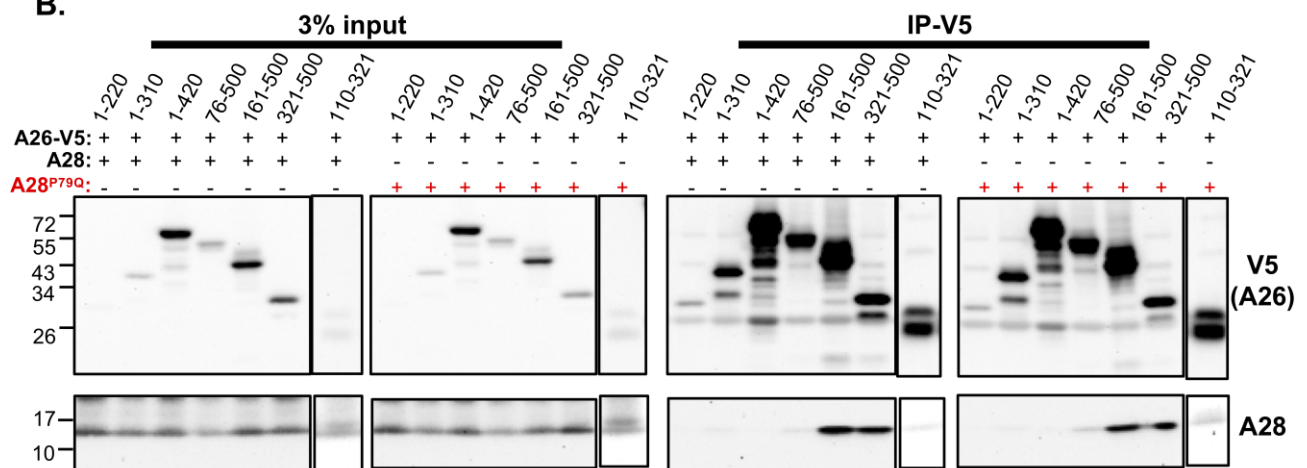


**Figure 13. The additional mutation revealed on WR<sup>HeLa-A56/K2</sup> virus.** (A). Line chart of G9<sup>H44Y</sup>, A28<sup>P79Q</sup> and A26 frameshift mutations in WR<sup>HeLa-A56/K2</sup> virus. The mutation frequency of A26 frameshift mutations generated from the sum of all mutation frequencies. (B). Immunoblot of A26 proteins from the WR<sup>HeLa-A56/K2</sup> P1, P5, P10, P20, and P35 pools of virus-infected cells collected at 24 hpi. D8 is a viral envelope protein that serves as a positive control. (C). Immunoblot of A26 proteins in the WR-G9<sup>H44Y</sup>+A28<sup>P79Q</sup>-HeLa-A56/K2 P1, P5, P10, P15, P20, P25, and P30 pools of virus-infected cells collected at 24 hpi. The WR-G9<sup>H44Y</sup>+A28<sup>P79Q</sup>-HeLa P1 and P30 pools serve as a control for comparing A26 protein on control virus through 30 passaging bouts. A26(C-) is an antibody that only recognizes the C-terminal of A26. D8 is a viral envelope protein that serves as a positive control.

**A.**



**B.**



**C.**

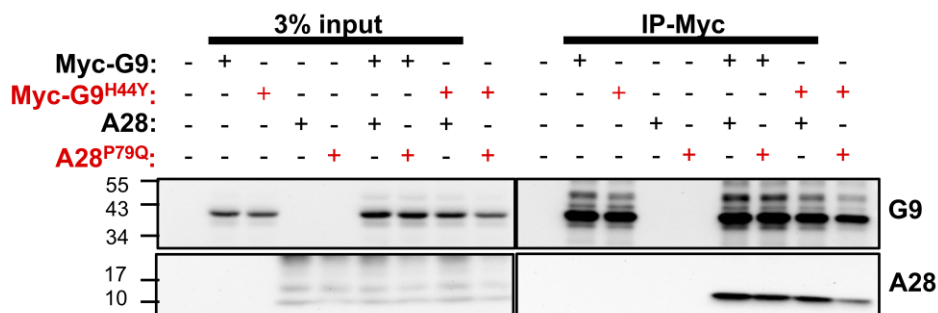


**Figure 14. Coimmunoprecipitation of wild type A28 protein, A28<sup>P79Q</sup> protein, A26, wild type G9 and G9<sup>H44Y</sup>.** (A). Co-IP of wild type A28 protein or A28<sup>P79Q</sup> protein with A26 in transient transfected cells. 293T cells were transfected with plasmids expressing A28, A28<sup>P79Q</sup> and/or A26-V5 and harvested 24 h later for co-IP with anti-V5 agarose beads, as described in the Materials and methods. The blot was probed with anti-A28 and anti-V5 antibodies. (B). Co-IP of wild type A28 protein or A28<sup>P79Q</sup> protein with different truncated variants of A26 in transient transfected cells. 293T cells were transfected with plasmids expressing A28 or A28<sup>P79Q</sup> with different truncated variants of A26-V5 and harvested 24 h later for co-IP with anti-V5 agarose beads, as described in the Materials and methods. The blot was probed with anti-A28 and anti-V5 antibodies. (C). Co-IP of wild type G9 or G9<sup>H44Y</sup> protein with wild type A28 protein or A28<sup>P79Q</sup> in transient transfected cells. 293T cells were transfected with plasmids expressing Myc-G9, Myc-G9<sup>H44Y</sup> and/or A28 or A28<sup>P79Q</sup> and harvested 24 h later for co-IP with anti-Myc agarose beads, as described in the Materials and methods. The blot was probed with anti-A28 and anti-G9 antibodies.



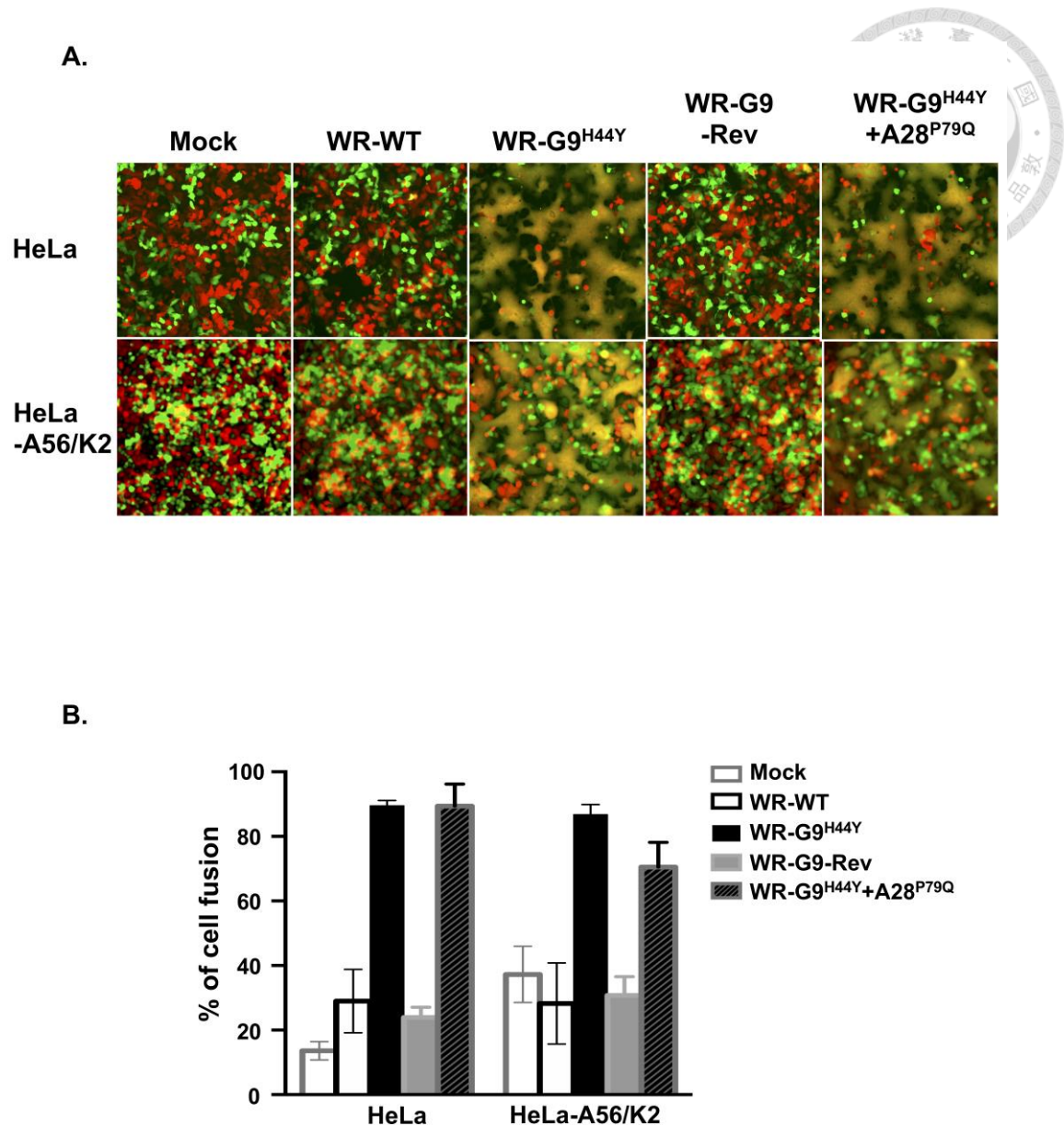


**Figure 15.** The EV of WR-G9<sup>H44Y</sup> and WR-G9<sup>H44Y</sup>+A28<sup>P79Q</sup> virus triggered a cell fusion phenotype on HeLa and HeLa-A56/K2 cells. (A). HeLa or HeLa-A56/K2 cells expressing GFP or RFP were seeded in a 1:1 ratio. The next day, these cells were infected with WR-WT, WR-G9<sup>H44Y</sup>, WR-G9-Rev or WR-G9<sup>H44Y</sup>+A28<sup>P79Q</sup> virus at an MOI of 5 PFU per cell and then photographed using a Zeiss Axiovert fluorescence microscope after 20 hpi. (B). Quantification of % cell fusion from the images described in (A). Images from three independent experiments were quantified using the image area of GFP<sup>+</sup>RFP<sup>+</sup> double-fluorescent cells divided by that of single-fluorescent cells. Data from three independent experiments.



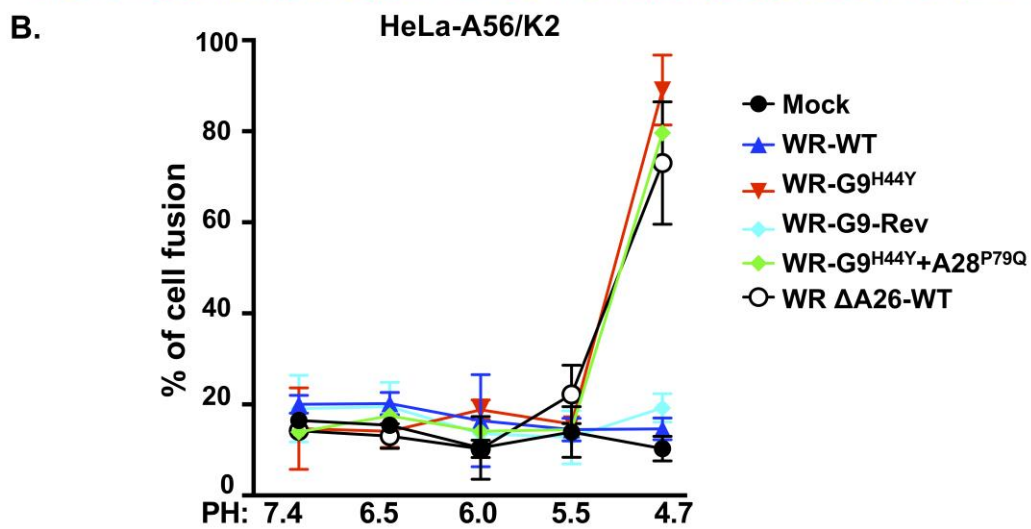
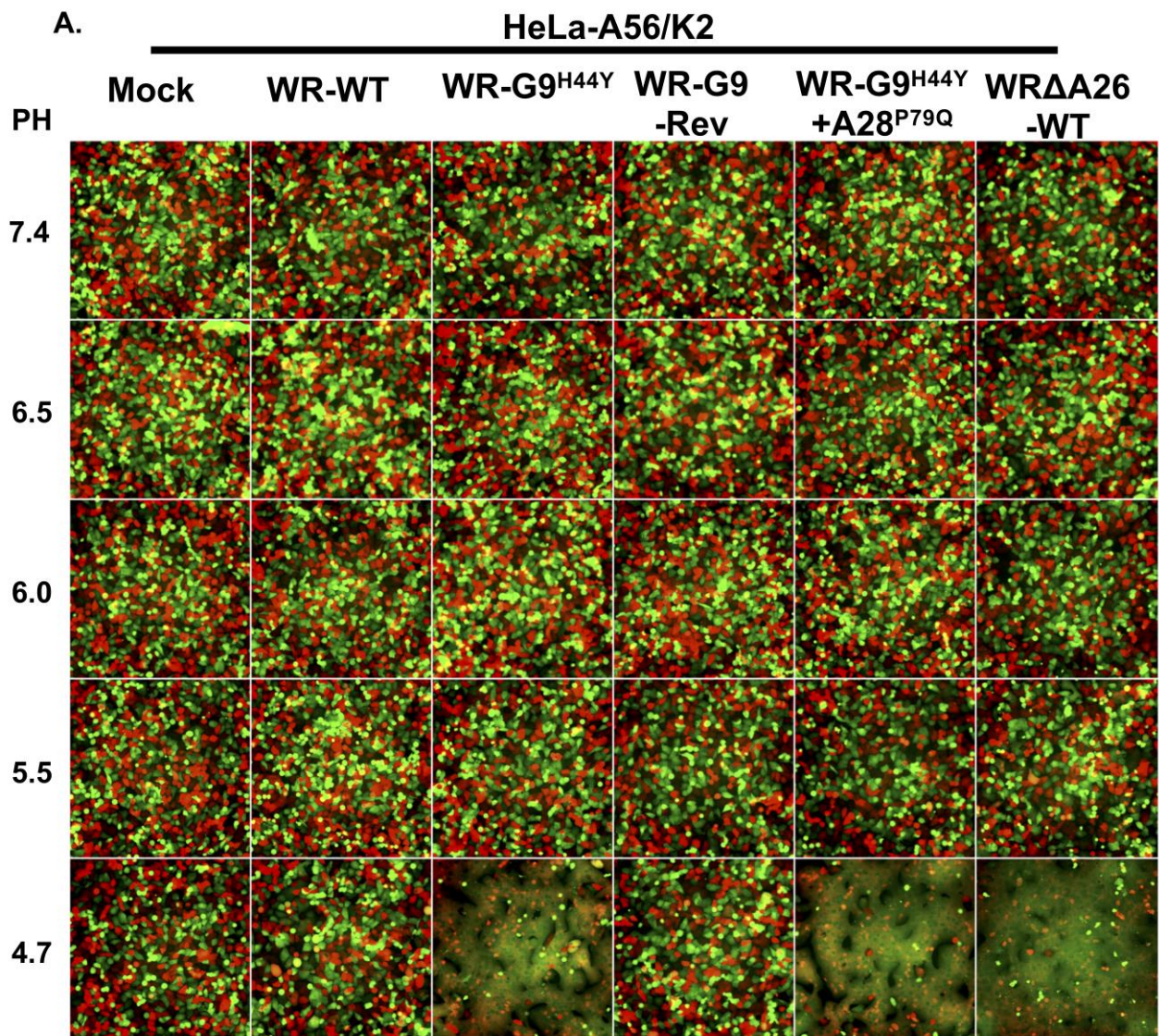


**Figure 16. Acid titration of WR-G9<sup>H44Y</sup> and WR-G9<sup>H44Y</sup>+A28<sup>P79Q</sup> virus-mediated fusion activation in HeLa-A56/K2 cells.** (A). HeLa-A56/K2 cells expressing GFP or RFP were seeded in a 1:1 ratio. The next day, these cells were pretreated with 40 µg/ml cordycepin for 60 min and subsequently infected with MV of WR-WT, WR-G9<sup>H44Y</sup>, WR-G9-Rev, WR-G9<sup>H44Y</sup>+A28<sup>P79Q</sup> or WRΔA26-WT virus at an MOI of 100 PFU per cell. Cordycepin was present in culture media throughout the experiments to inhibit viral early gene expression. After infection at 37 °C for 60 min, cells were treated with a buffer of pH 7.4, 6.5, 6.0, 5.5 or 4.7, respectively, at 37 °C for 3 min, washed with growth medium, further incubated at 37 °C for 1 h, and then photographed using a Zeiss Axiovert fluorescence microscope. (B). Quantification of % cell fusion from the images described in (A). Images from three independent experiments were quantified using the image area of GFP<sup>+</sup>RFP<sup>+</sup> double-fluorescent cells divided by that of single-fluorescent cells. Data from three independent experiments.

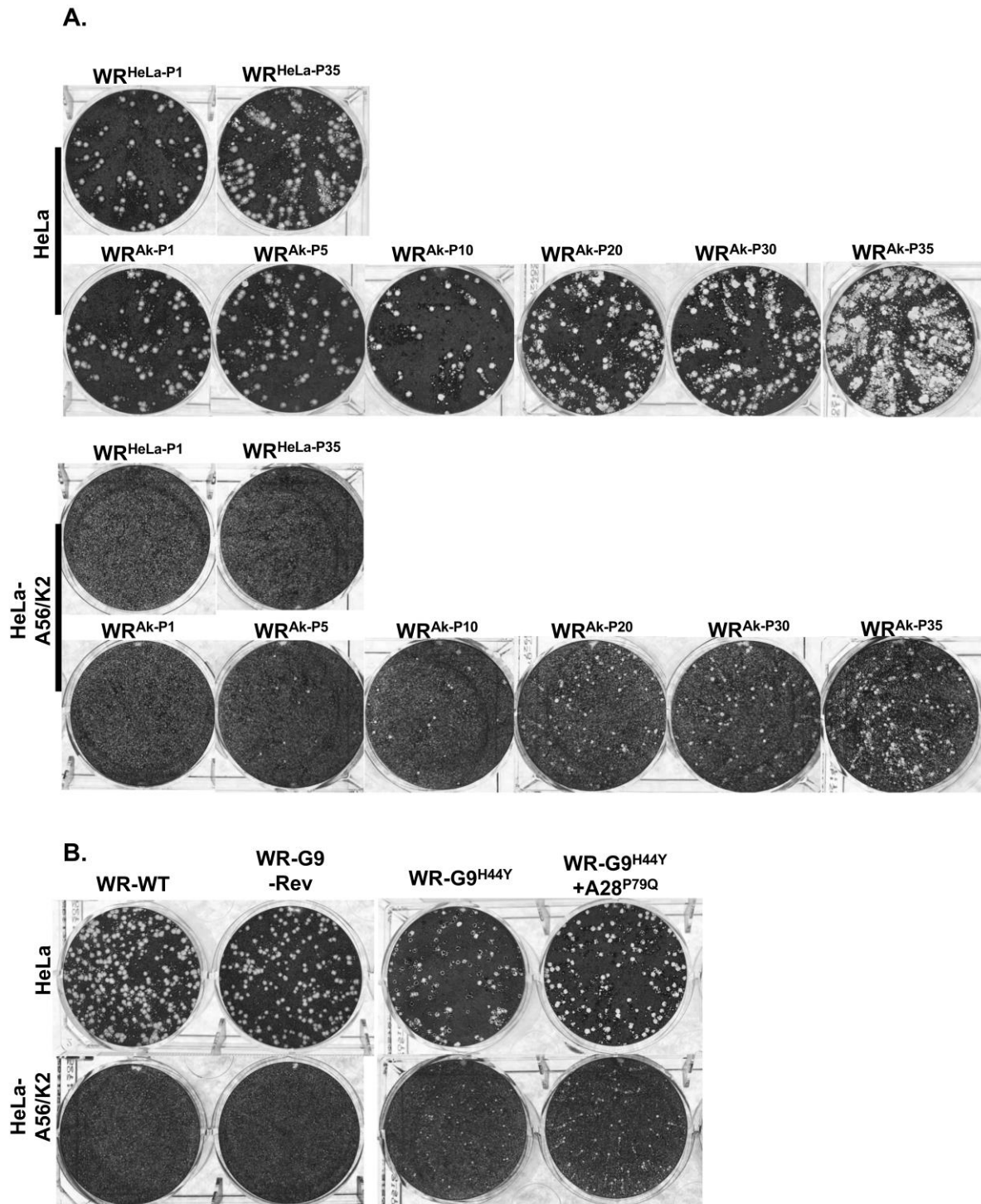


**Figure 17. EV spreading ability assessment by liquid plaque assay.** (A). The EV spreading morphology of WR<sup>HeLa-A56/K2</sup> viral pools P1 to P35 in HeLa and HeLa-A56/K2 cells and cell staining with 1% crystal violet after 3 dpi. (B). The EV spreading morphology of WR-WT, WR-G9-Rev, WR-G9<sup>H44Y</sup> and WR-G9<sup>H44Y</sup>+A28<sup>P79Q</sup> virus in HeLa and HeLa-A56/K2 cells and cell staining with 1% crystal violet after 3 dpi.

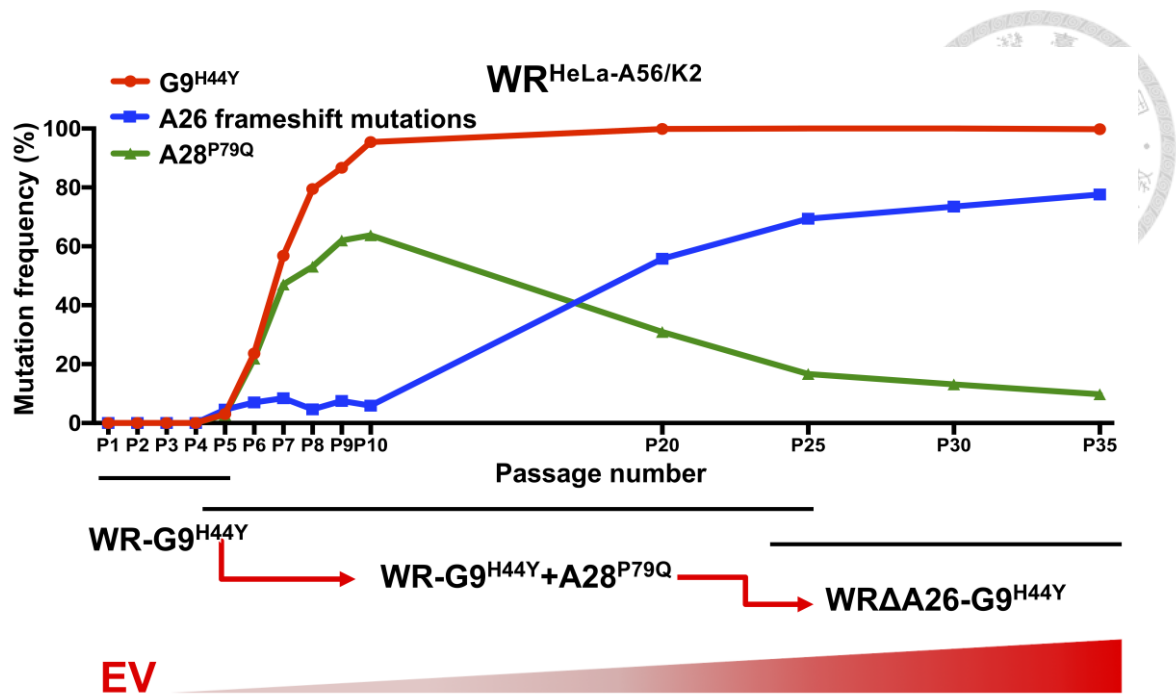
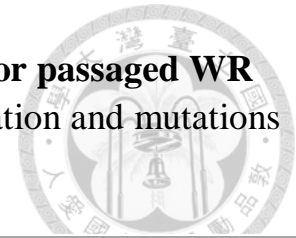


Figure 18. Hypothesis of the regulatory role of A28<sup>P79Q</sup> in EV spread.

**Supplementary 1. Table of whole genome sequencing data for passaged WR virus pools.** (The dataset was filtered with a cut-off of 1% variation and mutations resulting in amino acid changes are shown.)



| Passage number (P) | WR <sup>Hela</sup> |                   |                        | WR <sup>Hela-A56/K2</sup>                                                                                                                                                                                                                                                                                                                                                                                                                                                                                                                                                                                                  |                                                                                                                                                                                                                                                                                        |                                                                                                                                                                                                                          |
|--------------------|--------------------|-------------------|------------------------|----------------------------------------------------------------------------------------------------------------------------------------------------------------------------------------------------------------------------------------------------------------------------------------------------------------------------------------------------------------------------------------------------------------------------------------------------------------------------------------------------------------------------------------------------------------------------------------------------------------------------|----------------------------------------------------------------------------------------------------------------------------------------------------------------------------------------------------------------------------------------------------------------------------------------|--------------------------------------------------------------------------------------------------------------------------------------------------------------------------------------------------------------------------|
|                    | Nucleotide change  | Amino acid change | Mutation frequency (%) | Nucleotide change                                                                                                                                                                                                                                                                                                                                                                                                                                                                                                                                                                                                          | Amino acid change                                                                                                                                                                                                                                                                      | Mutation frequency (%)                                                                                                                                                                                                   |
| P1                 | N/D                | N/D               |                        | <b>J5L</b> 179dup<br><b>J5L</b> 179delA<br><b>I6L</b><br>1. 1084dup<br>2. 1084delA<br><b>F14L</b> 303dup<br><b>D12L</b> 614delA<br><b>A8R</b> 266delA<br><b>B12R</b> 696dup                                                                                                                                                                                                                                                                                                                                                                                                                                                | N60fs<br>N60fs<br>I362fs<br>I362fs<br>C102fs<br>N205fs<br>N89fs<br>E233fs                                                                                                                                                                                                              | 2.1<br>1.5<br>2.8<br>4.5<br>1<br>1.2<br>1.4<br>1                                                                                                                                                                         |
| P2                 | N/D                | N/D               |                        | <b>J5L</b> 179delA<br><b>I6L</b><br>1. 1084dup<br>2. 1084delA<br><b>B4R</b><br>1. 188delT<br>2. 293C>A<br>3. 525A>G<br>4. 788T>A<br>5. 1029A>G<br><b>C1L</b> 343A>G<br><b>C5L</b> 383A>G<br><b>F1L</b> 443C>G<br><b>F10L</b><br>1. 1147_1148delCC<br>2. 95A>T<br><b>F14L</b> 307A>G<br><b>E1L</b> 568T>C<br><b>E2L</b><br>1. 2180delT<br>2. 1783delA<br>3. 830A>G<br><b>E6R</b> 754G>A<br><b>O1L</b> 426delT<br><b>I2L</b> 168dup<br><b>I8R</b><br>1. 216delA<br>2. 704T>C<br>3. 1475G>A<br>4. 1570C>A<br><b>G2R</b><br>1. 155A>G<br>2. 371delT<br><b>G5R</b><br>1. 608C>T<br>2. 854C>T<br>3. 1225A>G<br><b>J3R</b> 161A>G | N60fs<br>I362fs<br>I362fs<br>L63fs<br>S98*<br>H175R<br>L263*<br>I403M<br>M115V<br>D128G<br>A148G<br>P383fs<br>N32I<br>K103E<br>S190P<br>L727fs<br>I595fs<br>E277G<br>A252Y<br>F142fs<br>I57fs<br>V73fs<br>L235S<br>R492E<br>L524I<br>Y52C<br>L124fs<br>A203V<br>S285F<br>I409V<br>E54R | 2.1<br>5.9<br>8.8<br>2.6<br>4.7<br>1.9<br>1.5<br>1<br>1.1<br>1.4<br>1.2<br>1.3<br>1.3<br>1.3<br>1.7<br>1.8<br>1.2<br>1.7<br>1.1<br>1.5<br>1.4<br>1.5<br>1.3<br>1<br>1.1<br>1.2<br>1.4<br>1.1<br>1.4<br>1.4<br>1.4<br>1.1 |

|    |     |     |  |                                                                                                                                                                                                                                                                                                                     |                                                                                                                                                   |                                                                                                                  |
|----|-----|-----|--|---------------------------------------------------------------------------------------------------------------------------------------------------------------------------------------------------------------------------------------------------------------------------------------------------------------------|---------------------------------------------------------------------------------------------------------------------------------------------------|------------------------------------------------------------------------------------------------------------------|
|    |     |     |  | <b>J6R</b> 630A>G<br><b>D11L</b> 388A>G<br><b>D12R</b> 614dup<br><b>A7L</b> 1183delA<br><b>A11R</b> 801A>T<br><b>A26L</b><br>1. 871T>C<br>2. 835G>A<br>3. 641T>A<br>4. 518C>T<br>5. 235C>T<br>6. 158A>G<br><b>A30L</b> 235A>G<br><b>A43R</b> 459delT<br><b>B7R</b><br>1. 182T>A<br>2. 186delT<br><b>B12R</b> 721T>C | I210M<br>I130V<br>N205<br>I395fs<br>K267N<br><br>Y291H<br>V279I<br>I214K<br>A173V<br>Q79*<br>H53R<br>M79V<br>I154fs<br><br>I61N<br>I63fs<br>F241L | 1.3<br>1.2<br>1.2<br>1<br>1.1<br><br>1.3<br>1.2<br>1.2<br>1.1<br>1<br>1.1<br>1.1<br>1.5<br><br>1.8<br>1.7<br>1.1 |
| P3 | N/D | N/D |  | <b>J5L</b> 179dup<br><b>B4R</b> 293C>A<br><b>I6L</b><br>1. 1084dup<br>2. 1084delA<br><b>E1L</b> 152T>C<br><b>H4L</b><br>1. 617delA<br>2. 348dup<br><b>D2L</b> 28delA<br><b>A22R</b> 559dup                                                                                                                          | N60fs<br>S98*<br><br>I362fs<br>I362fs<br>I51T<br><br>K296fs<br>N117fs<br>I10fs<br>M187fs                                                          | 3.3<br>5.7<br><br>1.6<br>4.8<br>1<br><br>2.1<br>1.4<br>1.8<br>1.2                                                |
| P4 | N/D | N/D |  | <b>J5L</b><br>1. 179dup<br>2. 179delA<br><b>I6L</b><br>1. 1084dup<br>2. 1084delA<br><b>H4L</b> 617delA<br><b>D4R</b> 328C>A                                                                                                                                                                                         | N60fs<br>N60fs<br><br>I362fs<br>I362fs<br>K206fs<br>L110I                                                                                         | 1.5<br>1.3<br><br>1.9<br>2.5<br>1<br>1.1                                                                         |
| P5 | N/D | N/D |  | <b>G9R</b> 130C>T<br><b>A28L</b> 236C>A<br><b>A26L</b> multiple mutations<br>1. 230delC<br>2. 112delA<br><b>J5L</b> 179dup<br><b>B4R</b> 293C>A<br><b>I6L</b><br>1. 1084dup<br>2. 1084delA<br><b>I8R</b> 1882C>A<br><b>D11L</b> 260delA                                                                             | H44Y<br>P79Q<br><br>P77fs<br>I38fs<br>N60fs<br>S98*<br><br>I362fs<br>I362fs<br>H628N<br>K87fs                                                     | 3.1<br>2.8<br><b>4.6</b><br><br>1.7<br>2.9<br>2.8<br>7<br><br>2.3<br>2.9<br>1.5<br>1.1                           |
| P6 | N/D | N/D |  | <b>G9R</b> 130C>T<br><b>A28L</b> 236C>A<br><b>A26L</b> multiple mutations<br>1. 230delC                                                                                                                                                                                                                             | H44Y<br>P79Q<br><br>P77fs                                                                                                                         | 23.6<br>21.9<br><b>7</b><br><br>1.1                                                                              |



|     |                                                                                                                                            |                                                    |                                      |                                                                                                                                                                                                                                                                                                   |                                                                                                                         |                                                                                                           |
|-----|--------------------------------------------------------------------------------------------------------------------------------------------|----------------------------------------------------|--------------------------------------|---------------------------------------------------------------------------------------------------------------------------------------------------------------------------------------------------------------------------------------------------------------------------------------------------|-------------------------------------------------------------------------------------------------------------------------|-----------------------------------------------------------------------------------------------------------|
|     |                                                                                                                                            |                                                    |                                      | 2. 112delA<br>3. 1471_1472delAT<br>4. 771_772dup<br><b>J5L</b><br>1. 179dup<br>2. 179delA<br><b>B4R</b> 293C>A<br><b>I6L</b><br>1. 1084dup<br>2. 1084delA<br><b>A24R</b> 11dup                                                                                                                    | I38fs<br>I491fs<br>L258fs<br><br>N60fs<br>N60fs<br>S98*<br><br>I362fs<br>I362fs<br>N4fs                                 | 3.5<br>1.2<br>1.2<br><br>1.7<br>1.1<br>6.5<br><br>1.9<br>2.5<br>1                                         |
| P7  | N/D                                                                                                                                        | N/D                                                |                                      | <b>G9R</b> 130C>T<br><b>A28L</b> 236C>A<br><b>A26L</b> multiple mutations<br>1. 112delA<br>2. 1471_1472delAT<br>3. 771_772dup<br>4. 188_189dup<br><b>J5L</b><br>1. 179dup<br>2. 179delA<br><b>B4R</b> 293C>A<br><b>I6L</b> 1084dup<br><b>F11L</b> 74G>T<br><b>A8R</b> 266dup<br><b>A24R</b> 11dup | H44Y<br>P79Q<br><br>I38fs<br>I491fs<br>L258fs<br>P64fs<br><br>N60fs<br>N60fs<br>S98*<br>I362fs<br>R25M<br>N89fs<br>N4fs | 56.7<br>47.1<br><b>8.3</b><br><br>3.7<br>1.2<br>2<br>1.4<br><br>1.4<br>2<br>3<br>1.2<br>1.2<br>1.1<br>1.7 |
| P8  | N/D                                                                                                                                        | N/D                                                |                                      | <b>G9R</b> 130C>T<br><b>A28L</b> 236C>A<br><b>A26L</b> multiple mutations<br>1. 112delA<br>2. 1471_1472delAT<br>3. 771_772dup<br><b>B4R</b> 293C>A<br><b>I6L</b> 1084delA                                                                                                                         | H44Y<br>P79Q<br><br>I38fs<br>I491fs<br>L258fs<br>S98*<br>I362fs                                                         | 79.5<br>53.1<br><b>4.7</b><br><br>1.3<br>1.5<br>1.9<br>3.4<br>1.2                                         |
| P9  | N/D                                                                                                                                        | N/D                                                |                                      | <b>G9R</b> 130C>T<br><b>A28L</b> 236C>A<br><b>A26L</b> multiple mutations<br>1. 112delA<br>2. 1471_1472delAT<br>3. 771_772dup<br>4. 188_189dup<br>5. 570G>A<br><b>B4R</b> 293C>A                                                                                                                  | H44Y<br>P79Q<br><br>I38fs<br>I491fs<br>L258fs<br>P64fs<br>W190*<br>S98*                                                 | 86.7<br>62<br><b>7.4</b><br><br>1.8<br>1.1<br>1.8<br>1.3<br>1.4<br>4.4                                    |
| P10 | <b>J5L</b><br>1. 179delA<br>2. 179dup<br><b>I6L</b> 1084delA<br><b>B4R</b> 293C>A<br><b>C5L</b> 598A>G<br><b>I4L</b> 276delA<br><b>D2L</b> | N60fs<br>N60fs<br>I362fs<br>S98*<br>R200K<br>K92fs | 1.1<br>1.7<br>5.3<br>4.8<br>1.2<br>1 | <b>G9R</b> 130C>T<br><b>A28L</b> 236C>A<br><b>A26L</b> multiple mutations<br>1. 771_772dup<br>2. 230delC<br>3. 188_189dup<br>4. 112delA.                                                                                                                                                          | H44Y<br>P79Q<br><br>L258fs<br>P77fs<br>P64fs<br>I38fs                                                                   | 95.4<br>63.8<br><b>5.9</b><br><br>1.4<br>1.2<br>1.7<br>1.6                                                |

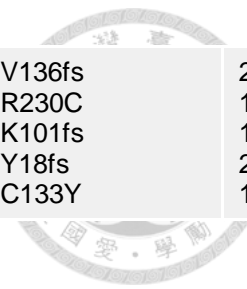
|     |                                                                                                                                                                                                                           |                                                                                                              |                                                                                      |                                                                                                                                                                                                                                                                                                                                                                                                                                                                                                                                                 |                                                                                                                                                                                                                                                                   |                                                                                                                                                                                                                   |
|-----|---------------------------------------------------------------------------------------------------------------------------------------------------------------------------------------------------------------------------|--------------------------------------------------------------------------------------------------------------|--------------------------------------------------------------------------------------|-------------------------------------------------------------------------------------------------------------------------------------------------------------------------------------------------------------------------------------------------------------------------------------------------------------------------------------------------------------------------------------------------------------------------------------------------------------------------------------------------------------------------------------------------|-------------------------------------------------------------------------------------------------------------------------------------------------------------------------------------------------------------------------------------------------------------------|-------------------------------------------------------------------------------------------------------------------------------------------------------------------------------------------------------------------|
|     | 1. 28dup<br>2. 28delA<br><b>A2L</b> 594delA<br><b>A18R</b> 49delA<br><b>A24R</b> 53delT<br><b>A28L</b> 24dup                                                                                                              | I10fs<br>I10fs<br>K198fs<br>M17fs<br>L18fs<br>I9fs                                                           | 1.6<br>1.1<br>1<br>1.4<br>1.1<br>1.3                                                 | <b>B4R</b> 293C>A                                                                                                                                                                                                                                                                                                                                                                                                                                                                                                                               | S98*                                                                                                                                                                                                                                                              | 5.5                                                                                                                                                                                                               |
| P20 | <b>J5L</b> 179delA<br><b>I6L</b> 1084dup<br><b>B4R</b><br>1. 293C>A<br>2. 12delT<br>3. 258dup<br><b>A26L</b><br>1. 230delC<br>2. 112delA<br>3.<br>677_680delCTAT<br><b>A56R</b> 682G>A                                    | N60fs<br>I362fs<br><br>S98*<br>F4fs<br>L87fs<br><br>P77fs<br>I38fs<br>S226fs<br>V228I                        | 1.7<br>2.9<br><br>37.9<br>2.2<br>1.1<br><br>1.3<br>1.7<br><br>1<br>1.5               | <b>G9R</b> 130C>T<br><b>A28L</b><br>1.236C>A<br>2. 24delT<br><b>A26L</b> multiple<br>mutations<br>1. 771_772dup<br>2. 230delC<br>3. 188_189dup<br>4. 112delA<br>5.1471_1472delAT<br>6.1420_1421delCT<br>7. 1245dup<br>8. 973delG<br>9. 947dup<br>10. 910dup<br>11. 578_579delTA<br>12. 570G>A<br>13. 421dup<br>14. 301_302dup<br>15. 149dup<br><b>J5L</b> 179dup<br><b>I6L</b><br>1. 1084delA<br>2. 1084dup<br><b>B4R</b> 293C>A<br><b>A32L</b> 670G>A<br><b>K2L</b> 67_69delAAT<br><b>F11L</b> 74G>T<br><b>J2R</b> 265G>A<br><b>A24R</b> 11dup | H44Y<br><br>P79Q<br>F8fs<br><br>L258fs<br>P77fs<br>P64fs<br>I38fs<br>I491fs<br>L474fs<br>D416fs<br>V325fs<br>R317fs<br>E304fs<br>V193fs<br>W190*<br>I141fs<br>S102fs<br>N50fs<br>N60fs<br><br>I362fs<br>I362fs<br>S98*<br>V224I<br>N23del<br>R25M<br>D89N<br>N4fs | 99.9<br><br>30.9<br>1<br><b>55.8</b><br><br>5.9<br>4.4<br>4.6<br>8.9<br>7.6<br>1.1<br>2.7<br>5.8<br>2.3<br>1.3<br>1.1<br>6.7<br>1.2<br>1.2<br>1.0<br>1.3<br><br>5.4<br>3.4<br>11.9<br>2.2<br>1<br>1.4<br>1<br>1.3 |
| P25 | <b>J5L</b><br>1. 179delA<br>2. 179dupA<br><b>I6L</b><br>1. 1084delA<br>2. 1084dup<br><b>B4R</b><br>1. 293C>A<br>2. 12delT<br>3. 258dup<br>4. 258del<br><b>A26L</b><br>1. 112delA<br>2. 1420_1421del<br><b>A32L</b> 370G>A | N60fs<br>N60fs<br><br>I362fs<br>I362fs<br><br>S98*<br>F4fs<br>L87fs<br>L87fs<br><br>I38fs<br>L474fs<br>A103T | 2<br>1.2<br><br>3.9<br>3.3<br><br>55.4<br>2.1<br>1.4<br>1.2<br><br>3.9<br>1.9<br>1.1 | <b>G9R</b> 130C>T<br><b>A28L</b> 236C>A<br><b>A26L</b> multiple<br>mutations<br>1. 771_772dup<br>2. 230delC<br>3. 188_189dup<br>4. 112delA<br>5.1471_1472del<br>6. 1245dup<br>7. 910dup<br>8. 578_579delTA<br>9. 570G>A<br>10. 421dup<br>11. 1189G>T                                                                                                                                                                                                                                                                                            | H44Y<br>P79Q<br><br>L258fs<br>P77fs<br>P64fs<br>I38fs<br>I491fs<br>D416fs<br>E304fs<br>V193fs<br>W190*<br>I141fs<br>E397*                                                                                                                                         | 100<br>16.7<br><b>69.4</b><br><br>7.5<br>8.5<br>2.9<br>12.9<br>9.4<br>4.1<br>1.7<br>1.1<br>12.6<br>2.7<br>1.4                                                                                                     |



|     |                                                                                                                                                                                                                                                                                                                                                                                                                                                            |                                                                                                                                                                                                     |                                                                                                                                                     |                                                                                                                                                                                                                                                                                                                                                                                                                                                                                                                                    |                                                                                                                                                                                                                                                      |                                                                                                                                                                                                      |
|-----|------------------------------------------------------------------------------------------------------------------------------------------------------------------------------------------------------------------------------------------------------------------------------------------------------------------------------------------------------------------------------------------------------------------------------------------------------------|-----------------------------------------------------------------------------------------------------------------------------------------------------------------------------------------------------|-----------------------------------------------------------------------------------------------------------------------------------------------------|------------------------------------------------------------------------------------------------------------------------------------------------------------------------------------------------------------------------------------------------------------------------------------------------------------------------------------------------------------------------------------------------------------------------------------------------------------------------------------------------------------------------------------|------------------------------------------------------------------------------------------------------------------------------------------------------------------------------------------------------------------------------------------------------|------------------------------------------------------------------------------------------------------------------------------------------------------------------------------------------------------|
|     | <b>K7R</b><br>1. 441del<br>2. 307G>T<br><b>G1L</b> 1695del<br><b>A8R</b> 266del<br><b>A56R</b> 682G>A                                                                                                                                                                                                                                                                                                                                                      | K147fs<br>G103*<br>F565fs<br>N89fs<br>V228I                                                                                                                                                         | 1.7<br>1.1<br>1<br>1<br>2.4                                                                                                                         | 12. 1120del<br>13. 514_521del<br>14. 217_220 del<br>15. 112dup<br><b>J5L</b><br>1. 179del<br>2. 179dup<br>3. 170T>A<br><b>I6L</b><br>1. 1084delA<br>2. 1084dup<br><b>B4R</b> 293C>A<br><b>A32L</b><br>1. 670G>A<br>2. 232C>A<br><b>K2L</b><br>1. 67_69del<br>2. 358dup<br><b>F11L</b> 74G>T<br><b>G1L</b> 1695del<br><b>H4L</b> 348del<br><b>A7L</b> 1585A>G<br><b>A8R</b> 266del                                                                                                                                                  | D374fs<br>I172fs<br>P73fs<br>I38fs<br>N60fs<br>N60fs<br>L57*<br>I362fs<br>I362fs<br>S98*<br>V224I<br>L78I<br>N23del<br>R120fs<br>R25M<br>F565fs<br>F116fs<br>I529V<br>N89fs                                                                          | 1.1<br>1.1<br>1.4<br>1<br>1.2<br>1.8<br>1<br>4.7<br>2.1<br>10.5<br>9.9<br>1.5<br>1.6<br>1.8<br>1.6<br>1<br>1.1<br>3.3<br>1.3                                                                         |
| P30 | <b>J5L</b><br>1. 179delA<br>2. 179dupA<br><b>I6L</b><br>1. 1084delA<br>2. 1375C>T<br><b>B4R</b><br>1. 293C>A<br>2. 12delT<br>3. 258dup<br><b>A26L</b><br>1. 112delA<br>2. 1420_1421del<br>3. 1442_1448del<br>4. 235dup<br><b>A32L</b><br>1. 370G>A<br>2. 286G>T<br><b>A52R</b> 401G>A<br><b>K7R</b><br>1. 441del<br>2. 307G>T<br><b>F15L</b> 303del<br><b>A7L</b> 376G>T<br><b>A8R</b> 266del<br><b>A24R</b> 11dup<br><b>A56R</b><br>1. 682G>A<br>2. 76del | N60fs<br>N60fs<br>I362fs<br>R459*<br>S98*<br>F4fs<br>L87fs<br>I38fs<br>L474fs<br>T481fs<br>Q79fs<br>A103T<br>A96S<br>C134Y<br>K147fs<br>G103*<br>K101fs<br>D126Y<br>N89fs<br>N4fs<br>V228I<br>I26fs | 1.4<br>1.8<br>5.2<br>1.5<br>63.6<br>3.7<br>1.9<br>4.9<br>1.9<br>1.1<br>1.8<br>3.6<br>1.6<br>1.7<br>3.3<br>1.2<br>1.1<br>3.6<br>1.2<br>2<br>3<br>1.1 | <b>G9R</b> 130C>T<br><b>A28L</b> 236C>A<br><b>A26L</b> multiple mutations<br>1. 771_772dup<br>2. 230delC<br>3. 188_189dup<br>4. 112delA<br>5. 1471_1472del<br>6. 1245dup<br>7. 570G>A<br>8. 421dup<br>9. 217_220 del<br>10. 112dup<br>11. 973del<br>12. 947dup<br>13. 149dup<br><b>J5L</b><br>1. 179del<br>2. 179dup<br><b>I6L</b><br>1. 1084delA<br>2. 1084dup<br><b>B4R</b><br>1. 293C>A<br>2. 350A>G<br><b>A32L</b><br>1. 670G>A<br>2. 232C>A<br><b>A52R</b><br>1. 81del<br>2. 369dup<br><b>A7L</b><br>1. 1585A>G<br>2. 1744G>C | H44Y<br>P79Q<br>L258fs<br>P77fs<br>P64fs<br>I38fs<br>I491fs<br>D416fs<br>W190*<br>I141fs<br>P73fs<br>I38fs<br>V325fs<br>R317fs<br>N50fs<br>N60fs<br>N60fs<br>I362fs<br>I362fs<br>S98*<br>E117R<br>V224I<br>L78I<br>K27fs<br>Q124fs<br>I529V<br>V582L | 100<br>13.1<br><b>73.5</b><br>5.2<br>6.3<br>3.3<br>10.7<br>6.5<br>5.4<br>21<br>1.9<br>1.7<br>1.5<br>6<br>2.2<br>1.8<br>2<br>1.3<br>3.5<br>2<br>10<br>1.5<br>17.8<br>2.5<br>1.5<br>1.1<br>11.3<br>1.1 |

|     |                                                                                                                                                                                                                                                                                                                                                                                                                                                                                                                                                                                                                                                                                                                 |                                                                                                                                                                                                                                                                                                                                                                 |                                                                                                                                                                                                                                                                            |                                                                                                                                                                                                                                                                                                                                                                                                                                                                                                                                                                                                                                                                                                                                                                |                                                                                                                                                                                                                                                                                                                                                                                               |                                                                                                                                                                                                                                                                                                               |
|-----|-----------------------------------------------------------------------------------------------------------------------------------------------------------------------------------------------------------------------------------------------------------------------------------------------------------------------------------------------------------------------------------------------------------------------------------------------------------------------------------------------------------------------------------------------------------------------------------------------------------------------------------------------------------------------------------------------------------------|-----------------------------------------------------------------------------------------------------------------------------------------------------------------------------------------------------------------------------------------------------------------------------------------------------------------------------------------------------------------|----------------------------------------------------------------------------------------------------------------------------------------------------------------------------------------------------------------------------------------------------------------------------|----------------------------------------------------------------------------------------------------------------------------------------------------------------------------------------------------------------------------------------------------------------------------------------------------------------------------------------------------------------------------------------------------------------------------------------------------------------------------------------------------------------------------------------------------------------------------------------------------------------------------------------------------------------------------------------------------------------------------------------------------------------|-----------------------------------------------------------------------------------------------------------------------------------------------------------------------------------------------------------------------------------------------------------------------------------------------------------------------------------------------------------------------------------------------|---------------------------------------------------------------------------------------------------------------------------------------------------------------------------------------------------------------------------------------------------------------------------------------------------------------|
|     |                                                                                                                                                                                                                                                                                                                                                                                                                                                                                                                                                                                                                                                                                                                 |                                                                                                                                                                                                                                                                                                                                                                 |                                                                                                                                                                                                                                                                            | 3. 1523A>C<br><b>K7R</b><br>1. 441del<br>2. 441dup<br><b>B11R</b> 74dup<br><b>N2L</b> 405del<br><b>K2L</b><br>1. 67_69del<br>2. 358dup<br><b>F5L</b> 688C>T<br><b>F11L</b> 74G>T<br><b>A11R</b> 71C>G<br><b>A24R</b> 11dup                                                                                                                                                                                                                                                                                                                                                                                                                                                                                                                                     | D508A<br><br>K147fs<br>L148fs<br>N25fs<br>V136fs<br><br>N23del<br>R120fs<br>R230C<br>R25M<br>S24C<br>N4fs                                                                                                                                                                                                                                                                                     | 1.2<br><br>1<br>1.1<br>1.5<br>1.4<br><br>3.1<br>2.4<br>1.8<br>1.6<br>1<br>1.3                                                                                                                                                                                                                                 |
| P35 | <b>J5L</b><br>1. 179delA<br>2. 179dupA<br><b>I6L</b><br>1. 1084delA<br>2. 1084dup<br><b>B4R</b><br>1. 293C>A<br>2. 12delT<br>3. 258dup<br>4. 258delT<br><b>A26L</b><br>1. 112delA<br>2. 1420_1421del<br>3. 1442_1448del<br>4. 235dup<br><b>A32L</b><br>1. 370G>A<br>2. 286G>T<br><b>A52R</b><br>1. 401G>A<br>2. 424G>A<br>3. 81dup<br>4. 81delA<br>5. 284G>A<br><b>K7R</b><br>1. 441del<br>2. 307G>T<br><b>A7L</b><br>1. 376G>T<br>2. 1568G>A<br><b>A18R</b> 49delA<br><b>A56R</b><br>1. 682G>A<br>2. 76del<br><b>F13L</b> 990C>A<br><b>F15L</b> 303delA<br><b>I4L</b> 1375C>T<br><b>H4L</b> 617delA<br><b>D10R</b> 310T>A<br><b>A55R</b> 827delA<br><b>C13L</b> 637delG<br><b>N2L</b><br>1. 405dup<br>2. 59C>T | N60fs<br>N60fs<br><br>I362fs<br>I362fs<br><br>S98*<br>F4fs<br>L87fs<br>L87fs<br><br>I38fs<br>L474fs<br>T481fs<br>Q79fs<br><br>A103T<br>A96S<br><br>C134Y<br>A142T<br>Y28fs<br>K27fs<br>G95D<br><br>K147fs<br>G103*<br><br>D126Y<br>C53Y<br>M17fs<br><br>V228I<br>I26fs<br>F330L<br>K107fs<br>R459*<br>K206fs<br>S104T<br>N276fs<br>L180fs<br><br>V136fs<br>A20V | 1.6<br>1.7<br><br>4.4<br>2.1<br><br>64.1<br>4.3<br>1.5<br>1.1<br><br>4.4<br>1.2<br>1.6<br>1.4<br><br>9<br>1.1<br><br>3.1<br>1.8<br>1.3<br>1.2<br>1.8<br><br>4.2<br>1<br><br>6.4<br>1.2<br>1<br><br>2.7<br>2.4<br>2.9<br>1.1<br>3.1<br>1<br>1.3<br>2.1<br>1.4<br><br>1<br>1 | <b>G9R</b> 130C>T<br><b>A28L</b> 236C>A<br><b>A26L</b> multiple mutations<br>1. 771_772dup<br>2. 230delC<br>3. 188_189dup<br>4. 112delA<br>5. 1471_1472delAT<br>6. 1420_1421delCT<br>7. 1245dup<br>8. 973delG<br>9. 947dup<br>10. 570G>A<br>11. 149dup<br>12. 1426_1427dup<br>13. 891delA<br>14. 217_220delCCAT<br>15. 112dup<br><b>J5L</b><br>1. 179delA<br>2. 179dup<br><b>I6L</b><br>1. 1084delA<br>2. 1084dup<br><b>B4R</b><br>1. 293C>A<br>2. 218delA<br>3. 430delT<br><b>A32L</b><br>1. 670G>A<br>2. 232C>A<br><b>A52R</b><br>1. 81del<br>2. 369dup<br>3. 198_199delCA<br><b>A7L</b><br>1. 1585A>G<br>2. 1744G>C<br><b>K7R</b> 441del<br><b>B11R</b> 74dup<br><b>B12R</b><br>1. 431dup<br>2. 696delA<br><b>D8L</b> 523_525 dup<br><b>K2L</b> 67_69delAAT | H44Y<br>P79Q<br><br>L258fs<br>P77fs<br>P64fs<br>I38fs<br>I491fs<br>L474fs<br>D416fs<br>V325fs<br>R317fs<br>W190*<br>N50fs<br>W477fs<br>G298fs<br>P73fs<br>I38fs<br><br>N60fs<br>N60fs<br><br>I362fs<br>I362fs<br><br>S98*<br>Y73fs<br>Y144fs<br><br>V224I<br>L78I<br><br>K27fs<br>Q124fs<br>Y66fs<br><br>I529V<br>V582L<br>K147fs<br>N25fs<br><br>N144fs<br>E233fs<br>N175_H176insN<br>N23del | 99.8<br>9.8<br><b>77.6</b><br><br>4.8<br>6.4<br>2.8<br>10.7<br>4.6<br>1.6<br>8.8<br>4<br>2<br>22.6<br>1.1<br>2.8<br>1.6<br>2.5<br>1.3<br><br>1.8<br>1.3<br><br>3<br>2.8<br><br>8.3<br>3.7<br>1.9<br><br>24.4<br>4.7<br><br>4.3<br>1.3<br>1.9<br><br>31.6<br>1.4<br>3.3<br>4.5<br><br>4.3<br>1.5<br>7.9<br>6.4 |

|  |  |  |  |                                                                                                          |                                             |                               |
|--|--|--|--|----------------------------------------------------------------------------------------------------------|---------------------------------------------|-------------------------------|
|  |  |  |  | <b>N2L</b> 405del<br><b>F5L</b> 688C>T<br><b>F15L</b> 303delA<br><b>A48R</b> 51dup<br><b>A51R</b> 398G>A | V136fs<br>R230C<br>K101fs<br>Y18fs<br>C133Y | 2.4<br>1.3<br>1<br>2.2<br>1.6 |
|--|--|--|--|----------------------------------------------------------------------------------------------------------|---------------------------------------------|-------------------------------|



**Supplementary 2. Acid titration of WR-G9<sup>H44Y</sup> and WR-G9<sup>H44Y</sup>+A28<sup>P79Q</sup> virus-mediated fusion activation in HeLa cells.**

